LUND UNIVERSITY

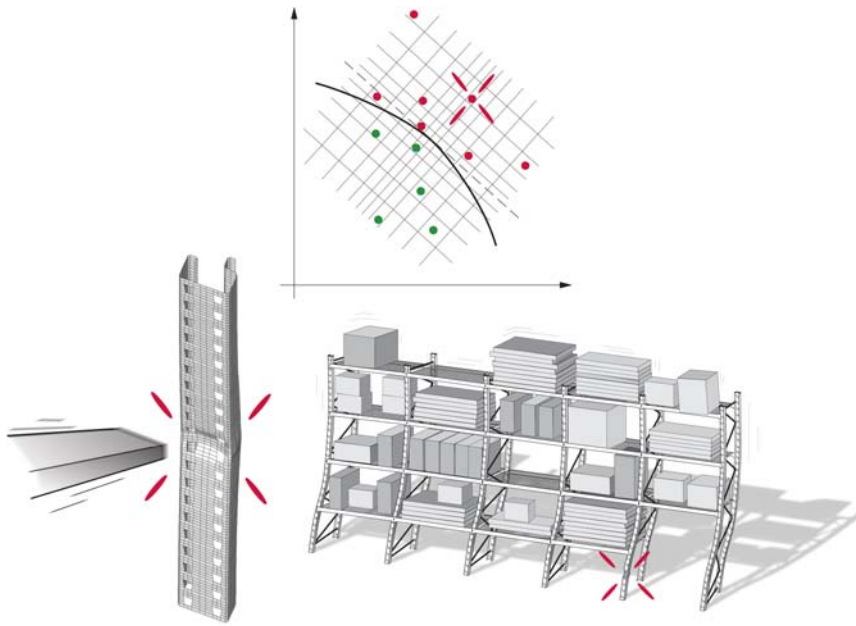

PROBABILISTIC ANALYSIS AND RELIABILITY OF ENGINEERING STRUCTURES

ANDERS OLSSON

Structural Mechanics

Doctoral Thesis

Structural Mechanics

ISRN LUTVDG/TVSM--02/1014--SE (1-154)
ISBN 91-628-5528-X ISSN 0281-6679

PROBABILISTIC ANALYSIS AND RELIABILITY OF ENGINEERING STRUCTURES

Doctoral Thesis by

ANDERS OLSSON

Printed by KFS i Lund AB, Lund, Sweden, December 2002.

For information, address:
Division of Structural Mechanics, LTH, Lund University, Box 118, SE-221 00 Lund, Sweden.
Homepage: http://www.byggmek.lth.se

To Martha,
David and Julia

Preface

The research presented in this thesis has been carried out at the Division of Structural Mechanics, Lund University, and comprises methods and applications for probabilistic analysis of structures. The work concerning the safety of racking systems in industry was financed by the Swedish Council for Work Life Research and carried out in cooperation with the Swedish National Testing and Research Institute. The work on methods for probabilistic analysis and structural reliability was financed by the Swedish Research Council (project no. 260-99-603), and the Swedish Research Council for Environment, Agricultural Sciences and Spatial Planning (project no. 2001-0414). The financial support from all sources is gratefully acknowledged.

I would like to thank my supervisors, Professor Göran Sandberg and Professor Ola Dahlblom, for all their support and encouragement during this work. They have given me valuable advice and suggestions, but also the opportunity to find my own path in the research during the course of the work. I am also very grateful to all other friends, colleagues and students at Structural Mechanics, former and present, for helping me in so many ways and for adding joy and companionship to the everyday work through various forms of collaboration and long coffee breaks.

Several people outside the Division of Structural Mechanics have been important to the present thesis. In particular, I would like to thank the members of the reference group for the racking systems project, and people from the industry of wooden roof trusses for discussions regarding relevant issues on roof-truss modelling and nail-plate joints.

Finally, I wish to express my deepest gratitude to my family, parents and friends for all their love and support throughout.

Lund, November 2002

Anders Olsson

Abstract

This thesis, consisting of six papers, concerns methods for probabilistic analysis of engineering structures. The work comprises evaluations of available methods, developments of new and improved methods, and applications of probabilistic analysis to engineering structures.

Comparative calculations using methods representing different strategies for stochastic finite element analysis were carried out, aiming at an evaluation with respect to computational efficiency, general applicability, and availability for practising engineers. Among the evaluated methods, the Monte Carlo simulation technique using Latin hypercube sampling was found to be attractive with respect to general applicability, since the handling of the stochastic variables is separate from mechanical modelling and numerical analysis. A method utilizing principal component analysis was suggested in order to bring Latin hypercube sampling in line with finite element analysis.

Methods for utilizing Latin hypercubes in importance sampling for structural reliability analysis were suggested. It was shown that simple importance sampling, as well as axis orthogonal importance sampling, can be considerably improved, with respect to computational efficiency, using Latin hypercube sampling instead of true random sampling. The improvement of the first method is dependent on a transformation of the stochastic variables in standard Gaussian space, resulting in a sample plan with one direction orthogonal to the tangent hyperplane of the failure surface at the design point.

The effects of damage caused by truck impacts to slender columns of racking systems were investigated by means of numerical simulations and laboratory tests. Three different thin-walled steel profiles were considered and it was found that even moderate geometrical imperfections result in considerable reduction of the load carrying capacity of individual columns. A study of the effects on entire racking systems was also performed in which damage magnitudes were regarded as probabilistic parameters.

Wooden roof trusses with nail-plate joints were analysed focusing on the influence of gaps between wooden members and misplaced nail-plates. Both issues arise as a consequence of lack of precision in the manufacturing process and the magnitudes of the imperfections were regarded as probabilistic parameters. Especially gaps between wooden members were shown to be of considerable importance for the deflection of roof trusses. In addition to the probabilistic analysis, a procedure was employed to optimize the nail-plate locations with respect to the deflection of a roof truss.

Keywords: probabilistic analysis, stochastic finite element analysis, Monte Carlo simulation, Latin hypercube sampling, principal component analysis, reliability, importance sampling, optimization, racking system, steel profile, roof truss, nail plate.

Contents

I Introduction and Overview

II Appended Papers

Part I

Introduction and Overview

Chapter 1

Introduction

1.1 Background

In all types of engineering, uncertainties of different kinds must be considered, in some way, by designers and engineers. For structural mechanics applications, the uncertainties often concern strength and stiffness values of structural members or connections. This includes geometrical and material properties. In many structures, also production errors or damage, caused by accidents or inadequate management, are uncertain parameters to be considered in the analysis. For large buildings and infrastructure projects, the properties of the foundation and surrounding environment are often difficult to determine with sufficient precision. The same holds for the loading, which may depend on natural phenomena such as snow and wind. To ensure a good safety level and serviceability of structures, at a competitive cost, it is thus necessary to have knowledge about statistical distributions and dependencies regarding various design parameters and external loads. Such knowledge often requires a patient collection of data or comprehensive laboratory experiments.

In addition to knowledge regarding the physical uncertainties, accurate mechanical models are required. Nowadays, elaborate numerical methods and models, including strategies for dealing with a variety of mechanical processes, have become widespread and are employed in everyday engineering design practice. Comprehensive general software, often based on the finite element method, are available. In most cases, however, these methods, models and software are developed for deterministic analysis in which various uncertainties are considered only through rough safety factors. This may be justified in some cases, but if knowledge regarding actual safety levels is required, the analysis must be extended to comprise probabilistic calculations considering the stochastic properties of the input parameters.

Quite extensive research has been carried out, aiming at the development of methods for probabilistic analysis of structural mechanics applications. Some strategies for probabilistic analysis are general in nature, others are specialized for the purpose of being employed in conjunction with some numerical procedure such as the finite element method. The methods developed are more or less suitable for different types of problems and differ considerably with respect to computational efficiency, general applicability, and availability for practising engineers. Considering the present standard, however, it must be concluded that further research and development of methods and software

are needed in order to reach a widespread standard comprising thorough probabilistic analysis in the design of engineering structures. To meet this aspiration, probabilistic methods and strategies must also be introduced to the engineering society through realistic and interesting applications.

A fruitful subdivision of probabilistic analysis is into two types of analyses, of which the first aims at calculating statistical distributions or some statistics such as mean values and standard deviations of relevant response parameters, such as stresses and deformations. The other type concerns the problem of calculating the risk of exceeding a certain level of some response and that a critical situation will arise. In most cases, the interest is then directed towards events that are highly unlikely to occur, for example a total or partial collapse of a building, and the methods suitable to handle this type of problem then become different from the methods suitable for the first type. Methods of the first type are presented below as stochastic finite element methods, since the dominating numerical tool in structural analysis today is the finite element method. Some of the methods, however, are equally applicable in conjunction with any other numerical or analytical procedure. Methods of the second type are presented as structural reliability methods.

1.2 Stochastic Finite Element Methods

The only method that has become widespread in engineering practice is the Monte Carlo simulation technique. Stochastic design parameters are sampled and a number of deterministic computations are carried out in order to provide information about the distribution, or some statistics of the response parameters. This is an accurate and simple approach, but also very expensive in terms of computer resources. Several methods possible to employ at a lower computational cost have been proposed. They can be divided into three main categories, denoted cat. $1-3$ below.

The cat.1 methods elaborate on the Monte Carlo sampling itself in order to reduce the sample size required to provide reliable statistics of the response. An example of a sampling technique belonging to this category is Latin hypercube sampling. Most of the work in this area has been carried out by mathematical statisticians (e.g. McKay et al. 1979; Iman and Conover 1982; Owen 1994) and elaborate sampling techniques are rarely employed in the field of structural analysis. A major advantage of these methods is that the consequent analysis using the sampled input data is identical to deterministic analysis. Thus full advantage can be taken of existing commercial codes developed for deterministic analysis (Sandberg et al. 1996).

The cat.2 methods also employ Monte Carlo simulations. However, the strategy is to reduce the computational work by using efficient solution techniques for the equation system of each run by making use of the similarity between the different equation systems. Two such methods are the Neumann expansion method, which several researchers (e.g. Yamazaki et al. 1988; Chakraborty and Dey 1996) have shown to be efficient and the preconditioned conjugate gradient method, which has been used in conjunction with the Neumann expansion method by Papadrakakis and Papadopoulos (1995).

The cat.3 methods do not compute the response statistics through Monte Carlo simulations but through series expansions of random variables. This category contains many different methodologies. One of the most well known is the Taylor series expansion

method, in which a truncated Taylor series of the response variable is established (e.g. Kleiber and Hien 1992).

1.3 Structural Reliability Methods

As stressed above, an important part of the analysis of an engineering structure is calculating the probabilities of failure or of unacceptable structural performance. For complex problems, the simplest and most adequate method is the standard Monte Carlo simulation technique. When the probabilities of failure are small, however, as they usually are in reliability analysis, this method is extremely time-consuming and expensive in terms of computer resources. Alternative methods must therefore be considered.

A widely employed method is the first order reliability method (FORM). In this method, the most likely failure point in the space of independent, standard Gaussian variables, the design point, is sought by the use of a search method such as the gradient projection method or the Haasofer-Lind method (Liu and Der Kiureghian 1991). When the design point is found, the failure surface, i.e. the boundary surface between the safe region and the failure region, is approximated by its tangent hyperplane at the design point, and the probability of failure can be calculated by integration. The accuracy of the method is dependent on the shape of the failure surface. If it diverges significantly from the tangent hyperplane, the method will give a considerable error in the estimate of the failure probability. The advantages of the method are that it is not too demanding in terms of the computer effort required and that it is fairly simple to employ.

The second order reliability method (SORM) is similar to the FORM, but the failure criterion is approximated by a second order function instead of a linear function. This increases the accuracy, but unfortunately also the computer effort required. SORM becomes expensive if the number of stochastic variables in the problem is large, but it is not certain that the estimated failure probability is accurate enough.

In order to improve the approximate result by FORM, the initial analysis can be supplemented with importance sampling. A simple and widely employed importance sampling approach is to move the sampling centre from the origin in standard Gaussian space to the design point on the failure surface (Schuëller and Stix 1987). About half the sample will then be located in the failure domain. This is, of course, much more efficient than if only a small fraction of the sample falls in the failure domain, which is the case when the sample is centred at the origin. The failure probability is calculated from the sum of the weight factors of all the realizations for which a failure occurs. The most straightforward sampling density to employ is the multivariate Gaussian distribution with standard deviations equal to one, but other sampling distributions and other sampling centres than the design point may be used and might be even more efficient. A discussion on the choice of importance sampling distribution is found in Melchers (1990).

In most cases, the design point is determined by some gradient-based search algorithm that works in standard Gaussian space, e.g. the gradient projection method or the Haasofer-Lind method (e.g. Liu and Der Kiureghian 1991). However, if discrete stochastic variables are involved, and a transformation from the basic stochastic variables into standard Gaussian space is not possible, importance sampling can be performed by moving the sampling centre according to information from a previous sampling (Dey

and Mahadevan 1998; Melchers 1990). This approach is usually less efficient than the gradient methods, but it does not require transformation to standard Gaussian space and it does not require the failure surface to be differentiable.

Another method is the axis orthogonal importance sampling method (Hohenbichler and Rackwitz 1988). The procedure starts by a FORM or a SORM analysis like the approach described above. Then a Monte Carlo sample, centred at the design point, is established on the tangent hyperplane of the failure surface. The sample space is thus reduced by one dimension, the direction orthogonal to the hyperplane. For each of the Monte Carlo realizations on the hyperplane, a line search is then carried out in the direction orthogonal to the hyperplane to find the intersection with the actual failure surface. A FORM analysis gives good start values for the line search. Finally, the failure probability can be estimated, by means of numerical integration of the probability density function, since the true position of the failure surface is calculated at a number of points distributed over the failure surface.

In the directional importance sampling method, the intersection with the failure surface is calculated for a set of directions crossing the origin. The directions are sampled with higher density towards regions where the failure surface is close to the origin. The approach is, according to Engelund and Rackwitz (1993), somewhat less efficient than the axis orthogonal importance sampling method, at least when the number of stochastic variables is large, but it may be employed directly on the basic stochastic variables (Ditlevsen et al. 1990). Also, directional sampling is most suitable for spherical, or almost spherical failure surfaces in Gaussian space (Bjerager 1988).

An important method, which must also be mentioned in this context, is the response surface method. In this method, the failure surface (with a function value equal to zero) is estimated by a polynomial by calculating function values at a number of positions in the space of the stochastic variables (e.g. Rajashekhar and Ellingwood 1993).

Chapter 2

Overview of the Present Work

2.1 Aim and Scope

The present work has been carried out with a focus on computational methods for probabilistic analysis of engineering structures, which are typically analysed by means of finite element calculations. The perspective has been from a structural mechanics point of view rather than from a mathematical statistics point of view, and the overall aims of the work have been:

- To compare and evaluate different methods and strategies for efficient probabilistic analysis of structural mechanics applications. The evaluation should comprise computational efficiency, general applicability, and availability for researchers and practising engineers in industry.
- To contribute with new and improved methods for stochastic finite element analysis and for structural reliability, towards more efficient probabilistic analysis with respect to the criteria above.
- To apply probabilistic analysis on complicated engineering applications with relevance for society and requested by industry.

The work is represented by six papers, appended in the present thesis, covering the aims stated above. Below follows a brief overview of the contents and essential results of the research with references to the appended papers.

2.2 Development and Evaluation of Methods

2.2.1 Comparison of Stochastic FE Methods

Different strategies have been suggested for stochastic finite element analysis, and *Paper I* supplies a comparison of methods representing the three different categories presented in the section of stochastic finite element methods of the introduction above. The comparison was carried out by means of a simple numerical example, namely a plate in tension, with Young's modulus represented by a spatial stochastic field with different variability and auto-correlation functions. The methods evaluated were: the Monte Carlo simulation method using true random sampling as well as different versions of the

Latin hypercube sampling plan, the Neumann series expansion method, and the Taylor series expansion method. All three methods were implemented in the same environment using the software MATLAB (1999), and much effort was spent on implementing the methods efficiently in order to make a fair evaluation.

Comparing the sampling methods, it was found that the Latin hypercube sampling plan was considerably more efficient than true random sampling. The efficiency of the Latin hypercube sampling was, however, to a large extent depending on an additional procedure for reduction of spurious correlation. All the sampling methods are very attractive with respect to general applicability since the probabilistic analysis is separated from the handling of the mechanical model. The Latin hypercube sampling plan is presented, in some detail, in a separate section below as it holds a unique position in this thesis and is considered in different ways by *Papers I–III* and *Papers V–VI*.

The Neumann expansion method, employed in conjunction with Monte Carlo simulations, elaborates on the solution of the equation systems defined by the mechanical modelling. The method was found to be considerably more efficient than the standard solution, i.e. solving the equation systems by means of Cholesky decompositions, especially for large systems. Unfortunately, the method involves the numerical solution of the FE model and thus requires changes in software developed for deterministic calculations.

The Taylor series expansion method is a perturbation method and does not involve Monte Carlo simulations. Therefore, it is not straightforward to compare the different strategies. The errors in the estimates of the statistics using the perturbation method are of a different kind than the errors of the sampling methods, which depend on insufficient sample sizes. The perturbation method is tedious to implement and involves mechanical processes and finite element procedures. This is, of course, an important drawback. It was shown, however, that for some applications, the Taylor series expansion method is very competitive in terms of computational efficiency.

2.2.2 Latin Hypercube Sampling

By exchanging true random sampling with Latin hypercube sampling (LHS), it is possible to ensure a good representation of the statistical target distribution of each marginal variable and thereby reduce the required number of Monte Carlo runs. Let n denote the required number of runs and k the number of random variables. The sampling space is then k-dimensional. An $n \times k$ matrix $\mathbf{P}$, in which each of the k columns is a random permutation of $1, \ldots, n$, and an $n \times k$ matrix $\mathbf{R}$ of independent random numbers from the uniform (0,1) distribution are established. These matrices form the basic sampling plan, represented by the matrix $\mathbf{S}$ as

$$\mathbf{S} = \frac{1}{n}(\mathbf{P} - \mathbf{R}) \tag{2.1}$$

Each element of $\mathbf{S}$, s_{ij}, is then mapped according to its target marginal distribution as

$$x_{ij} = F_{x_j}^{-1}(s_{ij}) \tag{2.2}$$

where $F_{x_j}^{-1}$ represents the inverse of the target cumulative distribution function for variable j. A vector $\mathbf{x}_i = [x_{i1}\ x_{i2}\ \ldots\ x_{ik}]$ now contains input data for one deterministic computation. Possible samples for two input variables and eight realizations, using true

random sampling and LHS respectively, are shown in Fig. 2.1. Note that the sample, using LHS, is spread over the entire sampling space as the generation of the sampling plan requires one image from each row and each column. When true random sampling is employed, there is a risk that the realizations form a cluster and parts of the sampling space will not be covered.

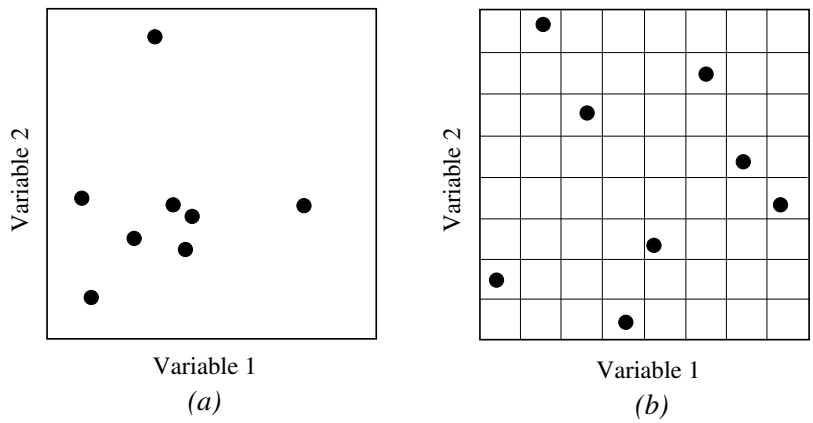

Figure 2.1: Two variables, independent and uniformly distributed, represented by (a) true random sampling and (b) Latin hypercube sampling.

Even though the marginal distribution of each variable is efficiently represented, there is a risk that a spurious correlation will appear, as shown in Fig. 2.2(a). However, it has been shown by Iman and Conover (1982) that such a spurious correlation can be reduced by modifications in the permutation matrix $\mathbf{P}$. The elements of $\mathbf{P}$, p_{ij}, are divided by the number of realizations plus one, and mapped on the Gaussian distribution with mean zero and standard deviation one as

$$y_{ij} = \Phi^{-1}_{(0,1)}\left(\frac{p_{ij}}{n+1}\right) \tag{2.3}$$

Then the covariance matrix of $\mathbf{Y}$, with elements y_{ij}, is estimated and Cholesky decomposed as

$$\mathbf{L}\mathbf{L}^T = cov(\mathbf{Y}) \tag{2.4}$$

where $\mathbf{L}$ is lower triangular. A new matrix $\mathbf{Y}^*$ with a sample covariance equal to the identity is computed as

$$\mathbf{Y}^* = \mathbf{Y}(\mathbf{L}^{-1})^T \tag{2.5}$$

and the ranks of the elements of the columns of $\mathbf{Y}^*$ become the elements in the columns of the matrix $\mathbf{P}^*$. If the elements of $\mathbf{P}$ in Eq. (2.1) are replaced by the elements of this matrix, the sampling matrix $\mathbf{S}$ will contain a considerably lower amount of undesired correlation. Fig. 2.2 illustrates the effect of the correlation-reduction procedure in a two-variable sampling plan, where a considerable spurious correlation is present in the preliminary sample.

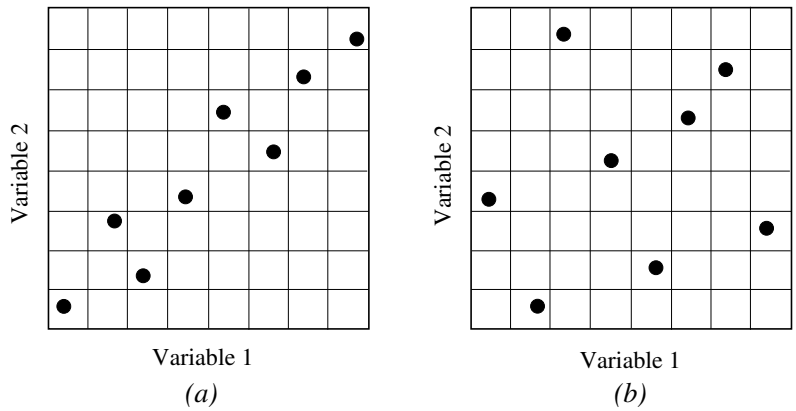

Figure 2.2: The effect of the correlation-reduction procedure in a two-variable example: (a) represents the sample prior to the reduction of spurious correlation and (b) represents the sample after the reduction of spurious correlation.

An important limitation of the correlation-reduction procedure is that the Cholesky decomposition, Eq. (2.4), requires that $cov(\mathbf{Y})$ is positive definite, which, in turn, requires that the number of realizations is higher than the number of stochastic variables, i.e. that $n > k$. Unfortunately, this requirement is a severe restriction in many applications. If the random field is discretized to coincide with the finite element mesh, the procedure requires the number of realizations to be larger than the number of finite elements in the mesh. If the random properties of adjacent elements are correlated, however, the original set of random variables can be represented by a smaller number of uncorrelated random variables. This was taken advantage of in a sampling procedure proposed in *Paper II*. The target covariance matrix, $\mathbf{C}$, can be factorized as

$$\mathbf{D} = \mathbf{Z}^T \mathbf{C} \mathbf{Z} \tag{2.6}$$

where $\mathbf{D}$ is the eigenvalue matrix of $\mathbf{C}$, and $\mathbf{Z}$ is the corresponding orthogonal eigenvector matrix. If $\mathbf{C}$ contains a significant correlation, the sum of the r largest eigenvalues, where r is a small number compared to the total number of eigenvalues, is approximately equal to the trace of $\mathbf{D}$. This means that if the r largest eigenvalues are stored in the diagonal $r \times r$ matrix $\tilde{\mathbf{D}}$, and the corresponding eigenvectors are stored in the $k \times r$ matrix $\tilde{\mathbf{Z}}$, the target covariance matrix is approximately equal to

$$\tilde{\mathbf{C}} = \tilde{\mathbf{Z}} \tilde{\mathbf{D}} \tilde{\mathbf{Z}}^T \tag{2.7}$$

The original set of k correlated random variables, with target covariance matrix $\mathbf{C}$, was thus replaced by a set of r uncorrelated random variables with target covariance matrix $\tilde{\mathbf{D}}$. When an LHS sample was produced, corresponding to the decoupled and reduced set of variables, and then transformed back in order to fit with the probability distributions of the original variables, the restriction $n > k$ was replaced by the restriction $n > r$. This restriction is more reasonable to fulfil for FE applications. Fig. 2.3 illustrates the reduction of the number of variables, which is performed by considering the decoupled variables with negligible variance as deterministic.

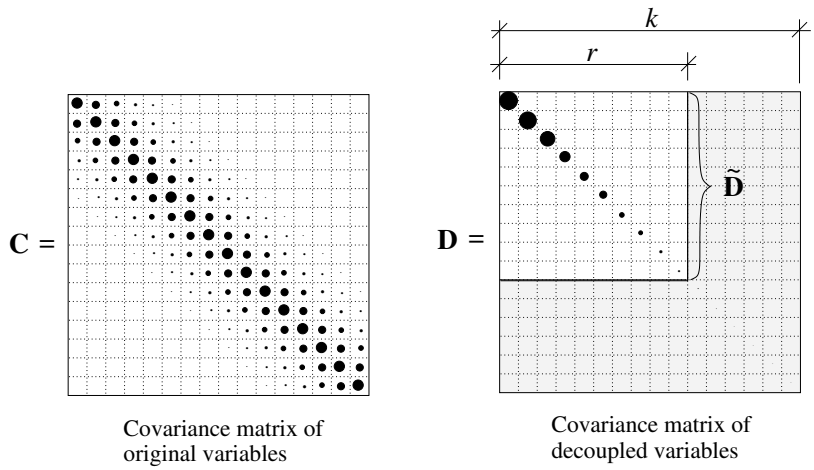

Figure 2.3: Illustration of original and diagonalized covariance matrices. Large dots represent high numbers and small dots represent small numbers. The shaded area of the decoupled covariance matrix only contains dots representing negligible variances, close to zero.

Numerical examples presented in *Paper II* showed that the computational efficiency of the procedure suggested by Iman and Conover (1982) was preserved when the procedure was employed on a transformed, decoupled set of variables. The method, of course, becomes somewhat more complicated than the original LHS, but it does not involve the mechanical modelling or the implementation of the FE software.

2.2.3 Structural Reliability and Importance Sampling

The importance sampling approach suggested by Schuëller and Stix (1987) is often suitable for structural reliability analysis when a FORM estimate of the reliability is insufficient. Centring the Monte Carlo sample at the design point, a reasonable sample size should be sufficient for estimating the probability of failure, which is calculated from the sum of the weight factors of all the realizations for which a failure occurs as

$$P_f = \frac{1}{N}\sum_{i=1}^{N}(W(\mathbf{v}_i)|g(\mathbf{v}_i) < 0) \tag{2.8}$$

where N is the number of realizations, $\mathbf{v}_i$ is a realization of the importance sampling distribution, $g(\mathbf{v}_i) < 0$ indicates failure for realization i, and $W(\mathbf{v}_i)$ is the corresponding weight factor calculated as

$$W(\mathbf{v}_i) = \frac{\phi_{\mathbf{u}}(\mathbf{v}_i)}{h_{\mathbf{v}}(\mathbf{v}_i)} \tag{2.9}$$

where $\phi_{\mathbf{u}}$ is the joint probability density function of the set $\mathbf{u}$ of stochastic variables u_j in standard Gaussian space, and $h_{\mathbf{v}}$ is the employed importance sampling density function.

Latin hypercube sampling may by employed for the sampling. A rotated orientation of the LHS plan, centred at the design point, with one direction orthogonal to the tangent hyperplane of the failure surface, was suggested in *Paper III*. Fig. 2.4 shows (a) an LHS sample centred at the design point in the original orientation, and (b) an LHS sample in the suggested orientation. It was shown by several application examples, representing different shapes of failure surfaces and problem sizes, that whereas LHS using the original orientation only slightly improved the computational efficiency compared to true random importance sampling, the suggested orientation of the LHS plan considerably improved the efficiency. It supplied a more accurate estimate of the failure probability using a constant sample size. The reason for the improvement is that the rotated orientation ensures a very good representation of the probability distribution function in the single most important direction, i.e. the direction orthogonal to the tangent hyperplane of the failure surface, and a good representation in the remaining directions in the plane of the tangent hyperplane. The closer the actual failure surface of the examples was to the tangent hyperplane, the better estimates were supplied by the method. However, even for highly non-linear failure surfaces, the method gave significant improvements compared to the alternative sampling methods.

In addition to the LHS modification applied on the described importance sampling method, *Paper III* suggests a similar improvement on another, even more efficient, importance sampling method, namely the axis orthogonal importance sampling method suggested by Hohenbichler and Rackwitz (1988). The suggested modification was shown to contribute considerably to increasing the computational efficiency of the method.

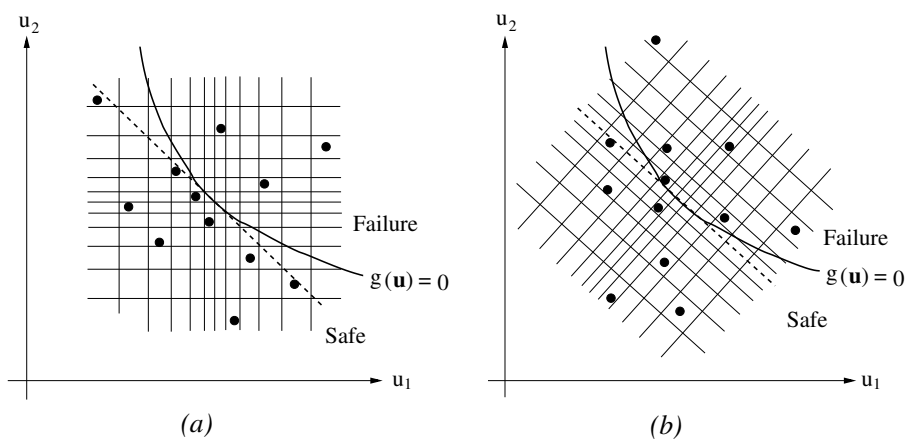

Figure 2.4: LHS importance sampling in (a) the original orientation and (b) a rotated orientation, in which one direction coincides with the direction orthogonal to the tangent hyperplane.

2.3 Engineering Applications

In addition to the applications employed in order to evaluate and compare the different strategies and methods presented above, two different types of structures are thoroughly considered in the present work, namely racking systems and roof trusses.

2.3.1 Damaged Columns and Joints in Pallet Racks

Racking systems used in industry are slender structures, often loaded by large quantities of goods, see Fig. 2.5. If the structural elements and connectors are damaged or removed, as they may be as a result of accidents or inadequate management, there is a significant risk of structural failure. In *Paper IV*, the influence of truck impacts on individual thin-walled columns was thoroughly investigated by means of numerical simulations on different profiles, as well as by laboratory tests. Not surprisingly, it was found that even moderate imperfections caused by truck impacts result in considerable reduction of the load-carrying capacity of these thin-walled columns.

The results of *Paper IV* constitute input to *Paper V*, in which the extent of the damage, at different positions in a pallet rack, was regarded as stochastic parameters. Assuming a certain probability distribution of the damage magnitudes of the columns, and with knowledge regarding the reduction of capacity of individual columns, the probability distribution of the remaining load-carrying capacity of an entire pallet rack was evaluated by probabilistic calculations. In addition to the analysis of damaged columns, *Paper V* comprises an analysis of the influence of uncertainties in the stiffness of beam-column connectors in pallet racks.

The probabilistic calculations were performed using Monte Carlo simulations and Latin hypercube sampling. The mechanical modelling was carried out using the deterministic finite element software ABAQUS (1996), which is a general and comprehensive software that admits advanced modelling including material and geometrical nonlinearities. *Paper V* considers a special application, but it also suggests a simple and general strategy for the handling of stochastic parameters of engineering structures in general.

2.3.2 Geometrical Imperfections in Roof Trusses

Wooden roof trusses with nail-plate joints are widely employed in modern roof construction. The large volume makes a detailed understanding of the mechanical behaviour of these structures vital, as it is necessary in order to secure a satisfactory safety level and serviceability of the structures and to achieve an optimal use of resources in terms of material consumption and manufacturing control.

In *Paper VI*, a roof truss with nail-plate joints was analysed with a focus on the influence of misplaced nail plates and gaps between wooden members, see Fig. 2.6. Misplacement of nail plates, as well as gaps between wooden members, occur as a consequence of lack of precision and insufficient control in the manufacturing process, and the magnitudes of the imperfections should be regarded as uncertain parameters. The influence of the imperfections on the deflection of a roof truss was investigated in *Paper VI* by means of probabilistic analysis and deterministic parameter studies, using a mechanical model capable of considering the non-linear stiffness of the nail-plate joints including contact pressure between the wooden members. It was found

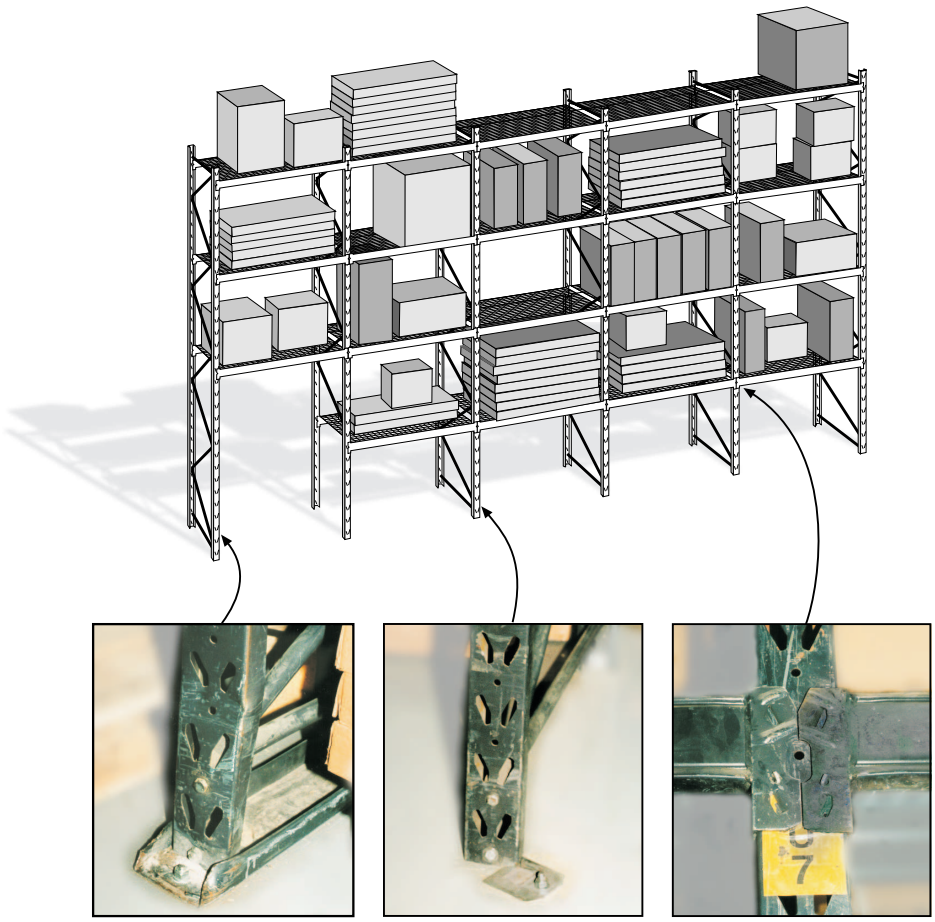

Figure 2.5: A typical pallet rack used in industry. Damaged columns and floor connectors are highlighted, as well as a beam-column connector.

that small initial gaps between wooden members, present at different locations in a 20^o W-truss, considerably increase the deflection, especially for heavy load cases. The influence of moderate misplacement of nail plates was also significant, but smaller than the influence of gaps.

In addition to the probabilistic analysis using Monte Carlo simulations, the ideal nail-plate locations were investigated by performing numerical optimization of these locations, aiming at a minimum deflection of the roof truss. The analysis showed that significant improvements could be achieved by small changes in the nail-plate locations in relation to the initial locations. The optimization was performed using a very effective procedure utilizing the elastic properties of the non-linear mechanical model, and it is interesting to note that a similar procedure can be employed in the search for the design point in a reliability analysis. No such analysis is presented in *Paper VI* as further developments of the mechanical model would be required in order to capture the small probabilities of failure or extreme deflection. However, in contrast to presently available

commercial software using very simple mechanical models, the employed model allows such modifications at a reasonable additional effort. Further research on geometrical imperfections in roof trusses should comprise this development of the mechanical model and the analysis should be carried out using efficient reliability methods.

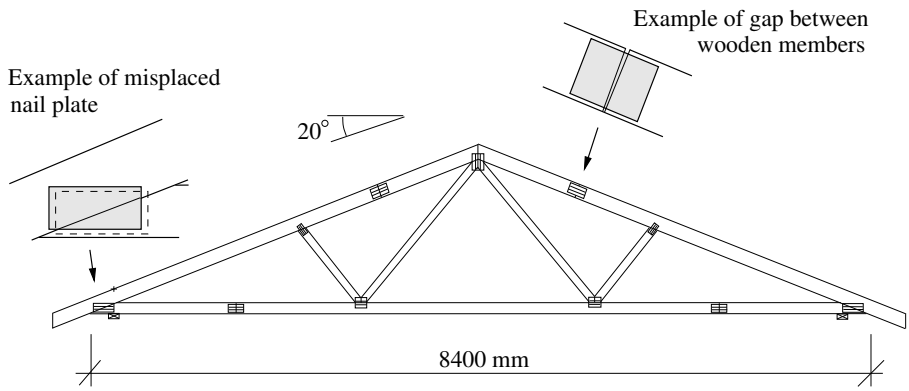

Figure 2.6: W-truss with nail-plate joints showing an example of a gap between two wooden members and a misplaced nail plate.

2.4 Concluding Remarks

The overall aim of the work presented in this thesis has been to add knowledge and contribute to an increased employment of efficient methods for probabilistic analysis of engineering structures. Hopefully, this aim has been obtained, even though it is hard to assess the result with respect to this general aspiration. In more precise terms, the most important results of the work can be summarized by the following items:

- By employing Latin hypercube sampling on a transformed, uncorrelated set of stochastic variables, the Latin hypercube sampling plan was brought into line with finite element analysis. The benefit of the transformation is that the restriction of a minimum number of Monte Carlo runs can be eased if the original stochastic variables are correlated.

- A novel orientation of the Latin hypercube sampling plan in conjunction with simple importance sampling for reliability analysis was introduced. In contrast to some previous attempts using Latin hypercube sampling, this approach was shown to contribute considerably to the computational efficiency of importance sampling. In addition, Latin hypercube sampling was efficiently employed in conjunction with axis orthogonal importance sampling.

- The general applicability of the Latin hypercube sampling plan was illustrated through applications considering randomly distributed damage to columns in racking systems and randomly distributed gaps between wooden members in roof trusses.

- Quantitative results were obtained concerning (1) the influence of truck impacts and damage of different magnitudes to individual thin-walled steel columns of racking systems, and (2) the influence of gaps between wooden members and the effect of misplaced nail plates on the deflection of wooden roof trusses.

Further work in the area should comprise application of advanced reliability methods, such as importance sampling using the Latin hypercube sampling plan, on realistic problems, such as racking systems and roof trusses analysed using advanced non-linear mechanical models. This would clearly illustrate the capability and efficiency of methods for probabilistic analysis of engineering structures, but also expose possible lack of applicability and pave the way for further research and development.

References

ABAQUS. (1996). Hibbit, Karlsson, and Sorensen, Inc., Pawtucket, R.I., USA.

Bjerager, P. (1988). "Probability integration by directional simulation," *Journal of Structural Engineering*, ASCE, **114**, 1285–1302.

Chakraborty, S., and Dey, S. S. (1996). "Stochastic finite element simulation of random structure on uncertain foundation under random loading," *Int. J. Mech. Sci.*, **38**, 1209–1218.

Dey, A., and Mahadevan, S. (1988). "Ductile structural system reliability analysis using adaptive importance sampling," *Structural Safety*, **20**, 137–154.

Ditlevsen, O., Melchers, R. E., and Gluver, H. (1990). "General multi-dimensional probability integration by directional simulation," *Computers and Structures*, **36**, 355–368.

Engelund, S., and Rackwitz, R. (1993). "A benchmark study on importance sampling techniques in structural reliability," *Structural Safety*, **12**, 255–276.

Hohenbichler, M., and Rackwitz, R. (1988). "Improvements of second-order reliability estimates by importance sampling," *Journal of Engineering Mechanics*, ASCE, **114**, 2195–2199.

Iman, R. L., and Conover, W. J. (1982). "A distribution-free approach to inducing rank correlation among input variables," *Communications in Statistics, Part B - Simulation and Computation*, **11**, 311–334.

Kleiber, M., and Hien, T. D. (1992). "The stochastic finite element method," *John Wiley & Sons*, Chichester, England.

Liu, P. L., and Der Kiureghian, A. (1991). "Optimization algorithms for structural reliability," *Structural Safety*, **9**, 161–177.

Melchers, R. E. (1990). "Search-based importance sampling," *Structural Safety*, **9**, 117–128.

MATLAB. (1999). "High-performance numerical computation and visualization software," *The Math Works Inc*, Natic Ma., USA.

McKay, M. D. Conover, W. J., and Beckman, R. J. (1979). "A comparison of three methods for selecting values of input variables in the analysis of output from a computer code," *Technometrics*, **21**, 239–245.

Owen, A. B. (1994). "Controlling correlations in Latin hypercube samples," *J. American Stat. Ass.*, **89**, 1517–1522.

Papadrakakis, M., and Papadopoulos, V. (1996). "Robust and efficient methods for stochastic finite element analysis using Monte Carlo simulation," *Compl. Meth. Appl. Mech. Engrg.*, **134**, 325–340.

Rajashekhar, M. R., and Ellingwood, B. R. (1993). "A new look at the response surface approach for reliability analysis," *Structural Safety*, **12**, 205–220.

Sandberg, G., Kjell, G., and de Maré, J. (1996). "Computational planning using Latin hypercube sampling," *Report TVSM–7118*, Lund Inst. of Techn., Div. of Struct. Mech., Lund, Sweden.

Schuëller, G. I., and Stix, R. (1987). "A Critical Appraisal of Methods to Determine Failure Probabilities," *Structural Safety*, **4**, 293–309.

Yamazaki, F., Shinozuka, M., and Dasgupta, G. (1988). "Neumann expansion for stochastic finite element analysis," *Journal of Engineering Mechanics*, ASCE, **114**, 1335–1354.

Part II

Appended Papers

Paper I

An Overview and Comparison of Methods for Stochastic Finite Element Analysis

by

Anders Olsson

Report TVSM-7135, Division of Structural Mechanics, Lund University

An Overview and Comparison of Methods for Stochastic Finite Element Analysis

Anders Olsson[1]

Report TVSM-7135, Division of Structural Mechanics, Lund University

Abstract

An overview of different methods for stochastic finite element analysis is presented, including different versions of the Latin hypercube sampling method, the Neumann expansion method for solving equation systems, and a perturbation method using Taylor series expansions. The methods are evaluated and compared by means of a numerical example, with respect to computational efficiency and general applicability. The Latin hypercube sampling method, including a procedure for reduction of spurious correlation, is shown to be very competitive in computational efficiency, especially if combined with the Neumann expansion method. Also, the sampling methods do not require any modifications of finite element software developed for deterministic analysis. The perturbation method, on the other hand, requires extensive modifications compared to deterministic analysis, but for some cases it gives a very good computational efficiency.
Keywords: stochastic finite element method, Latin hypercube sampling, correlation reduction, Neumann expansion, Taylor expansion, perturbation method.

1 Introduction

Nowadays elaborate deterministic numerical methods and models, including sophisticated strategies for dealing with a variety of mechanical processes, have become widespread and are employed in everyday engineering design practice. However, in most design cases the engineer is left with uncertainties about how to actually model a structure. The uncertainties can be directed towards the stiffness values of structural members or connections, geometrical or material properties. Production errors or damage, caused by accidents or inadequate management, are in many civil engineering structures uncertain parameters that should be considered in the analysis as well. Other issues are how the load is applied and, in dynamic analysis, the time history of the load.

There is a growing realization that unavoidable uncertainties must be considered in a computational scheme to produce reliable computational and engineering results. Traditionally, designers have used safety factors to provide increased confidence in the structural performance, but this approach does not take into account the special probability characteristics of a particular structure and does not provide the designer with

[1]Division of Structural Mechanics, Lund University, P.O. Box 118, SE-221 00, Lund, Sweden. Telephone: +46 46 222 46 89. Fax: +46 46 222 44 20.

adequate information about the reliability of the entire system. This has lead to rather extensive research aiming at combining efficient methods of structural analysis with stochastic analysis, where the influence of random variables is thoroughly evaluated.

The only method that has become widespread in engineering design practice is the Monte Carlo simulation technique. Probabilistic design parameters are sampled and a number of deterministic computations are performed to provide information about the distribution, or some statistics of response parameters. This is an accurate and simple approach, but also very expensive in terms of computer resources. Several methods that could be employed at a lower computational cost have been proposed. These can be divided into three main categories. The methods of the first category concern the sampling itself of the Monte Carlo technique in order to reduce the number of realizations required to provide reliable statistics of the response. To this category belong stratified sampling and Latin hypercube sampling. Most work in this area is carried out by mathematical statisticians [e.g., McKay et al. (1979); Iman and Conover (1982); Stein (1987); Owen (1994); Kjell (1995)], and elaborate sampling techniques are rarely employed in the field of structural analysis using finite elements. A major advantage of these methods is that the consequent analysis, i.e. the runs determined by the sample, is identical to the deterministic analysis. Thus, full advantage can be taken of existing commercial code developed for deterministic analysis (Sandberg and Olsson 1999; Olsson and Sandberg 2001).

The methods of the second category also employ Monte Carlo simulations. However, the strategy is to reduce the computational work by using efficient solutions techniques for the equation system of each run by making use of the similarity between the different realizations. The Neumann expansion method, and the preconditioned conjugate gradient method belong to this category. The Neumann expansion method in conjunction with the standard Monte Carlo method has been employed by several researchers and found to be efficient [e.g., Yamazaki et al. (1988); Chakraborty and Dey (1996)]. The preconditioned conjugate gradient method has been used in conjunction with the Neumann expansion method, and the standard Monte Carlo method by Papadrakakis and Papadopoulos (1996).

Methods of the third category do not compute the response statistics through Monte Carlo simulations but through series expansions of random variables. The most well-known methods are probably: the Taylor expansion method, in which a truncated Taylor series of the response variable is established (Liu et al. 1986; Kleiber and Hien 1992), and the Neumann expansion method, in which a truncated Neumann series is employed for the equation system (Shinozuka and Deodatis 1988; Spanos and Ghanem 1989) A comprehensive exposition of a wide range of stochastic finite element methods, from the second and third category, is given in Matthies et al. (1997).

The present paper gives a presentation of the most well-known methods from the different categories and apply them on a random field finite element problem. Comparisons on the accuracy, efficiency and general applicability of the different methods are presented. The paper does not comprise methods for reliability analysis, i.e. methods for estimating small probabilities of events such as failure.

2 Representation of Random Fields

This section contains some basics of the theory of random fields, and a brief account of the most commonly employed discretization methods in connection with finite elements. A thorough treatment of the theory of random fields is found in Vanmarcke (1984).

The random field, $H(\mathbf{x})$, of some physical property such as the modulus of elasticity, or the thickness of a plate can be expressed as the sum of its mean value function, $\mu(\mathbf{x})$, and its fluctuating component, $a(\mathbf{x})$, where $\mathbf{x}$ indicates the position vector,

$$H(\mathbf{x}) = \mu(\mathbf{x}) + a(\mathbf{x}) \tag{1}$$

The mean value is then a deterministic function of the spatial variables, whereby the fluctuating component is a random function, with a mean of zero, of the same variables,

$$E[a(\mathbf{x})] = 0 \tag{2}$$

Furthermore, the random field is represented by the auto-covariance function,

$$C_{aa}(\mathbf{x}, \mathbf{x}') = E[a(\mathbf{x})a(\mathbf{x}')] \tag{3}$$

where $\mathbf{x}$ and $\mathbf{x}'$ are two locations in the variable space. Higher order expectations might also be employed in the modeling of the random field. However, it is convenient, and often sufficient, to confine the statistics to the mean value function and the auto-covariance function. For Gaussian fields these statistics unambiguously determine the distribution. If the random variation is assumed to be homogeneous, i.e. the covariance between two points depends only on the relative position, $\boldsymbol{\xi} = \mathbf{x} - \mathbf{x}'$, the auto-covariance function can be expressed as

$$C_{aa}(\boldsymbol{\xi}, \sigma_0) = \sigma_0^2 \ \rho_{aa}(\boldsymbol{\xi}) \tag{4}$$

in which σ_0 is the standard deviation, the same at every location, and $\rho_{aa}(\boldsymbol{\xi})$ is an auto-correlation function with $\rho_{aa}(0) = 1$. Furthermore, if the random field is isotropic, i.e. the covariance between two points depends only on the distance, the auto-covariance function can be expressed as

$$C_{aa}(\boldsymbol{\xi}, \sigma_0) = \sigma_0^2 \ \rho_{aa}(|\boldsymbol{\xi}|) \tag{5}$$

It should be noted, however, that the finite element approaches presented herein are not limited to isotropic or homogeneous random fields.

The next step is to discretize the random field and its statistics to fit the consequent finite element analysis. Several discretization methods have been proposed. One of the most simple and widely employed is *the midpoint method* in which the value at the center point of each element is used to represent the random field within the element. The discretization of the random field may differ from the finite element mesh, but it is convenient, and often suitable, to assume that the random field discretization coincide with the finite element mesh. Another point discretization method is *the integration point method* in which the integration points are used to represent the random field. These two methods have the advantages of yielding positive definite covariance matrices and to allow other marginal distributions than the Gaussian. The major disadvantage

is that the finite element mesh has to be very fine in order to capture the correlation of the random field sufficiently, especially if the correlation length is short. Alternative methods are *the interpolation method*, which is based on representing the random field in terms of an interpolation rule involving a set of deterministic shape functions and the random nodal values of the field, and *the local averaging method*, which integrates the random field function over each element or domain. These latter methods are able to represent the random field with coarser meshes than the point discretization methods, but they are strictly valid only in the case of Gaussian random fields. Also, the local averaging method might in some cases lead to non-positive definite covariance matrices. More detailed descriptions, and several references on random field discretizations are given in Matthies et al. (1997).

The discretized random field is now represented by the mean value vector, and the covariance matrix, corresponding to the mean value function, and the auto-covariance function of the undiscretized random field. Using the midpoint method, letting the discretization of the random field coincide with the finite element mesh, the length of the mean value vector and the number of rows and columns in the symmetric covariance matrix are equal to the number of elements in the problem. The mean values at the center points of the k finite elements are derived as

$$m_i = \mu(\mathbf{x}_i), \qquad i = 1, 2, ..., k \tag{6}$$

and stored in the mean value vector $\mathbf{m}$. The covariance between each pair of element center points is computed as

$$C_{ij} = C_{aa}(\mathbf{x}_i, \mathbf{x}_j), \qquad \begin{matrix} i = 1, 2, ..., k \\ j = 1, 2, ..., k \end{matrix} \tag{7}$$

and stored in the covariance matrix $\mathbf{C}$.

3 Standard Monte Carlo Sampling

When the mean value vector and the covariance matrix are established, the Monte Carlo method can be employed to generate realizations that correspond to the statistics of the random field. For Gaussian random fields it is possible to generate a set of realizations with estimated statistics arbitrary close to the target statistics, and thereby to the joint distribution function, provided that a sufficiently large sample is considered. The procedure is to generate n independent Gaussian distributed random numbers with a mean of zero and a variance of one for each of the k variables. The random numbers are then stored in an $n \times k$ matrix $\mathbf{R}$. The correlation is met by performing Cholesky decomposition of the target covariance matrix $\mathbf{C}$ so that

$$\mathbf{L}\mathbf{L}^T = \mathbf{C} \tag{8}$$

where $\mathbf{L}$ is lower triangular. Then the covariance is applied as

$$\mathbf{U} = \mathbf{R}\mathbf{L}^T \tag{9}$$

yielding the $n \times k$ matrix $\mathbf{U}$ of Gaussian random numbers with a mean of zero, and a covariance in accordance with the target covariance matrix. The target mean values are applied by adding the mean value vector $\mathbf{m}$ to each row in $\mathbf{U}$.

The preservation of the Gaussian distribution from **R** to **U** is dependent on the fact that the sum of Gaussian variables is also a Gaussian variable. As other distributions are not preserved during this operation, the described procedure is only valid for Gaussian random fields. However, for non-Gaussian random fields the target covariance can be approached approximately by establishing **R** and **U** as if the field was Gaussian and then map the elements of **U** on the target distribution. This non-linear transformation is performed as

$$V_{ij} = F_j^{-1}\{\Phi_j[U_{ij}]\}, \qquad \begin{matrix} i = 1, 2, ..., n \\ j = 1, 2, ..., k \end{matrix} \tag{10}$$

where Φ_j represents the Gaussian cumulative distribution function, and F_j^{-1} represents the inverse of the target cumulative distribution function with respect to specified marginal statistics.

The transformation is illustrated in Fig. 1 and yields a sample with marginal distributions exactly approaching the target distributions, and correlation approximately approaching the target correlation. The closer the target marginal distributions are to the Gaussian distribution the better the approximation. The sampling method described above will in the following be designated SMC (Standard Monte Carlo).

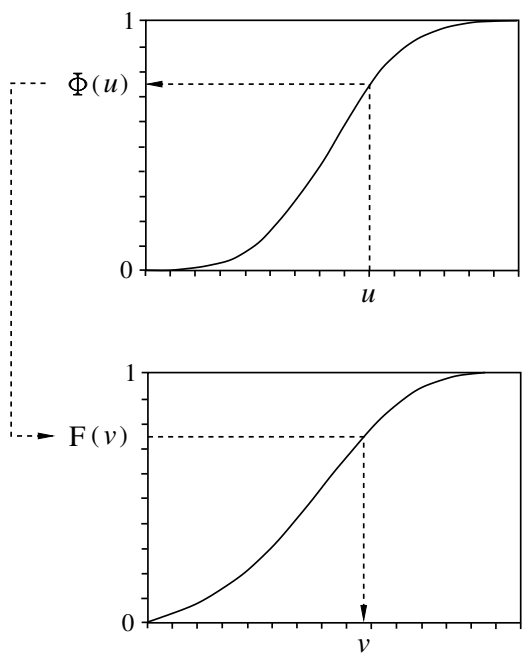

Figure 1: Transformation from Gaussian distribution, $\Phi(u)$, to non-Gaussian distribution, $F(v)$.

The correlation of **V** can be improved using an iterative algorithm proposed by Yamazaki and Shinozuka (1988). Yamazaki and Shinozuka applied the algorithm on the spectral density function of the stochastic field, but also outlined the corresponding procedure for the covariance matrix decomposition method according to the following:

$\mathbf{C}_1 := \mathbf{C}$
$\mathbf{C}_2 := cov(\mathbf{V})$

repeat until $\mathbf{C}_2 \approx \mathbf{C}$

for $i = 1 : number\ of\ variables$
for $j = 1 : number\ of\ variables$

$$\mathbf{C}_1(i,j) := \frac{\mathbf{C}_1(i,j)}{\mathbf{C}_2(i,j)}\mathbf{C}(i,j)$$

end
end

$\mathbf{L} := chol(\mathbf{C}_1)$
$\mathbf{U} := \mathbf{R}\mathbf{L}^T$

for $j = 1 : number\ of\ variables$
for $i = 1 : number\ of\ realizations$

$$\mathbf{V}(i,j) := F_j^{-1}\{\Phi_j[\mathbf{U}(i,j)]\}$$

end
end

$\mathbf{C}_2 := cov(\mathbf{V})$

end

where *cov* denotes estimation of the covariance, and *chol* denotes calculation of the lower triangular matrix by Cholesky decomposition. After a few iterations $\mathbf{C}_2 \approx \mathbf{C}$, and the algorithm is terminated. The sample stored in $\mathbf{V}$ then closely matches the target correlation. One problem, however, is that there are no guarantees that $\mathbf{C}_1$ remains positive definite during the iteration, not even if the midpoint method is used. If the covariance matrix is not positive definite the Cholesky decomposition can not be performed and the algorithm can not be employed.

4 Latin Hypercube Sampling

In order to reduce the required number of realizations, Latin hypercube sampling can be employed. This sampling scheme for computational planning was first proposed by McKay et al. (1979). As for the SMC method, the desired accuracy in the estimated distribution function determines the required number of realizations. Let n denote the required number of realizations and k the number of random variables. The sampling space is then k-dimensional. An $n \times k$ matrix $\mathbf{P}$, in which each of the k columns is a random permutation of (1,n), and an $n \times k$ matrix $\bar{\mathbf{R}}$ of independent random numbers from the uniform (0,1) distribution are established. Then the elements of the sampling matrix $\bar{\mathbf{V}}$ are determined as

$$\bar{V}_{ij} = F_j^{-1}\left(\frac{P_{ij} - \bar{R}_{ij}}{n}\right) \tag{11}$$

where F_j^{-1} represents the inverse of the target cumulative distribution function for variable j. Each row in $\bar{\mathbf{V}}$ now contains input for one deterministic computation. For two input variables and five realizations, a possible sampling plan is shown in Fig. 2. Note that the sample is spread over the entire sampling space as the generation of the Latin hypercube sampling plan requires one image from each row and each column. If n realizations from the entire sampling space had been chosen completely at random, as in SMC sampling, there is a risk that they would form a cluster and some parts of the sampling space would not be investigated.

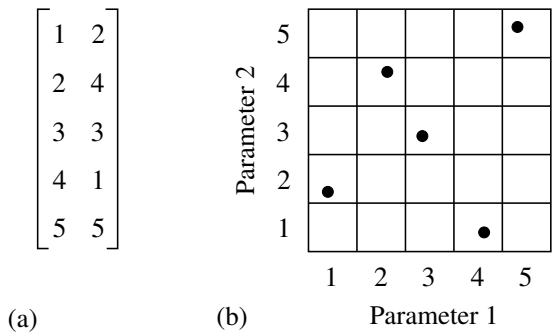

Figure 2: Latin cube, two variables and five realizations. The 5×2 matrix (a) determines the plan illustrated in (b).

Even though the marginal distribution of each variable is efficiently represented, there is a risk that some spurious correlation appears, Fig. 3(a). However, it has been shown (Iman and Conover 1982) that such spurious correlation can be reduced by modifications in the permutation matrix $\mathbf{P}$. The elements of $\mathbf{P}$ are divided by the number of realizations plus one, and mapped on the (0,1) Gaussian distribution,

$$Y_{ij} = \Phi_{(0,1)}^{-1}\left(\frac{P_{ij}}{n+1}\right) \tag{12}$$

Then the covariance matrix of $\mathbf{Y}$ is estimated and Cholesky decomposed as

$$\bar{\mathbf{L}}\bar{\mathbf{L}}^T = cov(\mathbf{Y}) \tag{13}$$

where $\bar{\mathbf{L}}$ is lower triangular. A new matrix $\mathbf{Y}^*$ with sample covariance equal to the identity is computed as

$$\mathbf{Y}^* = \mathbf{Y}(\bar{\mathbf{L}}^{-1})^T \tag{14}$$

and the ranks of the elements of the columns of $\mathbf{Y}^*$ become the elements in the columns of the matrix $\mathbf{P}^*$. If the elements of $\mathbf{P}$ in Eq. (11) is replaced by the elements of this matrix, the sampling matrix $\bar{\mathbf{V}}$ will contain a considerably lower amount of spurious correlation. Fig. 3 illustrates the effect of the correlation reduction procedure in a two variable sampling plan: (a) represents the sampling plan before, and (b) the sampling plan after the correlation reduction.

If the target correlation matrix is different from unity the target correlation is applied by replacing Eq. (14) with

$$\mathbf{Y}^* = \mathbf{Y}(\bar{\mathbf{L}}^{-1})^T\hat{\mathbf{L}}^T \tag{15}$$

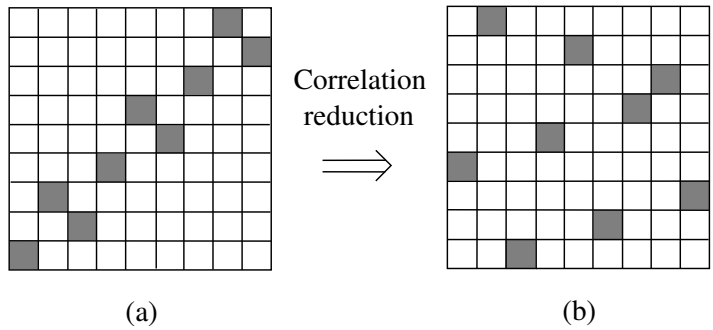

Figure 3: Spurious correlation of sampling plan (a) is reduced in plan (b).

where $\hat{\mathbf{L}}$ is the lower triangular matrix from the Cholesky decomposition of the target correlation matrix. The Latin hypercube sampling method without correlation reduction will in the following be designated LHS, and the Latin hypercube sampling with correlation reduction will be designated CLHS (correlation Latin hypercube sampling). As for SMC sampling, the correlation of $\bar{\mathbf{V}}$ will exactly approach the target correlation if the stochastic field is Gaussian, and approximately approach the target correlation if the stochastic field is non-Gaussian. An iterative algorithm, similar to the one described in the previous section, could be employed to improve the correlation in the non-Gaussian case.

It is important to note that the correlation reduction procedure described above requires the covariance matrix of $\mathbf{Y}$ to be positive definite. This means that the inequality

$$n > k \tag{16}$$

must be fulfilled for the CLHS method. Unfortunately this is a severe restriction in many applications. If the random field is discretized to coincide with the finite element mesh, the CLHS method requires the number of realizations to be higher than the number of finite elements in the mesh. This restriction could be relieved to some extent by employing a coarser mesh for the random field, but the representation of the random field would then deteriorate, and separate discretizations of the structure and the random field would be necessary. If the random properties of adjacent elements are correlated, however, the original set of random variables can be represented by a lower number of uncorrelated random variables. This representation is called principal component analysis and is commonly employed in conjunction with SMC sampling to decrease the computer effort of generating random numbers. Olsson and Sandberg (2001) showed that principal component analysis can also be efficiently used in combination with CLHS in order to relax the restriction of Eq. (16). The section below gives a presentation of the procedure.

4.1 Correlation Control in Transformed Variable Space

The target covariance matrix $\mathbf{C}$ can be factorized as

$$\mathbf{D} = \mathbf{Z}^T \mathbf{C} \mathbf{Z} \tag{17}$$

where $\mathbf{D}$ is the eigenvalue matrix of $\mathbf{C}$, and $\mathbf{Z}$ is the corresponding, orthogonal eigenvector matrix. If $\mathbf{C}$ contains significant correlation, the sum of the r largest eigenvalues, where r is a small number compared to the total number of eigenvalues, is approximately equal to the trace of $\mathbf{D}$. This means that if the r largest eigenvalues are stored in the diagonal $r \times r$ matrix $\tilde{\mathbf{D}}$, and the corresponding eigenvectors are stored in the $k \times r$ matrix $\tilde{\mathbf{Z}}$ the target covariance matrix is approximately equal to

$$\tilde{\mathbf{C}} = \tilde{\mathbf{Z}} \tilde{\mathbf{D}} \tilde{\mathbf{Z}}^T \tag{18}$$

The original set of k correlated random variables, with target covariance matrix $\mathbf{C}$, can thus be replaced by a set of r uncorrelated random variables with target covariance matrix $\tilde{\mathbf{D}}$. It is easy to transform the uncorrelated random variables back to the original variables. Let $\tilde{\mathbf{X}}$ be an $n \times r$ matrix of Gaussian distributed random numbers with target covariance matrix $\tilde{\mathbf{D}}$. The transformation to the corresponding $n \times k$ matrix $\mathbf{X}$ with covariance matrix close to $\mathbf{C}$ is then performed as

$$\mathbf{X} = \tilde{\mathbf{X}} \tilde{\mathbf{Z}}^T \tag{19}$$

When principal component analysis is employed in conjunction with Latin hypercube sampling the restriction of Eq. (16) is thus relaxed to

$$n > r \tag{20}$$

In many situations, as stated above, $r \ll k$. The Latin hypercube sampling on the uncorrelated variables starts by generating an $n \times r$ matrix $\tilde{\mathbf{P}}$ in which each of the r columns is a random permutation of (1,n). Then the procedure continues, equivalent to Eqs. (12)–(14), as

$$\tilde{Y}_{ij} = \Phi^{-1}_{(0,1)} \left(\frac{\tilde{P}_{ij}}{n+1} \right) \tag{21}$$

$$\tilde{\mathbf{L}} \tilde{\mathbf{L}}^T = cov(\tilde{\mathbf{Y}}) \tag{22}$$

$$\tilde{\mathbf{Y}}^* = \tilde{\mathbf{Y}} (\tilde{\mathbf{L}}^{-1})^T \tag{23}$$

Now the ranks of the elements of the columns of $\tilde{\mathbf{Y}}^*$ become the elements in the columns of the new matrix $\tilde{\mathbf{P}}^*$, and the final sampling matrix $\tilde{\mathbf{V}}$, in the original variable space, is established as

$$\tilde{V}_{ij} = F_j^{-1} \left(\Phi_j \left(Q_{ij} \right) \right) \tag{24}$$

where

$$\mathbf{Q} = \bar{\mathbf{Q}}\sqrt{\tilde{\mathbf{D}}}\tilde{\mathbf{Z}}^T \tag{25}$$

and

$$\bar{Q}_{ij} = \Phi^{-1}_{(0,1)}\left(\frac{\tilde{P}^*_{ij} - \tilde{R}_{ij}}{n}\right) \tag{26}$$

Note that the transformations Φ_j and F_j^{-1} are performed with respect to the specified marginal statistics of the k variables. The sampling matrix $\tilde{\mathbf{V}}$ represents the random field efficiently with respect to the marginal distributions, as well as to the correlation structure. The method will in the following be designated CTLHS (Correlation Transformed Latin Hypercube Sampling).

5 The Neumann Expansion Method

When the sample is determined, the deterministic solutions of the n equation systems must be computed. The system to be solved reads

$$\mathbf{K}\mathbf{u} = \mathbf{f} \tag{27}$$

where $\mathbf{K}$ is the stiffness matrix of one realization, $\mathbf{u}$ is the corresponding unknown displacement vector, and $\mathbf{f}$ is the force vector. A standard procedure is to perform a Cholesky decomposition of $\mathbf{K}$ and then solve the system by backward and forward substitutions. The major part of the computational work in this method is the Cholesky decomposition of $\mathbf{K}$ which has to be performed n times. An alternative method, proposed by Yamazaki et al. (1988), takes advantage of the similarity between the different stiffness matrices and employs the Neumann expansion technique to solve the systems. The stiffness matrix of each realization can be decomposed into two matrices,

$$\mathbf{K} = \mathbf{K}_0 + \Delta\mathbf{K} \tag{28}$$

where $\mathbf{K}_0$ is the non-fluctuating mean stiffness matrix, and $\Delta\mathbf{K}$ is the fluctuating part that is different for each realization. The displacement vector corresponding to the non-fluctuating part of the stiffness matrix can be obtained as

$$\mathbf{u}_0 = \mathbf{K}_0^{-1}\mathbf{f} \tag{29}$$

The actual inverse of the stiffness matrix is not computed, but the notation $\mathbf{K}_0^{-1}$ is used to represent a Cholesky decomposition with backward and forward substitutions. The Neumann expansion of $\mathbf{K}^{-1}$ takes the form

$$\mathbf{K}^{-1} = (\mathbf{K}_0 + \Delta\mathbf{K})^{-1} = \left(\mathbf{I} - \mathbf{J} + \mathbf{J}^2 - \mathbf{J}^3 + \ldots\right)\mathbf{K}_0^{-1} \tag{30}$$

where $\mathbf{J} = \mathbf{K}_0^{-1}\Delta\mathbf{K}$ and $\mathbf{I}$ denotes the identity matrix. This expression for $\mathbf{K}^{-1}$ in combination with Eq. (29) result in the following series expansion for the displacement vector,

$$\mathbf{u} = \mathbf{u}_0 - \mathbf{J}\mathbf{u}_0 + \mathbf{J}^2\mathbf{u}_0 - \mathbf{J}^3\mathbf{u}_0 + \ldots \tag{31}$$

Introducing the recursive equation

$$\mathbf{u}_i = \mathbf{K}_0^{-1}\Delta\mathbf{K}\mathbf{u}_{i-1}, \qquad i = 1, 2, \ldots \tag{32}$$

the series expression of the displacement vector can be written as

$$\mathbf{u} = \mathbf{u}_0 - \mathbf{u}_1 + \mathbf{u}_2 - \mathbf{u}_3 + \ldots \tag{33}$$

The series may be truncated after a fixed number of terms, or according to an error norm as for example

$$\frac{\|\mathbf{u}_i\|_2}{\left\|\sum_{k=0}^{i}(-1)^k\mathbf{u}_k\right\|_2} \leq \varepsilon \tag{34}$$

where ε is the allowable error and $\|\mathbf{u}\|_2$ is the vector norm defined by $\sqrt{\mathbf{u}^T\mathbf{u}}$. The major advantage of the Neumann expansion method is that only the non-fluctuating part of the stiffness matrix has to be factorized and this only once. The additional computational work consists of elementary matrix-vector multiplications and additions of matrices. Thus a considerable amount of computational resources can be saved by using this method. However, it must be checked that the series of each realization converges. This can be done by the error norm given by Eq. (34) in combination with a maximum number of terms, or by concluding that the series does not converge when

$$\|\mathbf{u}_i\|_2 \leq \|\mathbf{u}_{i+1}\|_2 \tag{35}$$

Yamazaki et al. (1988) showed that the convergence criterion of Eq. (34) can always be met by replacing the decomposition of Eq. (28) by

$$\mathbf{K} = m\mathbf{K}_0 + \Delta\mathbf{K}^* \tag{36}$$

where m is a scalar chosen to satisfy the convergence criterion. It is beyond the scope of the present paper to describe this modified procedure in detail, but it should be noted that in order to compute the value of the scalar m it is necessary to compute the eigenvalue of $\mathbf{J}$ with the largest absolute value. Unfortunately, the calculations required to find that eigenvalue appear to be more demanding, in terms of computational resources, than to perform the Cholesky decomposition of $\mathbf{K}$. Therefore, the Neumann expansion method should only be employed for applications where most of the realizations result in series that are convergent without modifications. If a small number of the realizations result in non-convergent series, the equation systems of these can be solved by the standard Cholesky decomposition method.

6 The Taylor Expansion Method

In this method, the unknown random field is approximated by a Taylor series expansion. The statistics of the random field are computed by integrating the product of this series expansion and the probability distribution of the input variables over the domain of these variables. An extensive description of the method is found in Kleiber and Hien (1992) and the notation employed below is similar to the notation used by Kleiber and Hien.

The stiffness relation of the structure reads

$$K_{\alpha\beta}u_\beta = f_\alpha \tag{37}$$

where $K_{\alpha\beta}$ and f_α are the stiffness matrix and force vector, respectively, and u_β represents the unknown random displacement field of the system. A Taylor series expansion of the displacement vector is established as

$$u_\alpha(s_\varrho) = u^0_\alpha(s^0_\varrho) + u^{,\rho}_\alpha(s^0_\varrho)\Delta s_\rho + \frac{1}{2}u^{,\rho\sigma}_\alpha(s^0_\varrho)\Delta s_\rho \Delta s_\sigma + \cdots \tag{38}$$

where $u^0_\alpha(s^0_\varrho)$ is the deterministic solution of the system corresponding to the mean values of the stochastic input variables, and $u^{,\rho}_\alpha(s^0_\varrho)$ and $u^{,\rho\sigma}_\alpha(s^0_\varrho)$ are the first and second derivatives of the displacement vector with respect to the stochastic input variables, s_ρ. The mean value vector and the covariance matrix of the displacements are defined as

$$E[u_\alpha] = \int_{-\infty}^{\infty}\int_{-\infty}^{\infty}\cdots\int_{-\infty}^{\infty} u_\alpha p_k(s_1, s_2, \ldots, s_k) ds_1 ds_2 \ldots ds_k \tag{39}$$

$$cov[u_\alpha, u_\beta] = \int_{-\infty}^{\infty}\int_{-\infty}^{\infty}\cdots\int_{-\infty}^{\infty}\{u_\alpha - E[u_\alpha]\}\{u_\beta - E[u_\beta]\}p_k(s_1, s_2, \ldots, s_k) ds_1 ds_2 \ldots ds_k \tag{40}$$

where $u_\alpha = u_\alpha(s_1, s_2, \ldots, s_k)$, p_k is the k-dimensional probability density function of the stochastic input variables and k is the number of stochastic input variables of the system. Substituting Eq. (38) into Eqs. (39)–(40), disregarding higher order moments than the second order, yields

$$E[u_\alpha] = u^0_\alpha + \frac{1}{2}u^{,\rho\sigma}_\alpha C^{\rho\sigma}_s \tag{41}$$

$$cov[u_\alpha, u_\beta] = u^{,\rho}_\alpha u^{,\sigma}_\beta C^{\rho\sigma}_s \tag{42}$$

where $C^{\rho\sigma}_s$ is the covariance matrix of the stochastic input variables. The derivatives of the displacements are obtained by partial derivatives of the system equation. The first and second order partial derivatives read

$$K^0_{\alpha\beta}(s^0_\varrho)u^{,\rho}_\beta(s^0_\varrho) = f^{,\rho}_\alpha(s^0_\varrho) - K^{,\rho}_{\alpha\beta}u^0_\beta(s^0_\varrho) \tag{43}$$

$$K^0_{\alpha\beta}(s^0_\varrho)u^{,\rho\sigma}_\beta(s^0_\varrho) = f^{,\rho\sigma}_\alpha(s^0_\varrho) - 2K^{,\rho}_{\alpha\beta}(s^0_\varrho)u^{,\sigma}_\beta(s^0_\varrho) - K^{,\rho\sigma}_{\alpha\beta}(s^0_\varrho)u^0_\beta(s^0_\varrho) \tag{44}$$

When the derivatives of the displacement vector are derived, they are substituted into Eqs. (41)–(42) and the displacement statistics are computed. The described procedure shows the basic concept of the Taylor expansion method. When the statistics of the displacements are computed, the statistics of secondary unknowns, such as strains and stresses, can be derived. This procedure, however, is not described in the present paper.

As in the sampling methods, the original set of stochastic input variables can be replaced by a set of uncorrelated stochastic input variables, i.e. principal components. The transformation of the covariance matrix is performed as

$$D_t^{\check{\rho}\check{\sigma}} = Z_{\check{\rho}\sigma} C_s^{\rho\sigma} Z_{\rho\check{\sigma}} \tag{45}$$

where $D_t^{\check{\rho}\check{\sigma}}$ is the diagonal covariance matrix of the new set of random variables, $t_{\check{\varrho}}$, and $Z_{\check{\rho}\sigma}$ contains the eigenvectors of $C_s^{\rho\sigma}$ corresponding to the $\check{k}$ largest eigenvalues of $C_s^{\rho\sigma}$. The expressions for the displacement statistics become

$$E[u_\alpha] = u_\alpha^0 + \frac{1}{2} u_\alpha^{,\check{\rho}\check{\sigma}} D_t^{\check{\rho}\check{\sigma}} \tag{46}$$

$$cov[u_\alpha, u_\beta] = u_\alpha^{,\check{\rho}} u_\beta^{,\check{\sigma}} D_t^{\check{\rho}\check{\sigma}} \tag{47}$$

where the displacement derivatives are derived from the partial derivatives of the system equation

$$K_{\alpha\beta}^0(t_{\check{\varrho}}^0) u_\beta^{,\check{\rho}}(t_{\check{\varrho}}^0) = f_\alpha^{,\check{\rho}}(t_{\check{\varrho}}^0) - K_{\alpha\beta}^{,\check{\rho}}(t_{\check{\varrho}}^0) u_\beta^0(t_{\check{\varrho}}^0) \tag{48}$$

$$K_{\alpha\beta}^0(t_{\check{\varrho}}^0) u_\beta^{,\check{\rho}\check{\sigma}}(t_{\check{\varrho}}^0) = f_\alpha^{,\check{\rho}\check{\sigma}}(t_{\check{\varrho}}^0) - 2K_{\alpha\beta}^{,\check{\rho}}(t_{\check{\varrho}}^0) u_\beta^{,\check{\sigma}}(t_{\check{\varrho}}^0) - K_{\alpha\beta}^{,\check{\rho}\check{\sigma}}(t_{\check{\varrho}}^0) u_\beta^0(t_{\check{\varrho}}^0) \tag{49}$$

The derivatives of the system matrix are computed as

$$K_{\alpha\beta}^{,\check{\rho}}(t_{\check{\varrho}}^0) = Z_{\check{\rho}\rho} K_{\alpha\beta}^{,\rho}(s_\varrho^0) \tag{50}$$

$$K_{\alpha\beta}^{,\check{\rho}\check{\sigma}}(t_{\check{\varrho}}^0) = Z_{\check{\rho}\sigma} K_{\alpha\beta}^{,\rho\sigma}(s_\varrho^0) Z_{\rho\check{\sigma}} \tag{51}$$

It should be emphasized, however, that as $D_t^{\check{\rho}\check{\sigma}}$ is diagonal, only the subset with index $\check{\rho} = \check{\sigma}$ has to be dealt with in Eqs. (46)–(51). Thus no mixed derivatives of the system matrix with respect to the transformed set of random variables have to be derived. This advantage, and the fact that the considered number of principal components is much lower than the original number of random variables, are the reasons why the method with transformation often can be employed at a considerably lower computational cost than the method without transformation. A disadvantage of the principal component approach is that the extremely sparse structure of the third order tensor $K_{\alpha\beta}^{,\rho}(s_\varrho^0)$ is damaged when transformed according to Eq. (50).

7 Numerical Example

To compare the accuracy and efficiency of the described methods, and to a certain degree illustrate the significance of the random field discretization, a numerical example is employed. All calculations are performed on a SGI Octane, 195 MHz computer, using the software MATLAB (1998). A square plate with unit side length and unit thickness is modeled by plane-stress Melosh elements. The material of the plate is assumed to be isotropic with stochastic modulus of elasticity and deterministic Poisson's ratio, $\nu = 0.3$. The plate is loaded with a deterministic, uniformly distributed load with unit magnitude. Nodal displacements in the y-direction are constrained along the lower edge, and nodal displacements in both directions are constrained at the lower left corner. Fig. 4 shows the geometry, loading, and boundary conditions of the structure. Note that in the deterministic case, with constant modulus of elasticity in the entire plate, the displacement field is computed exactly independently of the finite element mesh. Thus the need of a refined mesh is solely to capture the properties of the random field, i.e. the stochastic modulus of elasticity. A similar example was used by Yamazaki et al. (1988) to illustrate the advantages of using the Neumann expansion method in conjunction with SMC simulations.

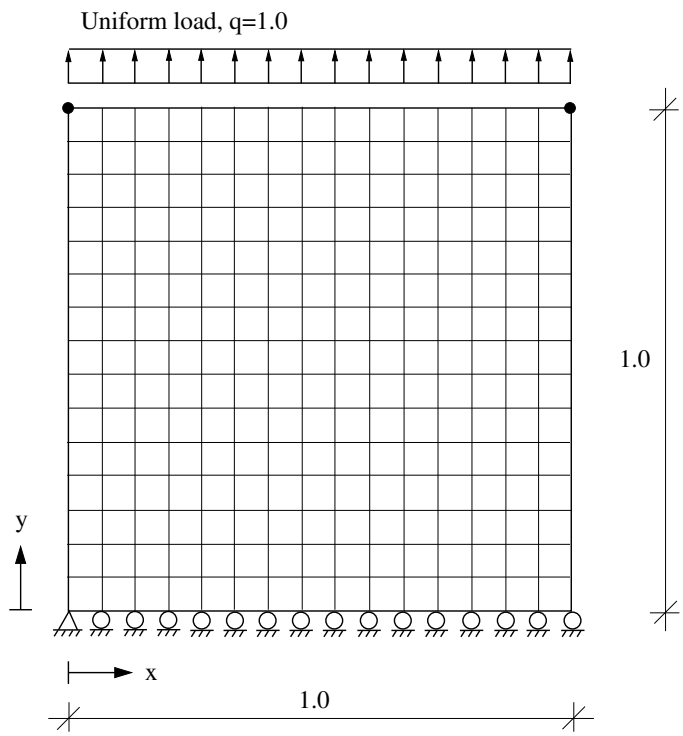

Figure 4: Square plate, loaded in tension, modeled by 15×15 *elements.*

7.1 Correlation and Discretization

A log-normal random field is adopted for the modulus of elasticity of the plate. The field is characterized by its mean value function, which is constant and equal to one in the entire plate, and the isotropic auto-covariance function,

$$C_{ij} = \sigma_0^2 \; exp \left[- \left(\frac{\left| \boldsymbol{\xi}_{ij} \right|}{d} \right)^2 \right] \tag{52}$$

in which σ_0 is the standard deviation of the random field, and d is a positive parameter such that a larger value indicates a stronger correlation. The random field is discretized using the midpoint method. Thus $\left| \boldsymbol{\xi}_{ij} \right|$ is the distance between the centroid of element i and the centroid of element j, and the size of the covariance matrix $\mathbf{C}$ is equal to the square of the number of elements in the plate. Fig. 5 shows the correlation according to Eq. (52) as a function of the distance, and the discretization of the correlation function corresponding to the midpoint method with 15 elements along the edge of the plate. It is quite clear from Fig. 5 that the discretization yields better approximations of the correlation function for large values of d.

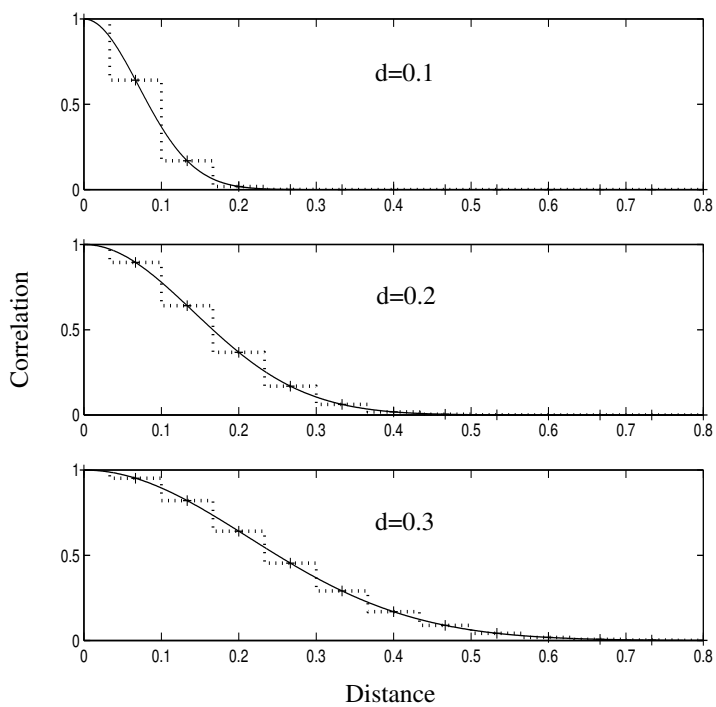

Figure 5: The correlation as a function of the distance.

The displacement field of the plate is now evaluated for all combinations of $d = 0.1$, 0.2, 0.3 and $\sigma_0 = 0.1$, 0.2, 0.3 in order to investigate how fine the finite element mesh has to be to capture the random field sufficiently well. Calculations are performed using 10, 15, 20, and 25 elements along the edge of the plate. The Latin hypercube

methods are employed, as they are more efficient than the SMC method in obtaining the statistics of the displacement field. A sample of 10,000 realizations is established for each calculation. The CLHS is used when possible, but in the models with fine mesh and strong correlation the covariance matrix becomes close to singular, resulting in numerical difficulties. In those cases the CTLHS is employed, considering a sufficiently large number of the eigenvalues of the covariance matrix. The quantities given in Table 1 are the mean value of the vertical displacement of the upper right corner of the plate, the variance of the same displacement, and the covariance between the vertical displacements of the upper left and upper right corners. An asterisk in Table 1 indicates that the CTLHS is used for that calculation. The significance of the values in Table 1 is not evaluated in the strict mathematical sense but five repetitive simulations of each model are performed showing that the errors should not exceed one unit of the last digit given of each value.

Fig. 5 illustrates that the same finite element mesh represents a different quality of the correlation function discretization depending on the value of the parameter d; the higher the value of d the better the representation. Thus a short correlation distance requires a finer mesh than a longer correlation distance. This is confirmed by the values in Table 1. In the following study of the performance of the different sampling methods and expansion methods, the correlation of the modulus of elasticity is determined by $d = 0.2$, and the 15×15 element mesh is employed.

Comparison of Different Methods

The efficiency of the different sampling methods is first and foremost dependent on the accuracy of the output distributions and statistics that can be achieved for a given number of realizations. The computer effort of generating the input sample is in most finite element applications comparatively low. As a measure of the ability of capturing the true values of the statistics the coefficient of variation, R, of the statistics is employed. A good performance of the applied sampling method results in a low coefficient of variation of the estimated output statistics. Naturally, also the bias due to the different sampling methods should be evaluated. A brief investigation on this matter is performed, though not thoroughly accounted for herein, showing that no significant bias appears in the evaluated statistics. However, it should be noted, that in some situations significant bias actually appears for the Latin hypercube methods with correlation control, e.g Kjell (1995).

The coefficient of variation of the statistics is evaluated for each combination of $\sigma_0 = 0.1,\ 0.2,\ 0.3$, and $n = 10,\ 100,\ 1000$. 100 calculations for each combination are performed in order to estimate the coefficient of variation of the statistics. The expression reads

$$R(\triangle) = \frac{\sqrt{\sum_{i=1}^{100} \left(\triangle_i - \triangle_{mean}\right)^2 / 99}}{\triangle_{mean}} \tag{53}$$

Standard deviation and element mesh		Mean value of vertical displacement			Variance of vertical displacement			Covariance of vertical displacements		
		$d = 0.1$	$d = 0.2$	$d = 0.3$	$d = 0.1$	$d = 0.2$	$d = 0.3$	$d = 0.1$	$d = 0.2$	$d = 0.3$
$\sigma_0 = 0.1$	10×10	1.00697	1.00807	1.00870	0.00120	0.00318	0.00519	-0.000350	-0.00099	-0.00147
	15×15	1.00721	1.00813	1.00873*	0.00116	0.00315	0.00515*	-0.000343	-0.00098	-0.00148*
	20×20	1.00735	1.00816*	1.00873*	0.00115	0.00313*	0.00514*	-0.000341	-0.00098*	-0.00148*
	25×25	1.00742	1.00818*	1.00874*	0.00114	0.00312*	0.00513*	-0.000340	-0.00098*	-0.00148*
$\sigma_0 = 0.2$	10×10	1.02776	1.03216	1.03474	0.00496	0.0132	0.0216	-0.00143	-0.00406	-0.0061
	15×15	1.02873	1.03243	1.03482*	0.00480	0.0131	0.0215*	-0.00141	-0.00404	-0.0061*
	20×20	1.02927	1.03255*	1.03487*	0.00474	0.0130*	0.0214*	-0.00140	-0.00403*	-0.0061*
	25×25	1.02955	1.03261*	1.03487*	0.00472	0.0130*	0.0214*	-0.00140	-0.00403*	-0.0061*
$\sigma_0 = 0.3$	10×10	1.0620	1.0720	1.0779	0.0117	0.0315	0.0519	-0.00334	-0.0096	-0.0144
	15×15	1.0642	1.0726	1.0781*	0.0114	0.0312	0.0516*	-0.00329	-0.0095	-0.0144*
	20×20	1.0654	1.0729*	1.0782*	0.0112	0.0311*	0.0515*	-0.00329	-0.0095*	-0.0144*
	25×25	1.0660	1.0730*	1.0782*	0.0112	0.0310*	0.0515*	-0.00327	-0.0095*	-0.0144*

Table 1: Statistics of the vertical displacements of the upper corners. When the CTLHS is used instead of the CLHS this is indicated by an asterisk.

where

$$\triangle_{mean} = \sum_{i=1}^{100} \triangle_i / 100 \tag{54}$$

and $\triangle$ represents the mean value, the variance, or the covariance. Actually, for the results presented in Table 2, 5×100 calculations are performed in order to verify the significance of the computed numbers. The relative error received using the Taylor expansion method is also given in Table 2. Even though this error is not equivalent to the coefficient of variation given for the sampling methods it can be used for a rough comparison of the different strategies.

Consider first the coefficient of variation of the mean value. It is quite clear that all the Latin hypercube methods perform excellently, at least ten times better than the SMC method. When applicable, the CLHS is the most efficient method but as it requires n to be higher than the number of stochastic variables, in the present case 15×15, it can not be used for $n = 10$, or $n = 100$. The CTLHS is suitable when the $n - 1$ largest eigenvalues are sufficient to represent the random field, and for $n = 100$, more than 99.99% of the eigenvalue sum is captured. The Taylor expansion method performs excellent when $\sigma_0 = 0.1$, but even for $\sigma_0 = 0.3$ the error is smaller than the coefficient of variation using any of the sampling methods with $n = 100$.

More interesting than the mean displacements is the ability to capture the variance and the correlation of the displacements as they normally require much larger samples. For example, using the SMC method with $n = 10$, and $\sigma_0 = 0.1$, the coefficient of variation of the variance amounts to 50% whereas the coefficient of variation of the mean value only amounts to 2%. Table 2 shows that the LHS is only slightly better than the SMC method, whereas the CLHS and the CTLHS are much more efficient. For example, using the CTLHS with $n = 100$, better results are achieved regarding the variance and correlation than using the LHS with $n = 1000$. Note that the CTLHS is almost as efficient as the CLHS. Furthermore, a comparison shows that the Taylor expansion method performs approximately as well as the CTLHS with $n = 100$. The performance of the Taylor expansion method is relatively better for small values of σ_0.

As a principal component representation is employed for the CTLHS, and can be employed for the Taylor expansion method, the number of eigenvalues required for the analysis should be studied. Fig. 6 shows, for $d = 0.1, 0.2, 0.3$, the relative error of the mean value and the relative error of the variance as functions of the number of eigenvalues considered. It is clear that the required number of eigenvalues decreases as the correlation of the random field increases.

As pointed out earlier, the sampling methods can be employed in conjunction with the Neumann expansion method in order to reduce the computational effort required for analyzing each realization. Realizations that, according to Eq. (35), do not result in a convergent series are solved with the standard Cholesky decomposition method. If the standard deviation of the random field is small, the number of such realizations is quite low compared to n, but they are important to detect as they otherwise would significantly affect the statistics of the displacement field. Table 3 shows the error of the displacement statistics, the same as in the previous tables, due to the approximations of the Neumann series expansions. The number of realizations treated with the standard Cholesky decomposition is given in parenthesis. The values of Table 3 are evaluated

Standard deviation and sampling method		Coefficient of variation of the mean value, $R(m)$			Coefficient of variation of the variance, $R(v)$			Coefficient of variation of the covariance, $R(c)$		
		$n = 10$	100	1000	$n = 10$	100	1000	$n = 10$	100	1000
$\sigma_0 = 0.1$	SMC	0.018	0.005	0.0019	0.5	0.14	0.05	1.1	0.3	0.11
	LHS	0.0012	0.00016	0.00005	0.4	0.12	0.04	1.1	0.3	0.10
	CLHS	–	–	0.000008	–	–	0.004	–	–	0.008
	CTLHS	–	0.0003	0.00002	–	0.03	0.005	–	0.06	0.010
	Taylor	0.00001			0.01			0.01		
$\sigma_0 = 0.2$	SMC	0.04	0.011	0.004	0.5	0.14	0.05	1.1	0.3	0.11
	LHS	0.0028	0.0006	0.00019	0.4	0.12	0.04	1.0	0.3	0.11
	CLHS	–	–	0.00004	–	–	0.008	–	–	0.019
	CTLHS	–	0.0006	0.00006	–	0.03	0.009	–	0.07	0.018
	Taylor	0.0002			0.05			0.03		
$\sigma_0 = 0.3$	SMC	0.05	0.016	0.006	0.5	0.15	0.05	1.2	0.3	0.11
	LHS	0.006	0.0013	0.0004	0.4	0.12	0.04	1.1	0.3	0.11
	CLHS	–	–	0.00008	–	–	0.010	–	–	0.02
	CTLHS	–	0.0009	0.00013	–	0.05	0.013	–	0.09	0.02
	Taylor	0.0006			0.10			0.08		

Table 2: The coefficient of variation of the statistics using the different sampling methods, and the relative error using the Taylor expansion method.

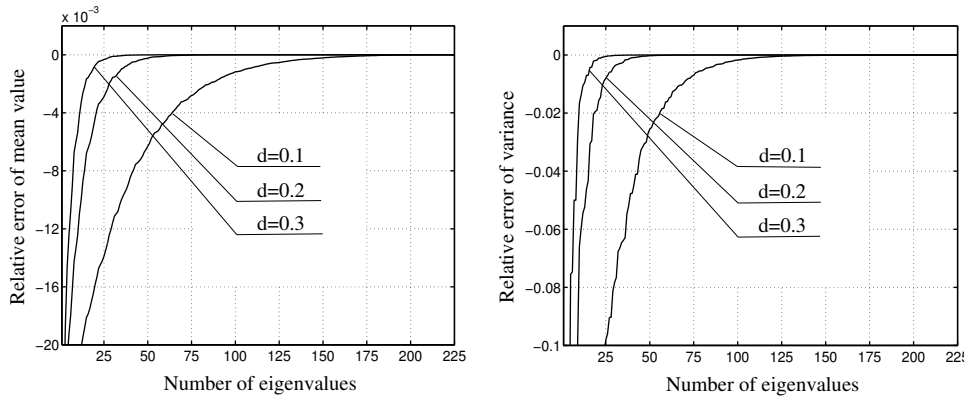

Figure 6: Relative error as a function of the number of eigenvalues.

using the CLHS with $n = 1000$, and $d = 0.2$, but it should be noted that the errors given are due to the use of the Neumann expansion method and would not decrease or increase if another number of realizations was considered or if any of the other sampling methods was employed instead of the CLHS.

Fig. 7 shows how the solution of the Neumann expansion method approaches the solution of the Cholesky decomposition method as the order of the expansion increases. The relative errors of the mean displacement and the variance of the displacement of the upper right corner are given as functions of the order of the Neumann series expansion for $d = \sigma_0 = 0.2$. It is noted that the error of the mean displacement according to the second order expansion, and the error of the variance of the displacement according to the first order expansion are comparable to the corresponding errors when the Taylor expansion method is employed.

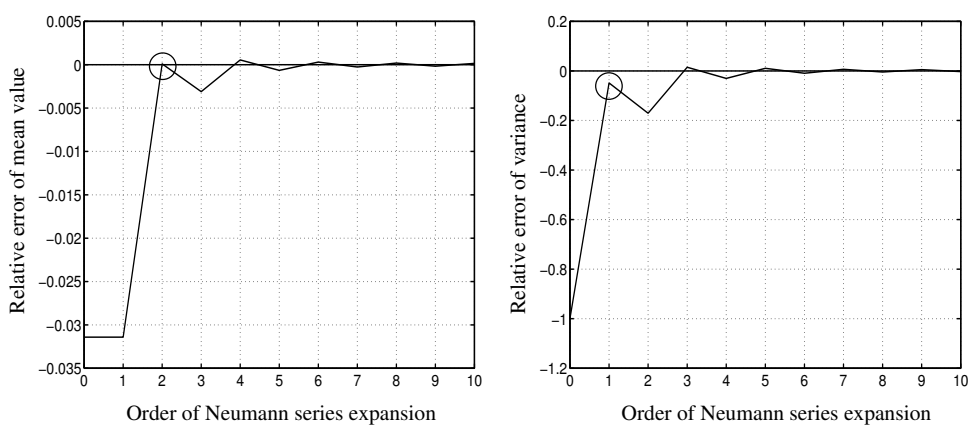

Figure 7: The relative error as a function of the order of the Neumann series expansion.

To compare the Neumann expansion method with the Cholesky decomposition method, and the sampling methods with the Taylor expansion method, the computational effort required for the different methods must be evaluated. However, it is not an easy task

statistics		2nd order		4th order		6th order		8th order	
mean	$\sigma_0 = 0.1$	0.000006	(0)	0.000009	(0)	0.0000010	(0)	0.00000012	(0)
value,	$\sigma_0 = 0.2$	0.00010	(6)	0.0005	(24)	0.0003	(39)	0.00015	(53)
	$\sigma_0 = 0.3$	0.0003	(219)	0.003	(704)	0.002	(1107)	0.0012	(1424)
variance,	$\sigma_0 = 0.1$	0.05	(0)	0.002	(0)	0.00013	(0)	0.000011	(0)
	$\sigma_0 = 0.2$	0.17	(6)	0.03	(24)	0.009	(39)	0.005	(53)
	$\sigma_0 = 0.3$	0.3	(219)	0.10	(704)	0.04	(1107)	0.02	(1424)
co-	$\sigma_0 = 0.1$	0.04	(0)	0.0017	(0)	0.00010	(0)	0.000009	(0)
variance,	$\sigma_0 = 0.2$	0.16	(6)	0.03	(24)	0.009	(39)	0.005	(53)
	$\sigma_0 = 0.3$	0.3	(219)	0.10	(704)	0.04	(1107)	0.02	(1424)

Table 3: The relative errors of the estimated statistics due to the approximations of the Neumann series expansions. The number of realizations evaluated by Cholesky decompositions are given in parenthesis.

to perform a fair comparison as the required computational effort very much depends on the implementation in the computer code. Therefore, it should be noted that even though much effort is spent on implementing the different methods efficiently, the relations between the CPU–times given in Tables 4–6 could be significantly different if the calculations were performed using another computer code. Nevertheless, Table 4 shows that the Neumann expansion method can be employed at a considerably lower cost than the standard Cholesky method, and the difference is more pronounced for large systems.

Table 5 shows the CPU–times required for generating one log-normal realization using the different sampling methods. The values given are valid for $n = 100$ and $n = 1000$, the latter in parenthesis. For small values of n, the major part of the cost is due to initial preparation of the sampling such as Cholesky decomposition or eigenvalue transformation of the covariance matrix. Considering the total computational costs of generating the sample and solving the corresponding equation systems, it appears most favorable to employ the CTLHS in conjunction with the Neumann expansion method.

Table 6 shows the CPU–times required using the Taylor expansion method with and without eigenvalue transformation. The displayed CPU–times for the latter alternative correspond to 100 considered eigenvalues. For small problems the values of Table 6 indicate that the eigenvalue transformation method is better only if the considered number of eigenvalues is much smaller than the number of original random variables. A comparison between the Taylor expansion method and the CTLHS method in conjunction with the Neumann expansion method is hard to perform as the types of error of the two approaches are different, and as the implementation might favor one of the approaches. From the evaluation of the square plate example none of the two alternative approaches can be regarded as superior to the other with respect to computational efficiency. The relative performance depends on the number of degrees of freedom and the number of stochastic variables of the problem, and on the variability of the stochastic input variables. Also, it matters how the random error of the sampling method is valued compared to the error of the Taylor expansion method due to the second order approximation.

element mesh	Cholesky	N. 2nd ord.	N. 4th ord.	N. 6th ord.	N. 8th ord.
15×15	0.047	0.022	0.036	0.050	0.064
25×25	0.241	0.077	0.130	0.184	0.238
50×50	2.430	0.441	0.787	1.137	1.506

Table 4: CPU-time required for the Cholesky and Neumann methods.

element mesh	SMC	LHS	CLHS	CTLHS (100)
15×15	0.008 (0.009)	0.014 (0.018)	– (0.018)	0.023 (0.018)
25×25	0.036 (0.028)	0.055 (0.051)	– (0.059)	0.282 (0.060)
50×50	1.116 (0.227)	1.255 (0.330)	– –	1.876 (0.346)

Table 5: CPU-time required for generating input samples.

element mesh	No transf.	eig.transf (100)
15×15	1.65	14.83
25×25	16.3	74.0
50×50	558	551

Table 6: CPU-time required for the Taylor expansion method.

8 Conclusions

The objective of this paper is to give an overview of different methods for stochastic finite element analysis and to compare the methods with respect to computational efficiency and general applicability. This has been done by analyzing a square plate with stochastic modulus of elasticity subjected to a deterministic loading.

The comparison of different Monte Carlo simulation methods showed that the Latin hypercube sampling is superior to the standard Monte Carlo method for estimating the mean value of the output quantity of the example problem, i.e. the displacement of a corner of the square plate. When estimating the variance of the same quantity, and the covariance with another displacement, the Latin hypercube sampling method was, however, only moderately more efficient than the standard Monte Carlo method. The correlation control procedure, on the other hand, was very efficient for reducing the coefficient of variation of the estimates of the variance and the covariance. Only about ten percent of the sample size needed for the standard Monte Carlo method was needed when using the correlation control Latin hypercube sampling to reach the same order of accuracy of the estimates of the variance and the covariance. When the problem comprised a high number of stochastic variables of the discretized stochastic field, a transformation into principal components was needed in order to limit the required number of realizations for the correlation control procedure. This transformation into uncorrelated variables did not have any significant negative effect on the correlation control procedure.

Irrespective of type of sampling, the Neumann expansion method can be employed to decrease the computational effort of solving the equation systems corresponding to the realizations. For large linear systems with moderate standard deviations of the input variables, considerable savings can be made using the Neumann expansion method instead of the Cholesky decomposition method. For example, the cost of calculating the Cholesky decomposition of the stiffness matrix of a mesh with 2,500 elements and a standard deviation of twenty percent (using matlab and taking advantage of the sparse structure of the stiffness matrix) was more than twice as high as solving the same system with the Neumann expansion method. One should, however, note that the use of the Neumann expansion method requires minor changes in the computer code of the finite element software developed for deterministic analyses.

The Taylor expansion method does not involve any sampling and it is not easy to compare it with the other methods. The method can be very efficient for some problems, but the computational costs grow rapidly with the number of stochastic variables and the method gives significant errors if the standard deviations of the variables are large. A rough summary of the results of the present investigation is that the computational efficiency is of the same order as the best sampling methods, but the relative efficiency

obviously depends to a high degree on the problem. It is, however, clear that the Taylor expansion method, in contrast to the sampling methods, has considerable limitations in general applicability and availability for everyday engineering design practices.

References

Chakraborty, S., and Dey, S. S. (1996). "Stochastic finite element simulation of random structure on uncertain foundation under random loading," *Int. J. Mech. Sci.*, **38**, 1209–1218.

Iman, R. L., and Conover, W. J. (1982). "A distribution-free approach to inducing rank correlation among input variables," *Communications in Statistics, Part B - Simulation and Computation*, **11**, 311–334.

Kjell G. (1995). "Computer experiments with application to earthquake engineering," *Rep. 1995:7, Studies in Statistical Quality Control and Reliability,* Dep. of Math. Stat. CTH, Gothenburg, Sweden.

Kleiber, M., and Hien, T. D. (1992). "The stochastic finite element method," *John Wiley & Sons*, Chichester, England.

Lawrence, M. A. (1987). "Basis random variables in finite element analysis," *Int. J. Num. Meth. Engrg.*, **24**, 1849–1863.

Liu, W. K. Belytschko, T., and Mani, A. (1986). "Random field finite elements," *Int. J. Num. Meth. Engrg.*, **23**, 1831–1845.

MATLAB. (1998). "High-performance numerical computation and visualization software", *The Math Works Inc*, Natic Ma., USA.

Matthies, H. G. Brenner, C. E. Bucher, C. G., and Soares, C. G. (1997). "Uncertainties in probabilistic numerical analysis of structures and solids – stochastic finite elements" *Structural Safety*, **19**, 283–336.

McKay, M. D. Conover, W. J., and Beckman R. J. (1979). "A comparison of three methods for selecting values of input variables in the analysis of output from a computer code," *Technometrics*, **21**, 239–245.

Olsson, A., and Sandberg, G. (2001). "On Latin Hypercube Sampling for Stochastic Finite Element Analysis," Accepted for publication in *J. Eng. Mech.*

Owen, A. B. (1994). "Controlling correlations in Latin hypercube samples," *J. American Stat. Ass.*, **89**, 1517–1522.

Papadrakakis, M., and Papadopoulos, V. (1996). "Robust and efficient methods for stochastic finite element analysis using Monte Carlo simulation," *Compl. Meth. Appl. Mech. Engrg.*, **134**, 325–340.

Sandberg, G. Kjell, G., and de Maré, J. (1997). "Computational planning using Latin hypercube sampling," *Report TVSM–7118*, Lund Inst. of Techn., Div. of Struct. Mech., Lund, Sweden.

Sandberg, G., and Olsson, A. (1999). "Failure sensitivity analysis of engineering structures," *Computers and Structures*, **72**, 525–534.

Shinozuka, M., and Deodatis, G. (1988). "Response variability of stochastic finite element systems," *J. Engrg. Mech.*, **114**, 499–519.

Spanos, P. D., and Ghanem, R. (1989). "Stochastic finite element expansion for random media," *J. Engrg. Mech.*, **115**, 1035–1053.

Stein, M. (1987). "Large sample properties of simulations using Latin hypercube sampling," *Technometrics*, **29**, 143–151.

Vanmarcke, E. (1984). "Random fields," *MIT Press*, Cambridge, Mass., USA.

Yamazaki, F., Shinozuka, M., and Dasgupta, G. (1988). "Neumann expansion for stochastic finite element analysis," *Journal of Engineering Mechanics*, ASCE, **114**, 1335–1354.

Yamazaki, F., and Shinozuka, M. (1988). "Digital generation of non-Gaussian stochastic fields," *Journal of Engineering Mechanics*, ASCE, **114**, 1383–1397.

Paper II

Latin Hypercube Sampling for Stochastic Finite Element Analysis

by

Anders Olsson and Göran Sandberg

Journal of Engineering Mechanics, ASCE 128(1) 121–125

Latin Hypercube Sampling for Stochastic Finite Element Analysis

Anders Olsson[1] and Göran Sandberg[2]

Journal of Engineering Mechanics, ASCE 128(1) 121–125

Abstract

A Latin hypercube sampling method, including a reduction of spurious correlation in input data, is suggested for stochastic finite element analysis. This sampling procedure strongly improves the representation of stochastic design parameters compared to a standard Monte Carlo sampling. As the correlation control requires the number of realizations to be larger than the number of stochastic variables in the problem, a principal component analysis is employed to reduce the number of stochastic variables. In many cases this considerably relaxes the restriction on the number of realizations. The method presented offers the same general applicability as the standard Monte Carlo sampling method but is superior in computational efficiency.

Keywords: finite element method, sampling design, stochastic processes.

1 Introduction

During the last two decades much effort has been directed towards reliable and efficient methods for probabilistic analysis of engineering structures. Several of the suggested approaches are closely connected to the finite element method, which is the dominating tool in deterministic analysis, and are called stochastic finite element methods. Some of the more well known are: the Taylor series expansion method (Liu et al. 1986) and the Neumann series expansion method, alternatively the preconditioned conjugate gradient method, in conjunction with Monte Carlo simulations (Yamazaki et al. 1988; Papadrakakis and Papadopoulos 1996). The only approach that has become widespread in engineering practice, however, is the Monte Carlo simulation technique. Probabilistic design parameters are sampled and a number of deterministic computations are performed to provide information about the distribution, or some statistics of response parameters. This is an accurate, simple, and indeed general approach, hence its popularity, but also very expensive in terms of computer resources.

In order to reduce the number of realizations required to provide reliable statistics of the response, and thereby reduce the computational cost, different sampling techniques such as stratified sampling and Latin hypercube sampling can be employed. Most work

[1]Division of Structural Mechanics, Lund University, P.O. Box 118, SE-221 00, Lund, Sweden. Telephone: +46 46 222 46 89. Fax: +46 46 222 44 20.

[2]Prof. Division of Structural Mechanics, Lund University, P.O. Box 118, SE-221 00, Lund, Sweden.

in this area has been carried out by mathematical statisticians (e.g. McKay et al. (1979); Iman and Conover (1982); Kjell (1995)), and elaborate sampling techniques are rarely employed in the field of structural analysis using finite elements. A major advantage of these methods is that the consequent analyses, i.e. the runs determined by the sample, are identical to the deterministic analysis. Thus full advantage can be taken of existing commercial codes developed for deterministic analyses (Sandberg and Olsson 1999).

In the present paper, the Latin hypercube sampling plan is brought into line with finite element analysis. The sampling plan is developed further to overcome a restriction implying that the number of realizations must exceed the number of correlated random variables. By means of a numerical example, the suggested method is compared to the standard Monte Carlo sampling method and the Latin hypercube sampling method according to McKay et al. (1979) and Iman and Conover (1982) with respect to computational efficiency.

2 Random Fields and Monte Carlo Simulations

The random field, $H(\mathbf{x})$, of a physical property such as the Young's modulus, or the thickness of a plate, can be expressed as the sum of its mean-value function, $\mu(\mathbf{x})$, and its fluctuating component, $a(\mathbf{x})$, where $\mathbf{x}$ indicates the position vector. The mean value is then a deterministic function of the spatial variables, whereby the fluctuating component is a random function with a mean of zero. The fluctuating component is represented by the autocovariance function,

$$C_{aa}(\mathbf{x}, \mathbf{x}') = E[a(\mathbf{x})a(\mathbf{x}')] \tag{1}$$

where $\mathbf{x}$ and $\mathbf{x}'$ are two locations in the variable space. If the random variation is assumed to be homogeneous and isotropic, i.e., the covariance between two points depends only on the distance, $\xi = |\mathbf{x} - \mathbf{x}'|$, the autocovariance function can be expressed as

$$C_{aa}(\xi, \sigma_0) = \sigma_0^2 \ \rho_{aa}(\xi) \tag{2}$$

in which σ_0 is the standard deviation, the same at every location, and $\rho_{aa}(\xi)$ is an autocorrelation function with $\rho_{aa}(0) = 1$.

In order to fit a finite element analysis, the stochastic input data must be discretized. One of the most simple discretization methods is the midpoint method, in which the value at the center point of each element is used to represent the random field within the element. Many other discretization methods have been presented and a thorough survey of several of these methods is given in Matthies et al. (1997). The discretized random field is represented by the mean-value vector, $\mathbf{m}$, and the covariance matrix, $\mathbf{C}$, corresponding to the mean-value function, and the autocovariance function of the undiscretized random field. It should be noted that the discretization of the random field may differ from the finite element mesh, but it is convenient, and suitable for our purpose, to assume that the random field discretization coincide with the finite element mesh. Thus, using the midpoint method, the length of the mean-value vector and the number of rows and columns in the symmetric covariance matrix are equal to the number of finite elements in the problem.

The Monte Carlo method can now be employed to generate realizations corresponding to the statistics of the random field. For Gaussian random fields it is possible

to generate a set of realizations with estimated statistics arbitrary close to the target statistics provided that a sufficiently large sample is considered. The procedure is to generate n independent Gaussian distributed random numbers with a mean of zero and a variance of one for each of the k variables. The random numbers are then stored in an $n \times k$ matrix $\mathbf{R}$. The correlation is met by performing a Cholesky decomposition of the target covariance matrix $\mathbf{C}$ so that

$$\mathbf{L}\mathbf{L}^T = \mathbf{C} \tag{3}$$

where $\mathbf{L}$ is lower triangular. Then the covariance is applied as

$$\mathbf{U} = \mathbf{R}\mathbf{L}^T \tag{4}$$

yielding the $n \times k$ matrix $\mathbf{U}$ of Gaussian random numbers with a mean of zero, and a covariance in accordance with the target covariance matrix. The target mean values are applied by adding the mean-value vector $\mathbf{m}$ $(1 \times k)$ to each row in $\mathbf{U}$. For non-Gaussian random fields the target covariance can be approached approximately by establishing $\mathbf{R}$ and $\mathbf{U}$ as if the field was Gaussian and then map the elements of $\mathbf{U}$ on the target distribution (Liu and Der Kiureghian 1986). The described sampling method will in the following be designated the standard Monte Carlo (SMC) method.

3 Latin Hypercube Sampling

In order to reduce the required number of realizations, Latin hypercube sampling can be employed. This sampling scheme for computational planning was first proposed by McKay et al. (1979). Let n denote the intended number of realizations and k the number of random variables. The sampling space is then k-dimensional. An $n \times k$ matrix $\mathbf{P}$, in which each of the k columns is a random permutation of $1, ..., n$, and an $n \times k$ matrix $\bar{\mathbf{R}}$ of independent random numbers from the uniform (0,1) distribution are established. Then the elements of the sampling matrix $\bar{\mathbf{V}}$ are determined as

$$\bar{V}_{ij} = F^{-1}\left(\frac{P_{ij} - \bar{R}_{ij}}{n}\right) \tag{5}$$

where F^{-1} represents the inverse of the target cumulative distribution function. Each row in $\bar{\mathbf{V}}$ now contains input for one deterministic computation. For two input variables and five realizations, a possible sampling plan is shown in Fig. 1. Note that the sample is spread over the entire sampling space as the generation of the Latin hypercube sampling plan requires one image from each row and each column. If n realizations from the entire sampling space had been chosen completely at random, as in SMC sampling, there is a risk that they would form a cluster and some parts of the sampling space would not be investigated.

Even though the marginal distribution of each variable is efficiently represented, there is a risk that a spurious correlation appears [Fig. 2(a)]. However, it has been shown (Iman and Conover 1982) that such a spurious correlation can be reduced by modifications in the permutation matrix $\mathbf{P}$. The procedure is as follows. The elements

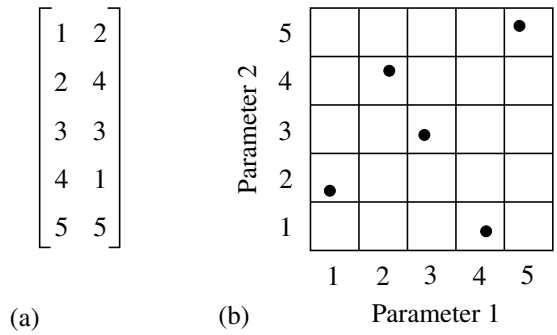

Figure 1: Latin cube, two variables and five realizations. The 5×2 matrix (a) determines the plan illustrated in (b).

of $\mathbf{P}$ are divided by the number of realizations plus one, and mapped on the (0,1) Gaussian distribution,

$$Y_{ij} = \Phi^{-1}_{(0,1)}\left(\frac{P_{ij}}{n+1}\right) \tag{6}$$

Then the covariance matrix of $\mathbf{Y}$ is estimated and Cholesky decomposed as

$$\bar{\mathbf{L}}\bar{\mathbf{L}}^T = cov(\mathbf{Y}) \tag{7}$$

where $\bar{\mathbf{L}}$ is lower triangular. A new matrix $\mathbf{Y}^*$ with sample covariance equal to the identity is computed as

$$\mathbf{Y}^* = \mathbf{Y}(\bar{\mathbf{L}}^{-1})^T \tag{8}$$

and the ranks of the elements of the columns of $\mathbf{Y}^*$ (permutations of $1, ..., n$) become the elements in the columns of the matrix $\mathbf{P}^*$. If the elements of $\mathbf{P}$ in Eq. (5) are replaced by the elements of this matrix, the sampling matrix $\bar{\mathbf{V}}$ will contain a considerably lower amount of spurious correlation. Fig. 2 illustrates the effect of the correlation-reduction procedure in a two variable sampling plan: (a) represents the sampling plan before, and (b) the sampling plan after the correlation reduction.

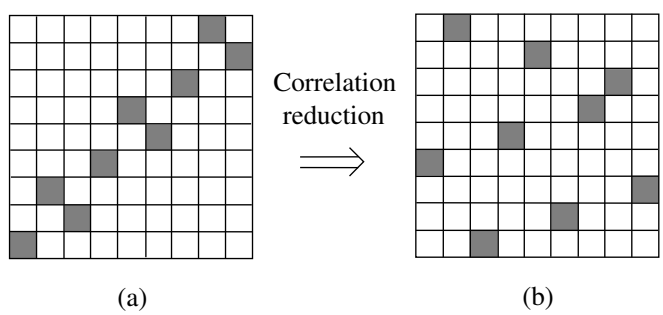

Figure 2: Unwanted correlation of sampling plan (a) is reduced in plan (b).

If the target correlation matrix is different from unity the target correlation is applied by replacing Eq. (8) with

$$\mathbf{Y}^* = \mathbf{Y}(\bar{\mathbf{L}}^{-1})^T \hat{\mathbf{L}}^T \tag{9}$$

where $\hat{\mathbf{L}}$ is the lower triangular matrix from the Cholesky decomposition of the target correlation matrix. The Latin hypercube sampling method without correlation reduction will in the following be designated as LHS, and the Latin hypercube sampling with correlation reduction will be designated as CLHS. As for SMC sampling, the correlation of $\bar{\mathbf{V}}$ will exactly approach the target correlation if the stochastic field is Gaussian, and approximately approach the target correlation if the stochastic field is non-Gaussian.

It is important to note that the correlation-reduction procedure described above requires the covariance matrix of $\mathbf{Y}$ to be positive definite. This means that the inequality

$$n > k \tag{10}$$

must be fulfilled for the CLHS method. Unfortunately, this is a severe restriction in many applications. If the random field is discretized to coincide with the finite element mesh, the CLHS method requires the number of realizations to be larger than the number of finite elements in the mesh. However, if the random properties of adjacent elements are correlated, the original set of random variables can be represented by a smaller number of uncorrelated random variables. This is taken advantage of in the sampling procedure proposed in the following section.

3.1 Correlation Control in Transformed Variable Space

The target covariance matrix $\mathbf{C}$ can be factorized as

$$\mathbf{D} = \mathbf{Z}^T \mathbf{C} \mathbf{Z} \tag{11}$$

where $\mathbf{D}$ is the eigenvalue matrix of $\mathbf{C}$, and $\mathbf{Z}$ is the corresponding orthogonal eigenvector matrix. If $\mathbf{C}$ contains a significant correlation, the sum of the r largest eigenvalues, where r is a small number compared to the total number of eigenvalues, is approximately equal to the trace of $\mathbf{D}$. This means that if the r largest eigenvalues are stored in the diagonal $r \times r$ matrix $\tilde{\mathbf{D}}$, and the corresponding eigenvectors are stored in the $k \times r$ matrix $\tilde{\mathbf{Z}}$ the target covariance matrix is approximately equal to

$$\tilde{\mathbf{C}} = \tilde{\mathbf{Z}} \tilde{\mathbf{D}} \tilde{\mathbf{Z}}^T \tag{12}$$

The original set of k correlated random variables, with target covariance matrix $\mathbf{C}$, can thus be replaced by a set of r uncorrelated random variables with target covariance matrix $\tilde{\mathbf{D}}$. This representation is called a principal component analysis and is commonly employed in conjunction with SMC to decrease the computer effort of generating random numbers. It is easy to transform the principal components, i.e. the uncorrelated random variables, back to the correlated space. Let $\tilde{\mathbf{X}}$ be an $n \times r$ matrix of Gaussian distributed random numbers with target covariance matrix $\tilde{\mathbf{D}}$. The transformation to the corresponding $n \times k$ matrix $\mathbf{X}$ with a covariance matrix close to $\mathbf{C}$ is then performed as

$$\mathbf{X} = \tilde{\mathbf{X}} \tilde{\mathbf{Z}}^T \tag{13}$$

When a principal component analysis is employed in conjunction with Latin hypercube sampling, with correlation reduction, it also contributes to relax the restriction of Eq. (10). The new restriction reads

$$n > r \tag{14}$$

and in many situations, as stated above, $r \ll k$. The Latin hypercube sampling on the uncorrelated variables starts by generating an $n \times r$ matrix $\tilde{\mathbf{P}}$ in which each of the r columns is a random permutation of $1, ..., n$. Then the procedure continues, equivalent to Eqs. (6)–(8), as

$$\tilde{Y}_{ij} = \Phi^{-1}_{(0,1)} \left(\frac{\tilde{P}_{ij}}{n+1} \right) \tag{15}$$

$$\tilde{\mathbf{L}}\tilde{\mathbf{L}}^T = cov(\tilde{\mathbf{Y}}) \tag{16}$$

$$\tilde{\mathbf{Y}}^* = \tilde{\mathbf{Y}}(\tilde{\mathbf{L}}^{-1})^T \tag{17}$$

Now the ranks of the elements of the columns of $\tilde{\mathbf{Y}}^*$ (permutations of $1, ..., n$) become the elements in the columns of the new matrix $\tilde{\mathbf{P}}^*$, and the final sampling matrix $\tilde{\mathbf{V}}$, in the original variable space, is established as

$$\tilde{V}_{ij} = F^{-1} \left(\Phi \left(Q_{ij} \right) \right) \tag{18}$$

where

$$\mathbf{Q} = \bar{\mathbf{Q}} \sqrt{\tilde{\mathbf{D}}} \tilde{\mathbf{Z}}^T \tag{19}$$

and

$$\bar{Q}_{ij} = \Phi^{-1}_{(0,1)} \left(\frac{\tilde{P}^*_{ij} - \tilde{R}_{ij}}{n} \right) \tag{20}$$

Note that the transformations Φ and F^{-1} are performed with respect to the specified marginal statistics of the k variables. The sampling matrix $\tilde{\mathbf{V}}$ represents the random field efficiently with respect to the marginal distributions, as well as to the correlation structure. This is confirmed by means of the numerical example below. The method will in the following be designated as transformed correlation Latin hypercube sampling (TCLHS).

4 Numerical Example

To compare the computational efficiency of the described methods, a numerical example is employed. A square plate with unit side length and unit thickness is modeled by plane-stress Turner-Clough elements. A square hole with a side length of 1/3 is located in the middle of the plate. The material is assumed to be isotropic with stochastic Young's modulus and deterministic Poisson's ratio, $\nu = 0.3$. The plate is loaded with a deterministic, uniformly distributed load with unit magnitude. Nodal displacements in the y-direction are constrained along the lower edge. Fig. 3 shows the geometry, loading, element mesh and boundary conditions of the structure.

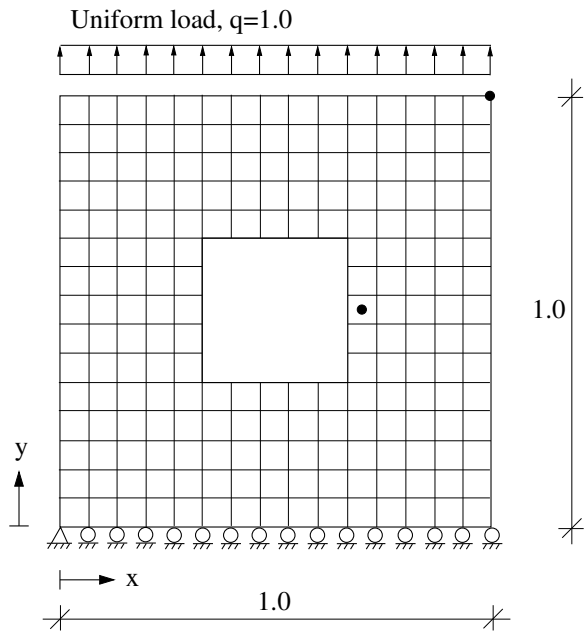

Figure 3: Square plate, loaded in tension, modeled by 200 *elements.*

A log-normal random field is adopted for the Young's modulus of the plate. The field is characterized by its mean-value function, which is constant and equal to one in the entire plate, and the isotropic autocovariance function,

$$C_{ij} = \sigma_0^2 \; exp\left[-\left(\frac{\xi_{ij}}{d}\right)^2\right] \tag{21}$$

in which $\sigma_0 = 0.2$ is the standard deviation, $d = 0.2$ is a positive parameter that determines the correlation length of the field, and ξ_{ij} is the distance between the centroid of element i and the centroid of element j. Fig. 4 shows the correlation according to Eq. (21) as a function of the distance, and the discretization of the correlation function corresponding to the midpoint method with 15 elements along the edge of the plate.

The displacement field and the stress field of the plate can now be estimated using any of the described sampling methods. The efficiency of the different sampling methods

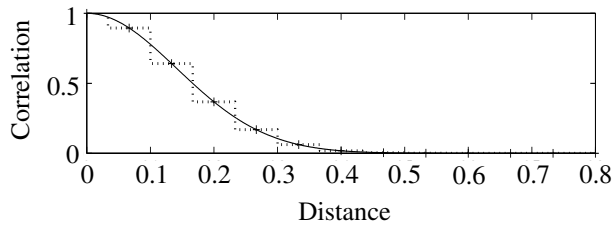

Figure 4: Correlation as function of distance.

depends primarily on the accuracy of the output distributions and statistics that can be achieved for a given number of realizations, and the computer effort of generating the input sample is in most finite element applications comparatively low. Consequently, it seems reasonable to evaluate the computational efficiency of the sampling methods by comparing the coefficient of variation of the structural response statistics when repeated simulations are performed. A good performance of the applied sampling method results in low coefficients of variation of the estimated output statistics. Naturally, the bias due to the different sampling methods should also be evaluated. A brief investigation into this matter is performed, though not thoroughly accounted for here, indicating that no significant bias appears in the evaluated statistics. However, it should be noted that in some situations a significant bias actually appears for Latin hypercube methods with correlation control. This has been illustrated by Kjell (1995).

For the evaluation of the coefficient of variation of the statistics, 500 simulations are performed for each sampling method with $n = 10$, $n = 100$, and $n = 1000$. In Table 1 the coefficients of variation of the mean values, and variances of two different structural response quantities are presented. These are the vertical displacement of the upper right corner of the plate, and the stress in vertical direction at the right edge of the square hole in the plate (the stress in the middle of the element marked in Fig. 3).

Consider first the coefficient of variation of the displacement and the stress mean values. It is quite clear that all the Latin hypercube methods perform excellently. When applicable, the CLHS is the most efficient method, but as it requires n to be higher than the number of stochastic variables, in the present case 200, it can not be used for $n = 10$, or $n = 100$. The TCLHS is suitable when the $n - 1$ largest eigenvalues are sufficient to represent the random field, and for $n = 100$, more than 99.99% of the eigenvalue sum is captured.

More interesting than mean displacements and mean stresses is the ability to capture the variance of displacements and stresses as the variance normally requires much larger samples. For example, using the SMC method with $n = 10$, the coefficient of variation of the variance amounts to 50%, for the displacement as well as for the stress, whereas the coefficient of variation of the mean values only amounts to 4% and 3% respectively. The results displayed in Table 1 show that the LHS is only slightly better than the SMC method, whereas the CLHS and the TCLHS are much more efficient. For example, using the TCLHS with $n = 100$, better results are achieved regarding the variance than using the LHS with $n = 1000$.

Sampling	mean(displacement[a])			variance(displacement[a])			mean(stress[b])			variance(stress[b])		
method	$n = 10$	100	1000	$n = 10$	100	1000	$n = 10$	100	1000	$n = 10$	100	1000
SMC	0.04	0.012	0.004	0.5	0.14	0.05	0.03	0.009	0.003	0.5	0.14	0.04
LHS	0.0028	0.0006	0.00018	0.4	0.11	0.04	0.005	0.0006	0.0002	0.4	0.12	0.04
CLHS	–	–	0.00003	–	–	0.007	–	–	0.00003	–	–	0.006
TCLHS	–	0.0007	0.00007	–	0.03	0.009	–	0.0005	0.00004	–	0.028	0.007

Table 1: Coefficient of variation of statistics using different sampling methods. [a]Vertical displacement of the upper right corner of the plate. [b]Stress in the y-direction in the element at the right edge of the square hole.

5 Conclusions

The objective of this paper is to introduce the correlation-controlled Latin hypercube sampling plan in transformed variable space for finite element applications. As the sampling plan is used only to establish input data for a number of deterministic runs, the method can be unimpededly employed for applications involving complicated mechanical processes such as geometrical and material non-linearities, and dynamics. Existing finite element codes, developed for deterministic analysis can, without modifications, be employed in conjunction with the sampling method.

The paper shows the superior efficiency of the suggested method compared to standard Monte Carlo sampling and Latin hypercube sampling without correlation control. It also shows the superior applicability of the method compared to correlation-controlled Latin hypercube sampling in original variable space.

Acknowledgements

This research was financed by the Swedish Research Council for Engineering Sciences. The support is gratefully acknowledged.

References

Iman, R. L., and Conover, W. J. (1982). "A distribution-free approach to inducing rank correlation among input variables," *Commun. in Stat. - Simul. Comput.*, 11(3), 311–334.

Kjell G. (1995). "Computer experiments with application to earthquake engineering," *Rep. No. 1995:7, Studies in Statistical Quality Control and Reliability,* Chalmers Univ. of Technology, Dept. of Math. Stat., Gothenburg, Sweden.

Liu, P.-L., and Der Kiureghian, A. (1986). "Multivariate distribution models with prescribed marginals and covariances," *Probabilistic Eng. Mech.*, 1, 105–112.

Liu, W. K. Belytschko, T., and Mani, A. (1986). "Random field finite elements," *Int. J. Numer. Methods Eng.*, 23, 1831–1845.

Matthies, H. G. Brenner, C. E., Bucher, C. G., and Soares, C. G. (1997). "Uncertainties in probabilistic numerical analysis of structures and solids – stochastic finite elements," *Struct. Safety*, 19(3), 283–336.

McKay, M. D., Conover, W. J., and Beckman R. J. (1979). "A comparison of three methods for selecting values of input variables in the analysis of output from a computer code," *Technometrics*, 21(2), 239–245.

Papadrakakis, M. and Papadopoulos, V. (1996). "Robust and efficient methods for stochastic finite element analysis using Monte Carlo simulation," *Comput. Methods Appl. Mech. Eng.*, 134, 325–340.

Sandberg, G., and Olsson, A. (1999). "Failure sensitivity analysis of engineering structures," *Comput. and Struct.*, 72, 525–534.

Yamazaki, F., Shinozuka, M., and Dasgupta, G. (1988). "Neumann expansion for stochastic finite element analysis," *J. Eng. Mech.*, 114(8), 1335–1354.

Paper III

On Latin Hypercube Sampling for Structural Reliability Analysis

by

Anders Olsson, Göran Sandberg and Ola Dahlblom

Structural Safety 25(1) 47–68

On Latin Hypercube Sampling for Structural Reliability Analysis

Anders Olsson[1], Göran Sandberg[2] and Ola Dahlblom[3]

Structural Safety 25(1) 47–68

Abstract

Latin hypercube sampling is suggested as a tool to improve the efficiency of different importance sampling methods for structural reliability analysis. In simple importance sampling, where the sampling centre is moved from the origin to the design point, standard Monte Carlo sampling can be replaced by Latin hypercube sampling. The efficiency improvement is then highly dependent on the choice of sampling directions. Different versions of Latin hypercube sampling are also successfully employed to improve the more efficient axis orthogonal importance sampling method. By means of different numerical examples, it is shown that more than 50% of the computer effort can be saved by using Latin hypercubes instead of simple Monte Carlo in importance sampling. The exact savings, however, are dependent on details in the use of Latin hypercubes and on the shape of the failure surfaces of the problems.

Keywords: Latin hypercube sampling, reliability, FORM, importance sampling, axis orthogonal, directional sampling.

1 Introduction

An important part of the analysis of any engineering structure is to calculate the probabilities of failure or of unacceptable structural performance. For complex problems, the simplest, most adequate and widely employed method is the standard Monte Carlo simulation technique (SMC). When the probabilities of failure are small, however, as they usually are in reliability analysis, such an analysis is extremely time-consuming and expensive in terms of computer resources. Alternative methods should therefore be considered.

In the first order reliability method (FORM), the most likely failure point in the space of independent, standard Gaussian variables, the design point, is sought by the use of a search method like the gradient projection method or the Haasofer-Lind method [11]. When the design point is found, the failure surface, i.e. the failure criterion, is approximated by its tangent hyperplane at the design point, and the probability of failure

[1]Division of Structural Mechanics, Lund University, P.O. Box 118, SE-221 00, Lund, Sweden. Telephone: +46 46 222 46 89. Fax: +46 46 222 44 20.

[2]Prof. Division of Structural Mechanics, Lund University, P.O. Box 118, SE-221 00, Lund, Sweden.

[3]Prof. Division of Structural Mechanics, Lund University, P.O. Box 118, SE-221 00, Lund, Sweden.

can be calculated by integration. In the second order reliability method (SORM), the failure criterion is approximated by a second order function instead of a linear function.

The approximation of the failure surface causes an error in the estimated probability. In order to improve the approximate result, or just to verify that the FORM/SORM approximation is acceptable, the initial analysis can be supplemented with importance sampling. Several importance sampling methods have been suggested during the last two decades and a brief overview of the most well-known methods is given in the following section.

Latin hypercube sampling (LHS), which is very efficient for estimating mean values and standard deviations in stochastic structural analysis, e.g. [15, 16, 19], is only slightly more efficient than the SMC for estimating small probabilities [6]. If, however, it is used in importance sampling, i.e. if the sampling is centred at the design point, it might be an interesting method for reliability analysis as well. This approach has been presented in a few publications, e.g. [18, 22], but when tested critically, the LHS on the basic stochastic variables, centred at the design point, is found to be considerably more efficient than the SMC version only if the probability of failure is dominated by a single basic stochastic variable. This is not the case in most realistic applications. It seems that the use of Latin hypercube sampling for reliability analysis has not yet been thoroughly evaluated, and that no efficient strategy has been presented in this area. In the present paper, Latin hypercube sampling is employed, in a fruitful way, in combination with two different well-known importance sampling methods. The efficiency of the proposed methods compared to SMC importance sampling and LHS importance sampling, as it has been previously presented, is evaluated for a number of numerical examples.

Several different designations of methods, some well known and others introduced herein, are employed in this paper. To make it easier for the reader, the employed methods and their abbreviations are listed in Table A1 of the Appendix.

2 Importance Sampling

A simple and widely employed importance sampling approach is to move the sampling centre from the origin in standard Gaussian space to the design point on the failure surface [20]. About half the sample will then be located in the failure domain. This is, of course, much more efficient than if only a small fraction of the sample falls in the failure domain, which is the case when the sampling is centred at the origin. The failure probability is calculated from the sum of the weight factors of all the realizations for which a failure occurs as

$$P_f = \frac{1}{N} \sum_{i=1}^{N} (W(\tilde{\mathbf{v}}_i) | g(\tilde{\mathbf{v}}_i) < 0) \tag{1}$$

where N is the number of realizations, $\tilde{\mathbf{v}}_i$ is a realization of the importance sampling distribution, $g(\tilde{\mathbf{v}}_i) < 0$ indicates failure for realization i, and $W(\tilde{\mathbf{v}}_i)$ is the corresponding weight factor calculated as

$$W(\tilde{\mathbf{v}}_i) = \frac{\phi_{\mathbf{u}}(\tilde{\mathbf{v}}_i)}{h_{\mathbf{v}}(\tilde{\mathbf{v}}_i)} \tag{2}$$

where $\phi_{\mathbf{u}}$ is the joint probability density function of the set $\mathbf{u}$ of stochastic variables u_j in standard Gaussian space, and $h_{\mathbf{v}}$ is the employed importance sampling density function. The most straightforward sampling density is the multivariate Gaussian distribution with standard deviations equal to one, but other sampling distributions and other sampling centres than the design point may of course be employed and might be even more efficient. Discussions on the choice of importance sampling distribution are found in [7, 12].

In most cases the design point is determined by some gradient-based search algorithm that works in standard Gaussian space, the gradient projection method or the Haasofer-Lind method [11] for example. However, if discrete stochastic variables are involved, and a transformation from the basic stochastic variables into standard Gaussian space is not possible, importance sampling can be performed by moving the sampling centre according to information from a previous sampling, [3, 4, 12]. This approach is usually less efficient than the gradient methods, but it does not require transformation to u-space. Moreover, it does not require the failure surface to be differentiable.

Another method is the axis orthogonal importance sampling method [7, 9]. As in the approach described above, the procedure starts by a FORM or a SORM analysis. Then a Monte Carlo sample, centred at the design point, is established on the tangent hyperplane of the failure surface. The sample space is thus reduced by one dimension, the direction orthogonal to the hyperplane. For each of the Monte Carlo realizations on the hyperplane, a line-search is then carried out in the direction orthogonal to the hyperplane to find the intersection with the actual failure surface. The FORM analysis, alternatively the SORM analysis, gives good start values for the line-search. Finally, the failure probability can be estimated, by means of numerical integration of the probability density function, since the true position of the failure surface is calculated at N points distributed over the failure surface.

In the directional importance sampling methods [1, 5, 13], the intersection with the failure surface is calculated for a set of directions crossing the origin. The directions are sampled with higher density towards regions where the failure surface is close to the origin. The approach is, according to [7], somewhat less efficient than the axis orthogonal importance sampling method, at least when the number of stochastic variables is large, but it may be employed directly on the basic stochastic variables [5]. Also, directional sampling is most suitable for spherical, or almost spherical failure surfaces in u-space [1].

Several thorough state-of-the-art reviews of importance sampling methods have been published over the years, e.g. [2, 8]. A comparative benchmark study on different methods is found in [7].

3 Latin Hypercube Sampling

Latin hypercube sampling was first proposed by McKay et al. [14] and has been further developed for different purposes by several researchers, e.g. [10, 15, 17, 21, 22]. To facilitate the presentation of the LHS importance sampling, the original and most simple form of the sampling plan for general Monte Carlo simulation purposes is presented below. Also, an important modification of the method, aiming at reduction of spurious correlation of the Latin hypercube sample is presented.

3.1 Standard Latin Hypercube Sampling

As for the SMC method, the desired accuracy of the estimated distribution function determines the number of realizations required. Let N denote the required number of realizations and K the number of random variables. The sampling space is then K-dimensional. An $N \times K$ matrix $\mathbf{P}$, in which each of the K columns is a random permutation of $1, \ldots, N$, and an $N \times K$ matrix $\mathbf{R}$ of independent random numbers from the uniform (0,1) distribution are established. These matrices form the basic sampling plan, represented by the matrix $\mathbf{S}$ as

$$\mathbf{S} = \frac{1}{N}(\mathbf{P} - \mathbf{R}) \tag{3}$$

Each element of $\mathbf{S}$, s_{ij}, is then mapped according to its target marginal distribution as

$$\hat{x}_{ij} = F_{x_j}^{-1}(s_{ij}) \tag{4}$$

where $F_{x_j}^{-1}$ represents the inverse of the target cumulative distribution function for variable j. A vector $\hat{\mathbf{x}}_i = [\hat{x}_{i1}\ \hat{x}_{i2}\ \ldots\ \hat{x}_{ik}]$ now contains input data for one deterministic computation.

A possible sampling plan for two input variables and five realizations is shown in Fig. 1. Note that the sample is spread over the entire sampling space as the generation of the LHS plan requires one image from each row and each column. If N realizations from the entire sampling space had been chosen completely at random, as in SMC sampling, there is a risk that they would form a cluster and some parts of the sampling space would not be investigated.

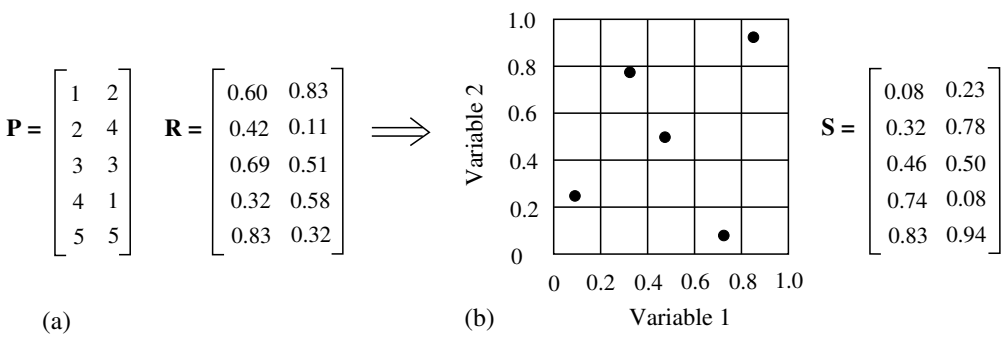

Figure 1: Latin cube, two variables and five realizations. The 5×2 matrix (a) determines the plan illustrated in (b).

3.2 Reduction of Spurious Correlation

Even though the marginal distribution of each variable is efficiently represented, there is a risk that some spurious correlation will appear, as shown in Fig. 2a. However, it has been shown [10, 17] that such a spurious correlation can be reduced by modifications in the permutation matrix $\mathbf{P}$. The elements of $\mathbf{P}$, p_{ij}, are divided by the number of

realizations plus one, and mapped on the Gaussian distribution with mean zero and standard deviation one as

$$y_{ij} = \Phi^{-1}_{(0,1)}\left(\frac{p_{ij}}{N+1}\right) \tag{5}$$

Then the covariance matrix of $\mathbf{Y}$ is estimated and Cholesky decomposed as

$$\bar{\mathbf{L}}\bar{\mathbf{L}}^T = cov(\mathbf{Y}) \tag{6}$$

where $\bar{\mathbf{L}}$ is lower triangular. A new matrix $\mathbf{Y}^*$ with a sample covariance equal to the identity is computed as

$$\mathbf{Y}^* = \mathbf{Y}(\bar{\mathbf{L}}^{-1})^T \tag{7}$$

and the ranks of the elements of the columns of $\mathbf{Y}^*$ become the elements in the columns of the matrix $\mathbf{P}^*$. If the elements of $\mathbf{P}$ in Eq. (3) are replaced by the elements of this matrix, the sampling matrix $\mathbf{S}$ will contain a considerably lower amount of undesired correlation. It should be noted, however, that the Cholesky decomposition of Eq. (6) requires that $cov(\mathbf{Y})$ is positive definite, which in turn requires that the number of realizations is higher than the number of stochastic variables, i.e that $N > K$. Fig. 2 illustrates the effect of the correlation-reduction procedure in a two variable sampling plan: (a) represents the sampling plan before, and (b) the sampling plan after the correlation reduction.

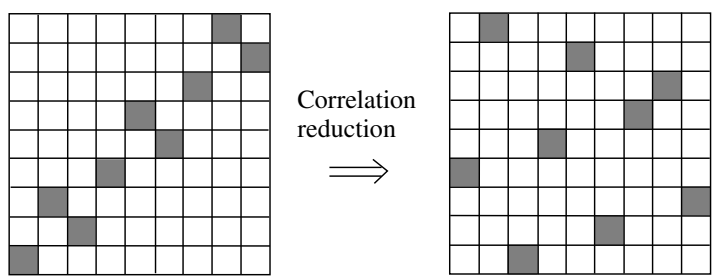

Figure 2: Undesired correlation of sampling plan (a) is reduced in plan (b).

If the target correlation matrix is different from unity, the target correlation is applied by replacing Eq. (7) with

$$\mathbf{Y}^* = \mathbf{Y}(\bar{\mathbf{L}}^{-1})^T\mathbf{L}^T \tag{8}$$

where $\mathbf{L}$ is the lower triangular matrix from the Cholesky decomposition of the target correlation matrix. The correlation of the sample $\hat{\mathbf{X}}$, Eq. (4), will approach the target correlation exactly if the stochastic variables are Gaussian, and approximately if the stochastic variables are non-Gaussian. An iterative algorithm may be employed to improve the correlation in the non-Gaussian case.

The sampling plan, including the correlation-reduction procedure, will in the following be called the correlation Latin hypercube sampling plan (CLHS), in contrast to the standard version, LHS. Finally, it is important to note that the correlation-reduction procedure may introduce some bias, i.e. unlike the LHS, the CLHS does not give an unbiased estimator.

4 Latin Hypercubes in Importance Sampling

Latin hypercubes can be employed instead of standard Monte Carlo in different ways and for different types of importance sampling. Below, the simple importance sampling method and the axis orthogonal importance sampling method are considered.

4.1 Latin Hypercubes in Simple Importance Sampling

When employed in simple importance sampling, the LHS plan is constructed as follows. First the transformation into standard Gaussian variables is performed as

$$\hat{u}_{ij} = \Phi^{-1}_{(0,1)}(s_{ij}) \tag{9}$$

where s_{ij} is an element of the matrix $\mathbf{S}$, Eq.(3). A vector $\hat{\mathbf{u}}_i = [\hat{u}_{i1}\ \hat{u}_{i2}\ \ldots\ \hat{u}_{ik}]$ now contains a realization in u-space centred at the origin. In the simple importance LHS (SILHS) [18, 22], the sample is then centred at the design point by adding the design point position vector, $\mathbf{m}$, to each realization, i.e.

$$\tilde{\mathbf{u}}_i = \hat{\mathbf{u}}_i + \mathbf{m} \tag{10}$$

As is clear from Eqs. (1)–(2), other distributions than the standard Gaussian could have been employed for the importance sampling distribution, but we make the straightforward assumption that Gaussian distributions with standard deviations equal to unity are employed for the importance sampling in u-space. The probability of failure is now calculated as

$$P_f = \frac{1}{N}\sum_{i=1}^{N}(W(\tilde{\mathbf{u}}_i)|g(\tilde{\mathbf{u}}_i) < 0) \tag{11}$$

where N is the sample size, $g(\tilde{\mathbf{u}}_i) < 0$ indicates failure for realization i, and $W(\tilde{\mathbf{u}}_i)$ is the corresponding weight factor calculated as

$$W(\tilde{\mathbf{u}}_i) = \frac{\phi_{\mathbf{u}}(\tilde{\mathbf{u}}_i)}{\phi_{\mathbf{u}}(\hat{\mathbf{u}}_i)} \tag{12}$$

where $\phi_{\mathbf{u}}$ represents the standard, K-dimensional, Gaussian probability density function centred at the origin.

Fig. 3a shows the SILHS plan in a two-variable example and the actual failure surface of the problem. From Fig. 3a it is clear that there is a risk that most of the realizations will be located on one side of the failure surface, in conformity with when standard importance Monte Carlo sampling (SIMC) is employed, even if about 50% of the sample should be located on each side. However, by introducing a transformed set of uncorrelated standard Gaussian variables, this can be avoided. The hypercube directions can

be rotated in such a way that one of the directions coincides with the normal of the approximating hyperplane, Fig. 3b. The new set of directions is established by first identifying the direction orthogonal to the tangent hyperplane of the failure surface at the design point. This direction is simply given by the unit vector in the direction of the position vector of the design point,

$$\mathbf{a}_1 = \frac{\mathbf{m}}{|\mathbf{m}|} \tag{13}$$

The remaining $K-1$ directions are chosen so that they are orthogonal to each other and to $\mathbf{a}_1$. This results in a square matrix $\mathbf{A}$, in which row p contains the unit vector $\mathbf{a}_p$ and with the property

$$\mathbf{A}^T\mathbf{A} = \mathbf{I} \tag{14}$$

Naturally, there is an infinite number of possible sets of directions satisfying Eq. (14). Only the direction vector $\mathbf{a}_1$ is clearly specified. It would be logical to choose the directions so that all mixed second derivatives of the failure function at the design point, with respect to the chosen directions, become zero [9], but this requires calculations of the second derivatives. In this paper no particular choice of orthogonal directions is recommended. When the method is employed in the evaluation problems below, a straightforward choice is made that results in numbers different from zero in just the first two positions of the second direction vector, numbers different from zero in just the first three positions of the third direction vector and so forth. A sample, centred at the origin, is then established, Eq. (3) and Eq. (9), but we let the coordinates of $\hat{\mathbf{u}}_i$ (for $i = 1:N$, $\hat{\mathbf{u}}_i$ is a row-vector with K components) refer to the set of directions defined by the rows of $\mathbf{A}$. A transformation to the original coordinate system is performed as

$$\hat{\mathbf{u}}_i^* = \hat{\mathbf{u}}_i\mathbf{A} \tag{15}$$

The sample is finally centred at the design point by adding the vector $\mathbf{m}$ to each realization, $\hat{\mathbf{u}}_i^*$, i.e.

$$\tilde{\mathbf{u}}_i^* = \hat{\mathbf{u}}_i^* + \mathbf{m} \tag{16}$$

Note that the only difference between the sample $[\tilde{\mathbf{u}}_1,\ \tilde{\mathbf{u}}_2,\ \ldots,\ \tilde{\mathbf{u}}_n]$, Eq. (10), and the sample $[\tilde{\mathbf{u}}_1^*,\ \tilde{\mathbf{u}}_2^*,\ \ldots,\ \tilde{\mathbf{u}}_n^*]$, Eq. (16), is, as shown in Fig. 3, that the Latin hypercube stratification is ensured in different sets of directions in u-space. Both samples correspond to the same target importance sampling function. They just represent it with different degrees of efficiency with respect to the failure function. In the following, the latter approach will be called the transformed importance Latin hypercube sampling (TILHS). If the actual failure surface is close to its tangent hyperplane, the TILHS can be expected to give very good estimates of the failure probability, even if the number of realizations is small, as a very good representation of the sampling distribution is ensured in the important direction orthogonal to the hyperplane. The uncertainty in the probability estimate arises mainly because of second- and higher-order derivatives of the failure function. Therefore, the method should be suitable for verification of the accuracy of a FORM analysis.

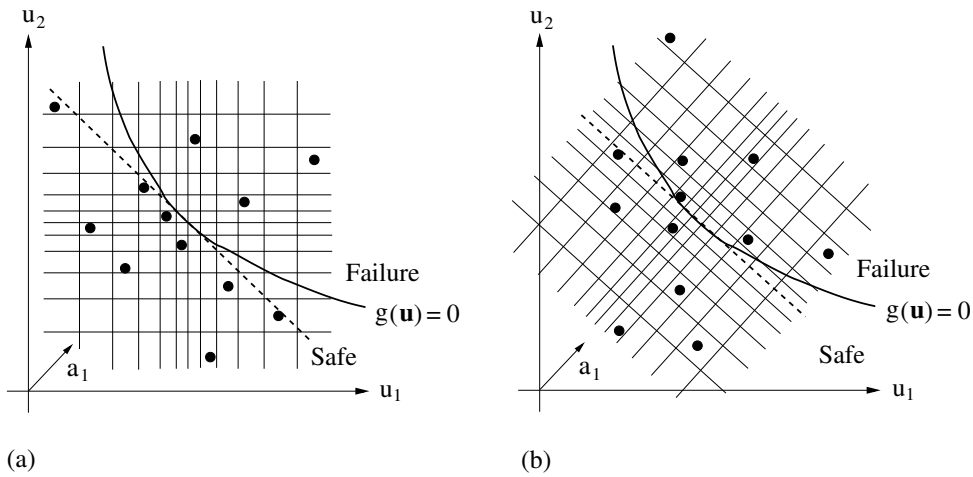

Figure 3: Latin hypercube importance sampling in (a) original coordinate system, SILHS, and (b) transformed coordinate system, TILHS.

4.2 Latin Hypercubes in Axis Orthogonal Importance Sampling

The axis orthogonal importance sampling, briefly described in the section about importance sampling, can easily be used in combination with Latin hypercubes. If the number of stochastic variables is K, the dimension of the tangent hyperplane is $K-1$. Thus an LHS or a CLHS sample in the $K-1$ dimensional standard Gaussian space is established in the directions of the tangent hyperplane. In the LHS version, an $N \times (K-1)$ matrix $\bar{\mathbf{P}}$, in which each of the $K-1$ columns is a random permutation of $1, \ldots, N$, and an $N \times (K-1)$ matrix $\bar{\mathbf{R}}$ of independent random numbers from the uniform (0,1) distribution are established. $\bar{\mathbf{P}}$ and $\bar{\mathbf{R}}$ form the sampling plan as

$$\bar{\mathbf{S}} = \frac{1}{N}(\bar{\mathbf{P}} - \bar{\mathbf{R}}) \tag{17}$$

Each element of $\bar{\mathbf{S}}$, $\bar{s}_{ij}$, is then mapped on the standard Gaussian distribution as

$$\bar{u}_{ij} = \Phi^{-1}_{(0,1)}(\bar{s}_{ij}) \tag{18}$$

Note that the coordinates given by $\bar{u}_{ij}$ now refer to a local coordinate system with axes defining the hyperplane. The probability of failure is calculated as

$$P_f = \frac{1}{N}\sum_{i=1}^{N} \Phi_{(0,1)}(-b_i) \tag{19}$$

where b_i is the root of

$$g\left([b_i \ \bar{\mathbf{u}}_i]\right) = 0 \tag{20}$$

The argument $[b_i \ \bar{\mathbf{u}}_i]$ is thus a row-vector with K components of which b_i constitutes the first component and $\bar{\mathbf{u}}_i$ constitutes the second to the Kth component. When searching for the solution of Eq. (20), using the Newton-Raphson algorithm in one dimension, a suitable start value for b_i is of course the distance between the origin and the design point, β. The transformation to the original coordinate system in u-space, which is needed for the g-function evaluations, is performed as

$$\bar{\mathbf{u}}_i^* = [b_i \ \bar{\mathbf{u}}_i] \, \mathbf{A} \tag{21}$$

The coordinates given by $\bar{\mathbf{u}}_i^*$ thus refer to the coordinate system of the basic variables in u-space.

Of course, the sample stored in $\bar{u}_{ij}$ may be established using the SMC or the CLHS as alternatives to the LHS, and the modifications are straightforward in the light of the previous sections of this paper. The axis orthogonal importance sampling using the different sampling procedures will in the following be called the axis importance Monte Carlo method (AIMC), the axis importance Latin hypercube sampling method (AILHS), and the axis importance correlation Latin hypercube sampling method (AICLHS) respectively. Fig. 4a illustrates the AIMC method, and Fig. 4b illustrates the AILHS or the AICLHS methods for a problem with two stochastic variables. Note that there is no difference between the AILHS and the AICLHS in a problem with only two stochastic variables.

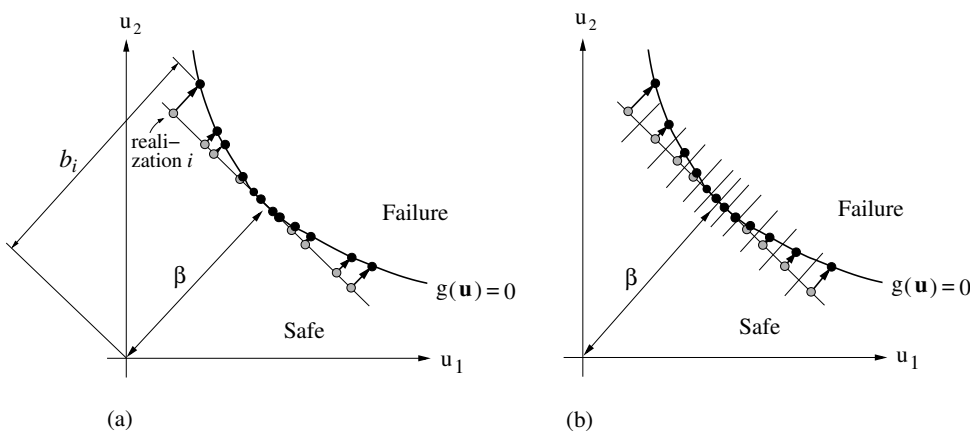

Figure 4: (a) AIMC sampling and (b) AILHS/AICLHS sampling. Line-search is employed to find the intersection with the actual failure surface.

5 Evaluation by Numerical Examples

The present evaluation of the proposed methods is limited to the analyses of three different example problems, each comprising a number of different cases. The purpose is to compare the new methods with the alternative importance sampling methods presented herein, and if we assume that each importance sampling is preceded by a

search for the design point in the standard Gaussian variable space, all the methods are equally applicable. Thus, we only focus on the computational efficiency of the different methods for different applications, i.e. we examine how much is gained when the TILHS is employed instead of the SIMC or the SILHS, and how much is gained when the AILHS or the AICLHS are employed instead of the AIMC. The example problems below allow us to study the following aspects, namely the importance of the shape of the failure surface, the significance of the probability level, and the significance of the number of stochastic variables in the problem.

5.1 Example 1

A simple spring system, Fig. 5, is loaded with two forces, f_1 and f_2. All the four spring stiffnesses and the magnitudes of the two forces are stochastic parameters and it is assumed that the system will collapse when the displacement d_2 exceeds a certain level. This is indeed a very small system of only six variables and only two degrees of freedom, but it could represent a simple model of many different engineering applications. We will consider four different cases. In the first case (a), a log-normal distribution with mean $\mu = 10$ and standard deviation $\sigma = 2$ is adopted for the spring stiffnesses as well as for the magnitudes of the forces. Failure occurs when $d_2 > 2.30$, which corresponds to a failure probability of 0.01. In case (b), the spring stiffnesses have the same properties as in case (a), but the forces are now uniformly distributed in the interval (7,13). In this case the failure criterion $d_2 > 2.17$ is adopted, which corresponds to the failure probability 0.01. Case (c) is identical to case (a), except that the failure criterion is changed to $d_2 > 2.98$, which corresponds to a failure probability of 0.0001. Case (d) is identical to case (b) except that the failure criterion is changed to $d_2 > 2.60$, which corresponds to a failure probability of 0.0001. The characteristics of cases (a)–(d) are summarized in Table 1.

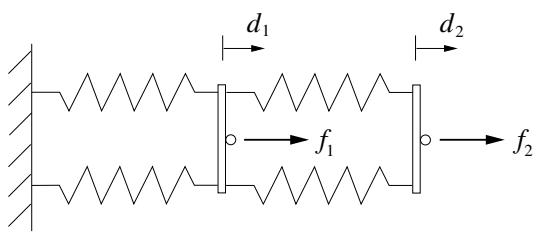

Figure 5: System with four springs, stochastic stiffness, loaded with two stochastic forces.

Using the FORM, the failure probabilities are estimated in case (a) to 0.009, in case (b) to 0.02, in case (c) to 0.00009, and in case (d) to 0.0003. From this we can conclude that the FORM gives good estimates for cases (a) and (c), but rather poor estimates for cases (b) and (d). Or to put it another way: in cases (b) and (d) the actual failure surface is not very close to a hyperplane. Using the SORM, the failure probabilities are calculated to 0.012 and 0.00014 for the cases (b) and (d) respectively. These results are of course closer to the true failure probabilities than the FORM results, and for problems with only a few stochastic variables the computational cost of using the SORM is moderate.

case	spring stiffnesses	force magnitudes	failure probability
(a)	log-normal	log-normal	0.01
(b)	log-normal	uniform	0.01
(c)	log-normal	log-normal	0.0001
(d)	log-normal	uniform	0.0001

Table 1: Summary of the characteristics of cases (a)–(d).

The different importance sampling methods are now employed. Neglecting the computational costs of generating the random numbers, establishing the Latin hypercube sampling plans and carrying out the necessary transformations, the efficiency of the different methods can be judged by the mean error of the failure probability estimate, when repeated simulations using the same number of g-function evaluations are performed. For the SIMC, the SILHS, and the TILHS, the number of g-function evaluations is equal to the number of realizations of the sample plus the number of g-function evaluations of the FORM analysis, whereas for the AIMC, the AILHS, and the AICLHS, about four to six g-function evaluations are required for each realization during the line-search procedure. Of course, for all the methods, the mean error will decrease for increasing sample sizes. The assumption that the computational costs of establishing the Latin hypercube sampling plans and carrying out the necessary transformations are comparatively small is justified for most realistic finite element applications.

Fig. 6 shows, for the four cases (a)–(d), the mean error of the estimated failure probability as a function of the number of g-function evaluations (not including the g-function evaluations carried out for finding the design point, i.e the FORM analysis) for the six importance sampling methods. For each evaluated sample size and each method, one thousand simulations are performed in order to calculate the mean error.

The TILHS is, in all the cases, the most efficient method using simple importance sampling centred at the design point. In (a) and (c), there is no significant difference between the performance of the SIMC and the SILHS, but the proposed method is much more efficient. Using the TILHS, it only takes slightly more than one third of the sample size, compared to the alternative methods, to reach a specified mean error, i.e. a level of accuracy. Cases (a) and (c) represent different failure probabilities, but this does not seem to have major effect on the relative performance of the methods. In cases (b) and (d), the SILHS is more efficient than the SIMC, but less efficient than the TILHS. To reach the same level of accuracy, about half the sample size is required, using the proposed method, compared to using the SIMC method. It is interesting to note that the proposed importance sampling method is considerably more efficient than the SIMC, even in the cases where the failure surface differs considerably from the approximating hyperplane employed in FORM analysis.

From Fig. 6 it is obvious that the axis orthogonal importance sampling method is much more efficient than the simple importance sampling method. This holds for all the different versions of the method using Monte Carlo sampling or Latin hypercube sampling. It is, however, also clear that the choice of SMC, LHS, or CLHS in the axis orthogonal importance sampling strongly influences its efficiency. In (a) and (c), the AILHS is only moderately more efficient than the AIMC, about 10–30%, but the

AICLHS is substantially more efficient. In (b) and (d), the AICLHS is only moderately more efficient than the AILHS, but both methods are much more efficient than the AIMC. Only about one third of the sample size, compared to the AIMC, is needed to reach the same level of accuracy using AILHS or AICLHS. In conclusion, large effects of using Latin hypercube sampling in different ways for importance sampling are shown by this example, but, as expected, differences are found for the different cases, i.e. for different shapes of the failure surface.

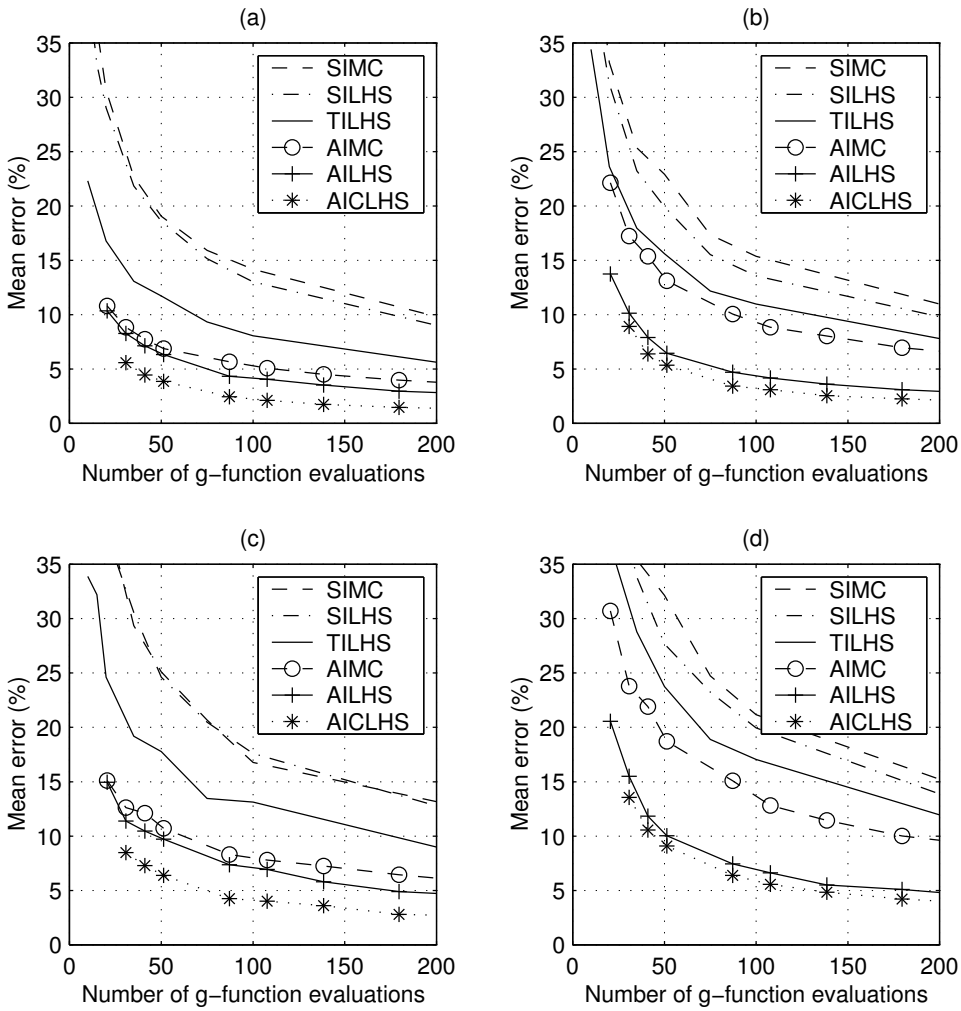

Figure 6: Mean error of estimated failure probability as a function of the number of g-function calls using the six importance sampling methods.

5.2 Example 2

We now compare the importance sampling methods by considering an example problem with a higher number of degrees of freedom and a high dimensional stochastic variable space.

A square plate with unit side length and unit thickness is modelled by four-node, plane-stress elements with two degrees of freedom at each node. A square hole with a side length of 1/3 is located in the middle of the plate. The material is assumed to be isotropic with stochastic Young's modulus and deterministic Poisson's ratio, $\nu = 0.3$. The plate is loaded with a deterministic, uniformly distributed load with unit magnitude. Nodal displacements in the y-direction are constrained along the lower edge. Fig. 7 shows the geometry, loading, element mesh and boundary conditions of the structure.

A log-normal random field is adopted for the Young's modulus of the plate. The field is described by its mean-value function, which is constant and equal to one in the entire plate, and the isotropic auto-covariance function,

$$c_{ij} = \sigma_0^2 \; exp\left[-\left(\frac{\xi_{ij}}{l} \right)^2 \right] \tag{22}$$

in which $\sigma_0 = 0.2$ is the standard deviation, $l = 0.2$ is a positive parameter determining the correlation length of the field, and ξ_{ij} is the distance between two points in the plate. c_{ij} is the auto-covariance between the two points. In discretized form, using the midpoint method, ξ_{ij} is the distance between the centroid of element i and the centroid of element j, and c_{ij} becomes the element in row i and column j of the $r \times r$ covariance matrix $\mathbf{C}$, where r is the number of finite elements in the problem. Fig. 8 shows the correlation in continuous form as a function of the distance, and the discretization of the correlation function according to the midpoint method in which the midpoint position of each element is used to represent the random field within the element.

The present discretization gives a problem with two hundred correlated stochastic variables. However, a transformation into uncorrelated variables is performed by calculating the eigenvalues and the eigenvectors of the covariance matrix, $\mathbf{C}$. The eigenvalues give the variances of the transformed variable set, and, by regarding the variables with a small variance as deterministic, the number of stochastic variables is reduced to one hundred. The stochastic variable set, in u-space, thus consists of one hundred standard Gaussian variables. Details about the transformations between the u-space and the basic variables are given in [15].

We now focus on two different failure criteria, namely (a), failure occurs when the vertical displacement of the centre of the upper edge of the plate exceeds 2.00, and (b), failure occurs when the stress in the vertical direction at the right edge of the square hole in the plate (the stress in the middle of the element marked in Fig. 7) exceeds 2.53. Each of these criteria corresponds to a failure probability of 0.01. FORM analysis gives, for case (a), a failure probability of 0.007, and, for case (b), a failure probability of 0.01. SORM gives, for both cases, a failure probability of 0.01.

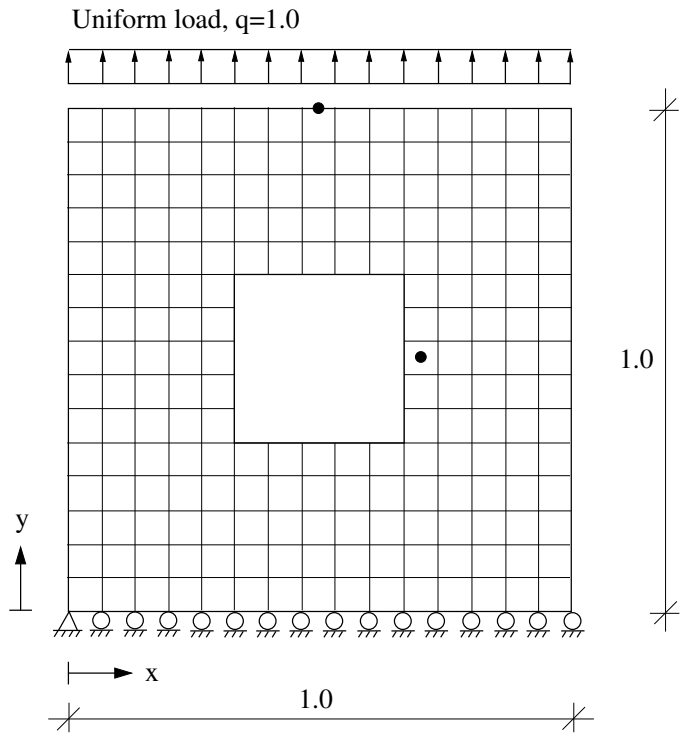

Figure 7: Square plate, loaded in tension, modelled by 200 elements. The two dots indicate positions in the plate with relevance to the failure criteria.

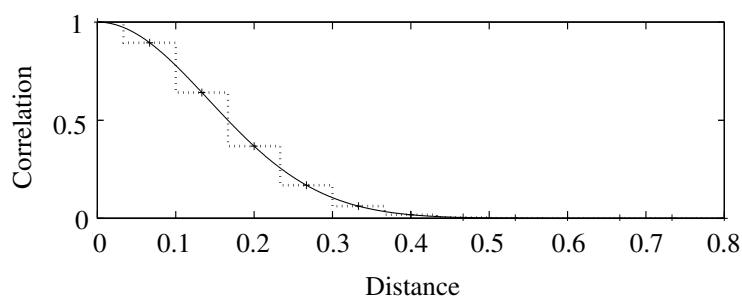

Figure 8: Correlation as a function of the distance in continuous and discretized form.

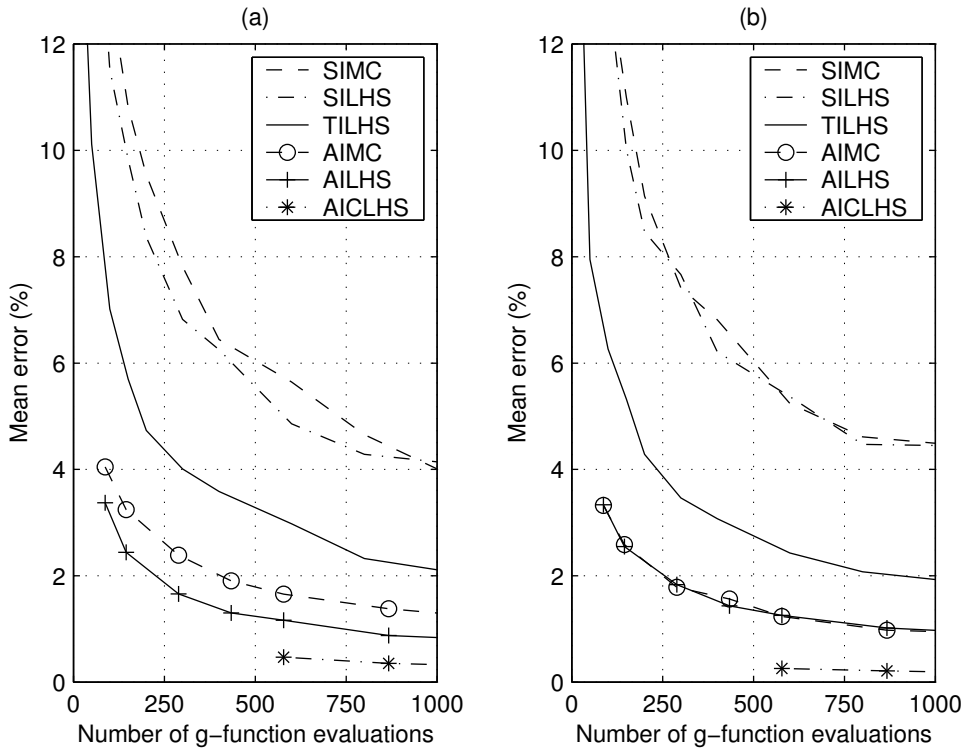

Figure 9: Mean error of the estimated failure probability as a function of the number of g-function evaluations. For case (a), failure occurs when the vertical displacement of the centre of the upper edge exceeds 2.00 units. For case (b), failure occurs when the stress in the vertical direction at the right edge of the square hole exceeds 2.53 units.

When the position of the design point is calculated, importance sampling is performed using the different methods. The mean errors, using the failure probability estimates for different sample sizes, are displayed in Fig. 9. The comparison shows that the TILHS produces much better results than the SIMC or the SILHS. In case (a), for which the FORM does not give a very accurate result, only about one third of the sample size is required to reach a certain degree of accuracy when the TILHS is used compared to when the SIMC or the SILHS are used. In case (b), for which the FORM gives a very accurate result, the superior efficiency of the proposed method is even more pronounced. It can be noted that the SILHS is not significantly more efficient than the SIMC.

The axis orthogonal importance sampling is, as in the previous example problem, much more efficient than the simple importance sampling. For case (a), the AILHS is about twice as efficient as the AIMC, but for case (b) there is no significant difference between these two methods. The AICLHS, on the other hand, is far more efficient for both cases. This implies that there are important dependencies between different orthogonal directions of the failure surface and that the reduction of spurious correlation of the CLHS sample on the hyperplane is of great importance. Fig. 10 shows histograms of the failure probability estimates of case (a) using the AIMC, the AILHS, and the

AICLHS with a sample size of one hundred, i.e. about six hundred g-function evaluations for each simulation. One thousand simulations are carried out for each method and the strong variance reduction effect of using the AICLHS is quite obvious. A drawback, however, of the CLHS method, and thereby the AICLHS method, is that the sample size must be greater than the number of stochastic variables, in this case one hundred, which, due to the line-search procedure, corresponds to somewhat less than six hundred g-function evaluations. A discussion on this restriction is found in [15].

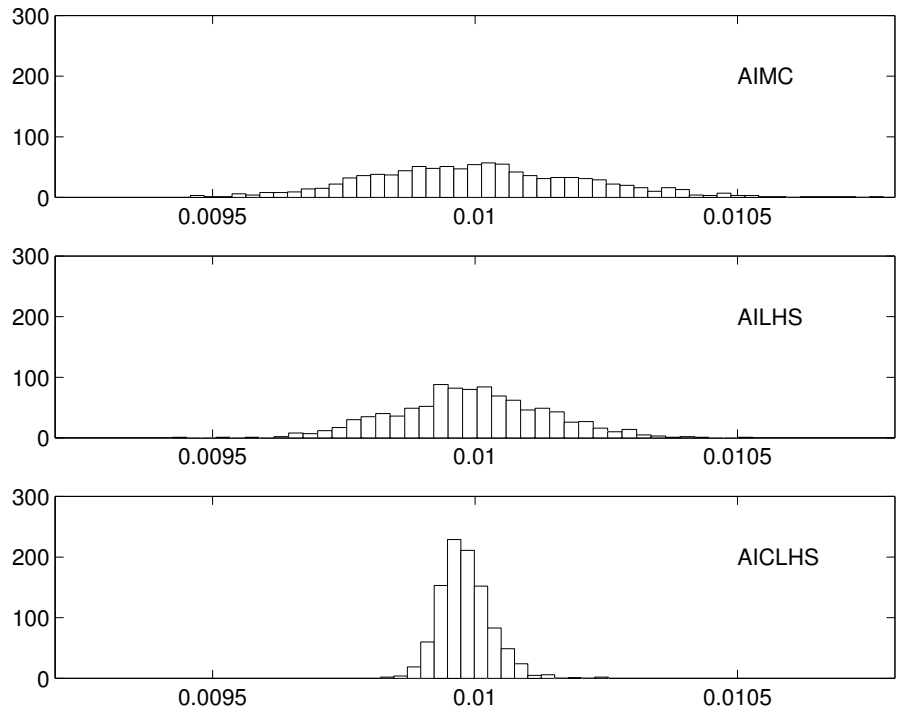

Figure 10: Histograms of the failure probability estimates of case (a) using the AIMC, the AILHS, and the AICLHS with a sample size of one hundred realizations. One thousand simulations of each kind were carried out.

In conclusion, this example with a high number of degrees of freedom and a high number of stochastic variables gives approximately the same picture of the different methods as the previous example. Very good estimates of the failure probability can be achieved using, for example, the AICLHS with about six hundred g-function evaluations. A SORM analysis, that also gives very good estimates, requires about five thousand g-function evaluations in addition to the cost of the FORM analysis.

5.3 Example 3

The examples above examine the ability of the different importance sampling methods for different systems, failure criteria, and number of stochastic variables. This far, however, the failure surfaces have not been highly nonlinear, i.e. analyses using SORM resulted in fairly accurate estimates of the failure probabilities. Now an example problem with a highly nonlinear failure surface in u-space will be employed in order to examine the importance sampling methods for such cases.

The sum of ten independent, exponentially distributed variables, x_i, $i = 1, 2, \ldots, 10$, with parameter $\lambda = 1$ must not (a) excced a certain level, and (b) go below a certain level corresponding to a failure probability of 0.01. For cases (a) and (b) respectively, the failure criteria are expressed as

$$g_{(a)}(\mathbf{x}) = -\sum_{i=1}^{10} x_i + C_{(a)} \tag{23}$$

and

$$g_{(b)}(\mathbf{x}) = \sum_{i=1}^{10} x_i - C_{(b)} \tag{24}$$

In standard Gaussian space, the same failure criteria are expressed as

$$g_{(a)}(\mathbf{u}) = \sum_{i=1}^{10} ln\left[\Phi_{(0,1)}(-u_i)\right]/\lambda + C_{(a)} \tag{25}$$

and

$$g_{(b)}(\mathbf{u}) = -\sum_{i=1}^{10} ln\left[\Phi_{(0,1)}(-u_i)\right]/\lambda - C_{(b)} \tag{26}$$

The values of the constants are $C_{(a)} = 18.783$ and $C_{(b)} = 4.130$. For case (a), the failure surface will have a positive curvature, i.e. the safe region will be convex, and for case (b), the failure surface will have a negative curvature. The same problems, i.e. positive and negative curvatures, are also considered at a lower failure probability. Cases (c) and (d) correspond to cases (a) and (b) respectively at a failure probability of 0.0001 with constants $C_{(c)} = 26.193$ and $C_{(d)} = 2.198$. The characteristics of cases (a)–(d) are summarized in Table 2.

The four cases have been analysed using the FORM and the SORM with the following results. Probability of failure according to FORM/SORM: case (a) 0.00060/0.018;

case	failure surface	failure probability
(a)	positive curvature	0.01
(b)	negative curvature	0.01
(c)	positive curvature	0.0001
(d)	negative curvature	0.0001

Table 2: Summary of the characteristics of cases (a)–(d).

case (b) 0.094/0.020; case (c) 0.0000021/0.00023; case (d) 0.0035/0.00015. The FORM results are thus completely inaccurate and the SORM results are wrong by approximately a factor of two.

Fig. 11 shows, for the four cases (a)–(d), the mean error of the estimated failure probability as a function of the number of g-function evaluations for the six importance sampling methods. For each evaluated sample size and each method, five thousand simulations are performed to calculate the mean error. This high number of simulations is needed in order to make reliable comparisons between the efficiency of the different methods because the problems are highly nonlinear and some of the simulations give very poor estimates of the failure probabilities.

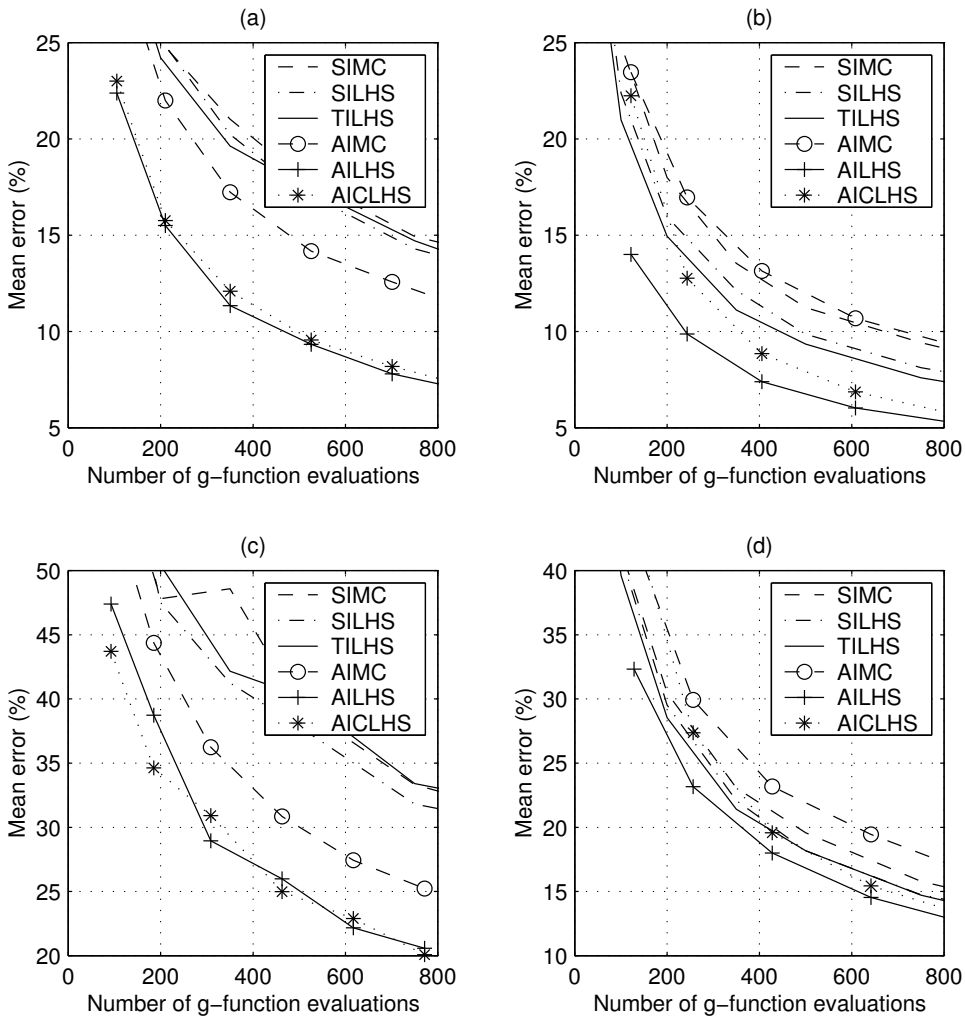

Figure 11: Mean error of estimated failure probability as a function of the number of g-function calls using the six importance sampling methods.

For cases (a) and (c), only small differences in efficiency are found between the simple importance sampling methods, SIMC, SILHS and TILHS. One explanation for this is that the failure surface is highly nonlinear. As previously stated in this paper, it is for cases with failure surfaces fairly close to their tangent hyperplanes that a large effect using TILHS instead of SIMC or SILHS can be expected. An additional explanation, valid for problems with convex safe regions, is that in some of the simulations individual realizations of the importance sampling distribution may fall in the failure region even if they are located far from the design point, but relatively close to the origin, i.e. individual realizations may be assigned very high weight factors according to Eq. (12). This gives very large errors for a small part of the simulations giving that the errors of the simulations are not normally distributed. This problem is not avoided by using SILHS or TILHS. According to [7], it can be favourable for this type of problems to employ a more spread importance sampling distribution with a standard deviation larger than one.

The axis orthogonal importance sampling methods are, as in the previous examples, considerably more efficient than the simple importance sampling methods for cases (a) and (c). The positive curvature of the failure surface gives that a great deal of the realizations contribute significantly to the failure probability estimation, i.e even if a realization on the tangent hyperplane is far from the origin, the point of intersection between the failure surface and the direction vector orthogonal to the hyperplane, through the realization, may be relatively close to the origin. Thus, it is important to use the Latin hypercube stratification to reach a good representation of the importance sampling density function. The AICLHS method, however, does not perform better than the AILHS method, and there are at least two reasons for this. The first reason is that the exact correlation between the different stochastic variables does not seem to be particularly important for this function, which simply is the sum of ten equally distributed variables. Thus the variance-reduction effect of using the AICLHS instead of the AILHS is not very large. The other reason is that the AICLHS method gives a biased estimate of the failure probability for this problem. Fig. 12 shows the histograms of the failure probability estimates of case (a) using the AIMC, the AILHS, and the AICLHS with a sample size of 50 realizations, i.e. about 350 g-function evaluations for each simulation. The variance-reduction effect of using the AILHS or the AICLHS is quite obvious, as well as the bias effect of using the AICLHS, i.e. the mean estimate of the failure probability is clearly below 0.01 using the AICLHS. In Fig. 12, it can also be seen that the mean errors of the failure probability estimates are not distributed as Gaussian variables.

For case (b), significant, although not large, differences in efficiency are found between the SIMC, the SILHS, and the TILHS methods, but for case (d), the differences between the simple importance sampling methods are very small. For both cases, the TILHS method is the most efficient. Cases (b) and (d) consider a negative curvature of the failure surface and only a small part of the realizations using simple importance sampling is located in the failure region if the sampling is centred at the design point. Moreover, only realizations close to the design point contribute significantly to the failure probability estimates. On the other hand, there is no risk that individual realizations will give huge contributions to the failure probability estimates as for cases (a) and (c). It would probably be efficient for these cases [7] to use an importance sampling

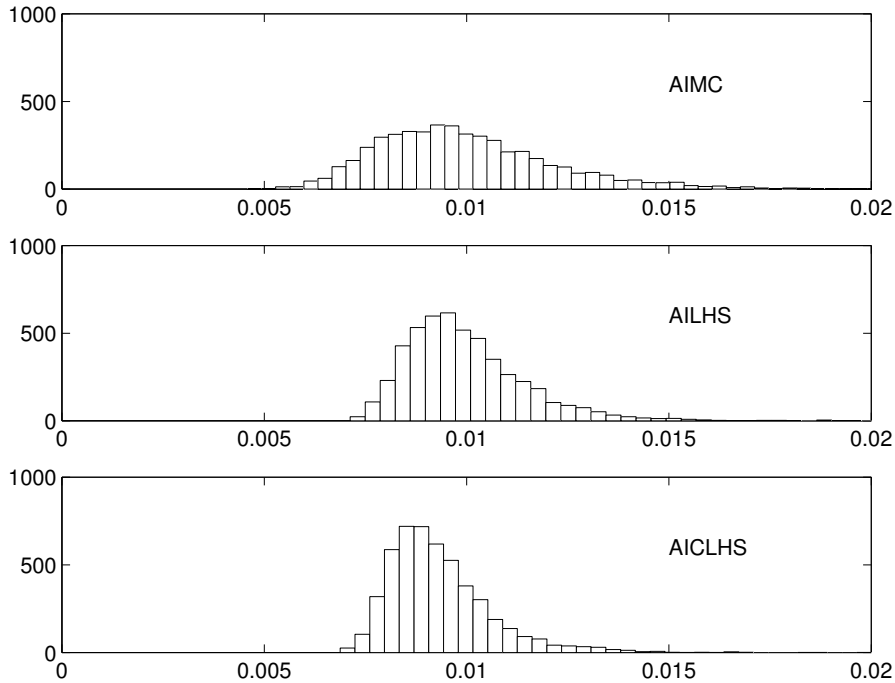

Figure 12: Histograms of the failure probability estimates of case (a) using the AIMC, the AILHS, and the AICLHS with a sample size of fifty realizations. Five thousand simulations of each kind were carried out.

distribution with standard deviation smaller than one.

For cases (b) and (d), the axis importance sampling methods are not generally more efficient than the simple importance sampling methods. As a matter of fact, the AIMC gives the poorest estimates of all the six methods. The benefit of using the AILHS instead of the AIMC is, however, quite large. The AILHS is almost twice as efficient as the AIMC. The AICLHS underestimates the probability of failure, especially for a small sample size. Therefore, even if the method gives the best variance reduction, it does not give the smallest mean error when estimating the failure probability.

6 Conclusions

The objective of this paper is to introduce Latin hypercube sampling as an efficient and generally applicable tool in importance sampling for structural reliability analysis. In simple importance sampling, where the sampling is centred at the design point, Latin hypercube sampling can be employed instead of simple Monte Carlo sampling. To reach a superior efficiency, however, it is shown that the sampling directions should be transformed, so that one of the directions become orthogonal to the tangent hyperplane of the failure surface at the design point. For problems with failure surfaces fairly close to their tangent hyperplanes, the suggested method performs much better than simple

importance sampling using standard Monte Carlo. Typically, better accuracy is reached at half the sample size using transformed Latin hypercubes compared to using standard Monte Carlo importance sampling. The exact savings, however, differ between different problems.

This paper also presents a combined use of Latin hypercube sampling and axis orthogonal importance sampling. The axis orthogonal importance sampling is, in general, more efficient than simple importance sampling, and the suggested combination with Latin hypercube sampling is shown to perform very well. The Latin hypercube sample is established on the tangent hyperplane of the failure surface, and a line-search procedure is carried out for each realization in the direction orthogonal to the hyperplane in order to find the intersection with the failure surface. A more elaborate version of the Latin hypercube sampling plan, including reduction of spurious correlation, may also be employed in axis orthogonal importance sampling. This method is even more efficient for many problems, especially for moderately curved failure surfaces, but gives biased estimates of the failure probability. The bias can be severe for small sample sizes and highly nonlinear failure surfaces. In general, however, the benefits of using Latin hypercubes in axis orthogonal importance sampling, with or without reduction of spurious correlation, are at least as large as using transformed Latin hypercubes in simple importance sampling.

The use of Latin hypercubes does not put any serious restrictions on the applicability of the importance sampling methods and the benefits of Latin hypercubes can be added to the benefits of elaborate and efficient importance sampling strategies. Therefore, Latin hypercube sampling has the qualifications to become a widely employed tool in reliability analysis. In the future, when new efficient importance sampling methods are developed, the possibility of increasing their efficiency further by the use of Latin hypercubes should also be investigated.

Acknowledgements

This research was financed by the Swedish Research Council for Engineering Sciences, and by the Swedish Council for Building Research. Their support is gratefully acknowledged.

Appendix

Table A1 summarizes the different methods presented and compared in the paper. Some of the methods and designations are widely accepted, whereas others are introduced here.

Abbreviation	Full name	Comment
FORM	First Order Reliability Method	Approx. of the failure surface with a hyperplane
SORM	Second Order Reliability Method	2nd order approx. of the failure surface
SMC	Standard Monte Carlo	True random sampling
LHS	Latin Hypercube Sampling	Simple Latin hypercube sampling
CLHS	Correlation Latin Hypercube Sampling	LHS with reduction of spurious correlation
SIMC	Standard Importance Monte Carlo	SMC but centred at the design point
SILHS	Standard Importance Latin Hypercube Sampling	LHS but centred at the design point
TILHS[a]	Transformed Importance Latin Hypercube Sampling	Transformed hypercube directions
AIMC	Axis Importance Monte Carlo	SMC sampling on the hyperplane
AILHS[a]	Axis Importance Latin Hypercube Sampling	LHS sampling on the hyperplane
AICLHS[a]	Axis Importance Correlation Latin Hypercube Sampling	CLHS sampling on the hyperplane

Table A1: *Summary of methods and abbreviations employed in the paper.*
[a] *To the authors' knowledge, these methods have not been presented before.*

References

[1] Bjerager P. Probability integration by directional simulation. Journal of Structural Engineering. ASCE 1988;114(8):1285–302.

[2] Bjerager P. On computational methods for structural reliability analysis. Structural Safety 1990;9(2):79–96.

[3] Bucher CG. Adaptive sampling – an iterative fast Monte Carlo procedure. Structural Safety 1988;5(2):119–26.

[4] Dey A, Mahadevan S. Ductile structural system reliability analysis using adaptive importance sampling. Structural Safety 1988;20(2):137–54.

[5] Ditlevsen O, Melchers RE, Gluver H. General multi-dimensional probability integration by directional simulation. Computers & Structures 1990;36(2):355–68.

[6] Pebesma EJ, Heuvelink GBM. Latin hypercube sampling of Gaussian random fields. Technometrics 1999;41(4):303–12.

[7] Engelund S, Rackwitz R. A benchmark study on importance sampling techniques in structural reliability. Structural Safety 1993;12(4):255–76.

[8] Hurtado JE, Barbat AH. Monte Carlo techniques in computational stochastic mechanics. Archives of Computational Methods in Engineering 1998;5(1):3–30.

[9] Hohenbichler M, Rackwitz R. Improvements of second-order reliability estimates by importance sampling. Journal of Engineering Mechanics. ASCE 1988;114(12):2195–9.

[10] Iman RL, Conover WJ. A distribution-free approach to inducing rank correlation among input variables. Communications in Statistics, Part B – Simulation and Computation 1982;11(3):311–34.

[11] Liu PL, Der Kiureghian A. Optimization algorithms for structural reliability. Structural Safety 1991;9(3):161–77.

[12] Melchers RE. Search-based importance sampling. Structural Safety 1990;9(2):117–28.

[13] Moarefzadeh MR, Melchers RE. Directional importance sampling for ill-proportioned spaces. Structural Safety 1999;21(1):1–22.

[14] McKay MD, Conover WJ, Beckman RJ. A comparison of three methods for selecting values of input variables in the analysis of output from a computer code. Technometrics 1979;21(2):239–45.

[15] Olsson AMJ, Sandberg GE. Latin hypercube sampling for stochastic finite element analysis. Journal of Engineering Mechanics. ASCE 2001;128(1):121-5.

[16] Olsson A. Modelling damage and stochastic properties in engineering structures. Report TVSM-3037. Lund (Sweden): Lund Institute of Technology; 1999.

[17] Owen AB. Controlling correlations in Latin hypercube samples. Journal of the American Statistical Association 1994;89(428):1517–22.

[18] Portielje R, Hvitved-Jacobsen T, Schaarup-Jensen K. Risk analysis using stochastic reliability methods applied to two cases of deterministic water quality models. Water Research 2000;34(1):153–70.

[19] Sandberg G, Olsson A. Failure sensitivity analysis of engineering structures. Computers & Structures 1999;72(4-5):525–34.

[20] Schuëller GI, Stix R. A critical appraisal of methods to determine failure probabilities. Structural Safety 1987;4(4):293–309.

[21] Stein M. Large sample properties of simulations using Latin hypercube sampling. Technometrics 1987;29(2):143–51.

[22] Žiha K. Descriptive sampling in structural safety. Structural Safety 1995;17(1):33–41.

Paper IV

Load-Carrying Capacity of Damaged Steel Columns with Channel Sections

by

Anders Olsson, Göran Sandberg and Per-Erik Austrell

Journal of Structural Engineering, ASCE 125(3) 338–343

Load-Carrying Capacity of Damaged Steel Columns with Channel Sections

Anders Olsson[1], Göran Sandberg[2] and Per-Erik Austrell[3]

Journal of Structural Engineering, ASCE 125(3) 338–343

Abstract

The influence of damage on the load-carrying capacity of thin-walled steel columns with channel sections is investigated. The axial load-carrying capacity is evaluated for different profiles, and different damage magnitudes are dealt with. The profiles selected for the analysis are commonly used as upright members in rack and shelving systems in industry. The type of damage corresponds primarily to truck impacts. The strategy presented, however, is generally applicable to different types of profiles, and suitable for parameter studies of different types of damage, load cases, and boundary conditions. The main part of the analysis consists of numerical simulations using the finite element method, but a verifying laboratory test series is also presented. The results of the numerical simulations are in good agreement with the laboratory tests, and show that even very small defects in the thin-walled columns significantly reduce the axial load-carrying capacity.

1 Introduction

Thin-walled steel profiles with channel sections are commonly employed in civil engineering structures to resist lateral and axial loads. The sections are easily assembled to other structural members through welding or bolting. They are inexpensive to manufacture and fabricate as they may be pressed or rolled from flat steel sheets or coiled strips. Although these profiles perform very well as structural members in relation to their weights, they are susceptible to different types of buckling including distortion of the cross section, local buckling, and torsional instability. They are also sensitive to initial imperfections and damage.

Much research has been aimed towards accurate and efficient analysis of thin-walled beam columns in terms of conventional beam theory, finite strip analysis, and finite element analysis. Conventional beam theory proceeds from the kinematic assumption that the cross section does not distort. The modes of deformation are limited to extension, bending about two principal axes and torsion. However, beam theory can be

[1]Division of Structural Mechanics, Lund University, P.O. Box 118, SE-221 00, Lund, Sweden. Telephone: +46 46 222 46 89. Fax: +46 46 222 44 20.

[2]Prof. Division of Structural Mechanics, Lund University, P.O. Box 118, SE-221 00, Lund, Sweden.

[3]Assoc. Prof. Division of Structural Mechanics, Lund University, P.O. Box 118, SE-221 00, Lund, Sweden.

extended by also incorporating distortional modes of deformation. This approach has been employed by Davies and Leach (1992) using a generalized beam theory developed by Schardt (1989). Another method for analysis of thin-walled beam columns is the finite strip method, where the thin-walled member is subdivided into longitudinal strips. This method includes distortional modes because each strip is free to deform both in and out of its plane. Buckling of channel sections for storage racks without imperfections has been analyzed using this method by Hancock (1985). Nonlinear material models have also been incorporated. Clarke (1994) and Rasmussen and Rondal (1997) used a Ramberg Osgood model and studied the influence of material parameters on the buckling behavior.

The method used in this study employs large displacement finite element analysis, material nonlinearity, and modeling by use of shell elements. This is necessary due to the complexities involved in modeling the geometry, the boundary conditions, and the material. It is then possible to model details in the geometry such as holes or local defects. Moreover, the initial damage is modeled by indentation of a rigid surface laterally into the beam columns, causing plastic deformations. Hence, this approach is suitable when local deformations and strains at some place along the beam column must be captured in detail. The disadvantage compared to the other methods is the computational cost related to model preparation and the required number of degrees of freedom.

The purpose here is to suggest and apply a strategy for investigating the effects of damage for thin-walled steel columns. The work is comprised within a project concerning failure sensitivity of pallet racks. Upright members in such structures are usually of the type described above, and if they are damaged (for example by truck impacts or because second-hand, crooked or squeezed components are used) the load-carrying capacity is reduced and the risks of failure and accidents are increased. The scope of the present investigation is restricted to three different profiles, and the type of damage considered is related to truck impacts. The main part of the analysis consists of numerical simulations using the finite element software ABAQUS (*ABAQUS* 1996). However, a laboratory test series is also performed.

2 Profiles and Modeling

The three profiles selected for this study are frequently used in rack and shelving systems. One of the profiles selected for this study has an asymmetric cross section while the other two have symmetric cross sections, one C profile and one Ω profile. Fig. 1 shows one repetitive segment of each profile with corresponding element meshes. To bring down the required number of elements some simplifications in the modeling were adopted. The asymmetric profile has impresses on its broad side along the upright axis. These were neglected in the model. Further, small circular holes, occurring in all three profiles were modeled by reductions in thickness of strips along the upright axis at the location of these holes. The simplifications were performed after comparisons with finer models, considering impresses and circular holes in detail. The comparisons showed that the simplified models were able to capture the global, linear elastic stiffness, and overall deformation modes of the columns when loaded as in the simulations below. The simplified modeling of perforation in thin-walled columns has earlier been employed, and

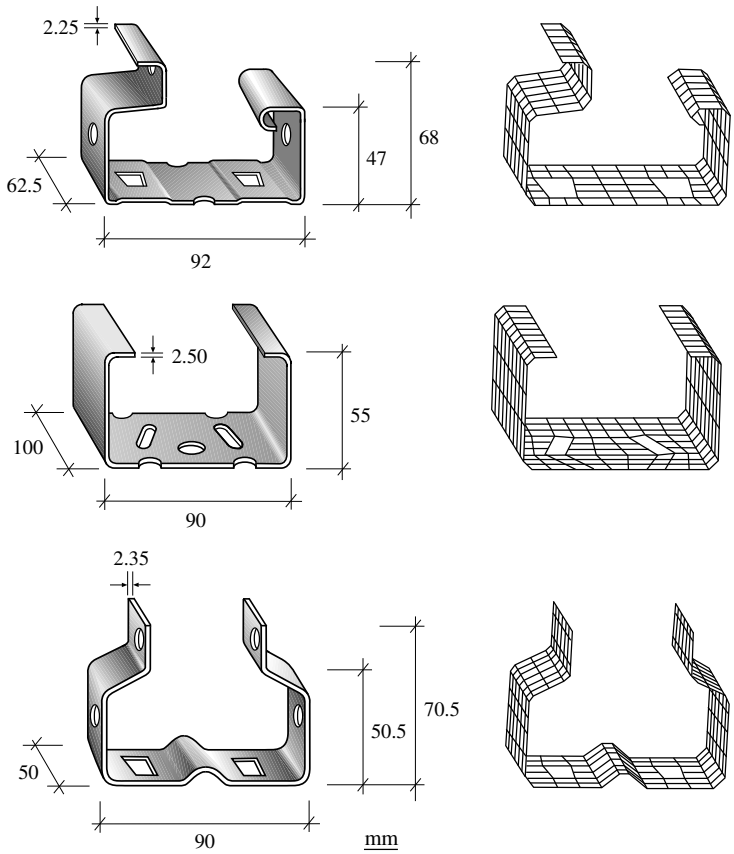

Figure 1: Repetitive segments of the three profiles with corresponding element meshes.

shown to be valid, by Mroz (1995).

A four-node, thin-shell element (ABAQUS element S4R5) with five degrees of freedom at each node, and reduced integration was used in the analysis. The element contains no drilling degree of freedom corresponding to rotation in the plane of the element. The element allows for large deformations but requires the strains to be small. The material properties were founded on tension tests of the steel sheets from which the profiles were fabricated. An isotropic, elastic-ideal plastic material model, von Mises yield criterion, with a yield stress of 385 MPa and Young's modulus of 212 GPa were adopted. Initial stresses in the profiles due to the forming procedure were not considered in the modeling.

3 Numerical Simulations

The columns considered are employed as upright members in pallet racks. The length of the columns was set to 1,250 mm, which corresponds to a typical height of one compartment in a pallet rack in industry. In most cases, however, upright members are continuous without joints from the floor to the top of the rack. This, combined with the fact that the stiffness of the connectors at the floor and at the horizontal beams varies from one racking system to another, makes it difficult to achieve appropriate and generally applicable boundary conditions for the columns. Therefore only the extreme cases, rigid supports and pin-ended supports, were dealt with. In all the simulations performed, warping and distortion of the cross sections were prevented at the ends of the columns.

Each simulation was divided into a number of displacement-controlled preloading steps where the columns were damaged laterally by indentation of a rigid body, and an axial compression step where the remaining load-carrying capacity was evaluated. The simulations were divided into three groups with different boundary conditions and load cases. Simulations I and II consider impact normal to the broad side. In simulation I the columns are rigidly supported and in simulation II the columns are pin-end supported. Simulation III considers impact to the corners of the columns with pin-ended supports. Each simulation was performed for all three profiles, and different magnitudes of damage were considered.

3.1 Simulation I

The preloading, damaging part of this simulation was divided into three steps. Fig. 2 shows these steps and the consequent axial compression. First the broad side at the middle of each column was indented by a rigid body pressed normally to the broad side. The thickness of the rigid body was 40 mm but the edges were rounded off with a radius of 5 mm so that only 30 mm initially came in contact with the structure. There was no friction between the rigid body and the deformable structure. The columns were supported so that they were free to rotate around the inplane axis of the cross section, parallel to the broad side (dotted axis in the left part of Fig. 2) but no twisting was allowed around the normal of the cross section at the ends. Then the rigid body was released and lost contact with the structure. In the third step the ends of the columns were bent so that the cross section normals at the supports ended up parallel to the original upright axis. The reason why the ends were bent back to their original orientation in a separate step was that the alternative, to keep the ends rigid from the beginning, would yield a highly unstable behavior of the column when the rigid body was released in the second load step. Elastic energy would rapidly be released and thus cause major numerical difficulties. However, if a dynamic analysis had been carried out it would probably be possible to deal with that behavior as the mass inertia would contribute to stabilize the structural response.

The extent of the damage was represented by the average of the displacements of two nodes, in the middle of each column in the direction normal to the broad side. The nodes are indicated in Fig. 3 where the deformations of the midsections are also shown for 10 mm damage. Fig. 4 shows the entire columns with the same magnitude of damage. The preloading part of the simulation also initiated the mode of failure for

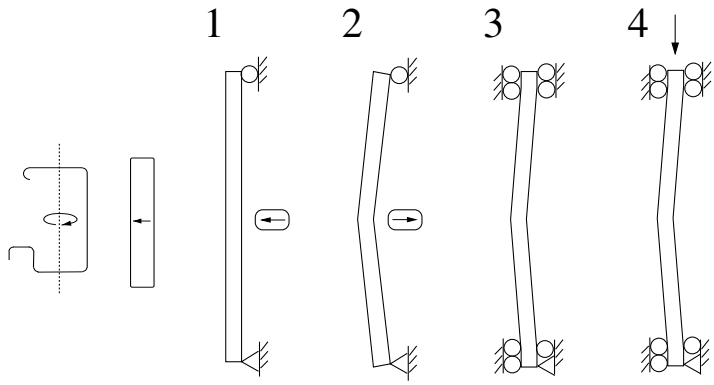

Figure 2: Boundary conditions and load steps in simulation I.

the columns and, as shown in Figs. 3 and 4, all three profiles failed in a combination of flexural and distortional buckling.

In the final step, axial compression was applied to the columns. Different magnitudes of damage, caused by the preloading steps, resulted in different reductions of the load-carrying capacity. Fig. 5 shows the axial load-carrying capacity as a function of the damage magnitude for the three profiles. A value of 100% corresponds to the load-carrying capacity of undamaged columns, which for the asymmetric profile was 183 kN, for the C profile 173 kN, and for the Ω profile 187 kN. The asymmetric profile and the Ω profile were affected by damage in the same extent. The load-carrying capacity was reduced by 50% for damage of approximately 12 mm.

The C profile did not lose as much load-carrying capacity as the other profiles for small damage, but when the rigid body displacement in the first preloading step was increased over a certain magnitude (40 mm) the cross section of the C profile distorted substantially during the third preloading step. This resulted in severe damage, but the representation of damage as defined was not able to capture the distortional part of the deformation. To capture this behavior, it would be necessary to introduce a more sophisticated definition of damage. However, it would then be cumbersome to compare the effects of damage to different profiles as the definition of damage would differ. It would also be more complicated to use the computational results to evaluate the influence of damage to columns in industrial racking systems.

The axial compression stiffness was also affected by damage. Fig. 6 shows, for the asymmetric profile, the axial force as a function of the axial compressive deformation for a number of different damage magnitudes, 0–12 mm in steps of 2 mm. The stiffness decreased with increasing damage magnitudes. However, it can also be seen in Fig. 6 that the load-carrying capacity at the maximum loading was less sensitive to additional axial compressive deformation for columns with large damage. This is an advantageous quality in statically indeterminate systems which are able to redistribute the paths of the loading to other parts of the structure when some structural members are damaged.

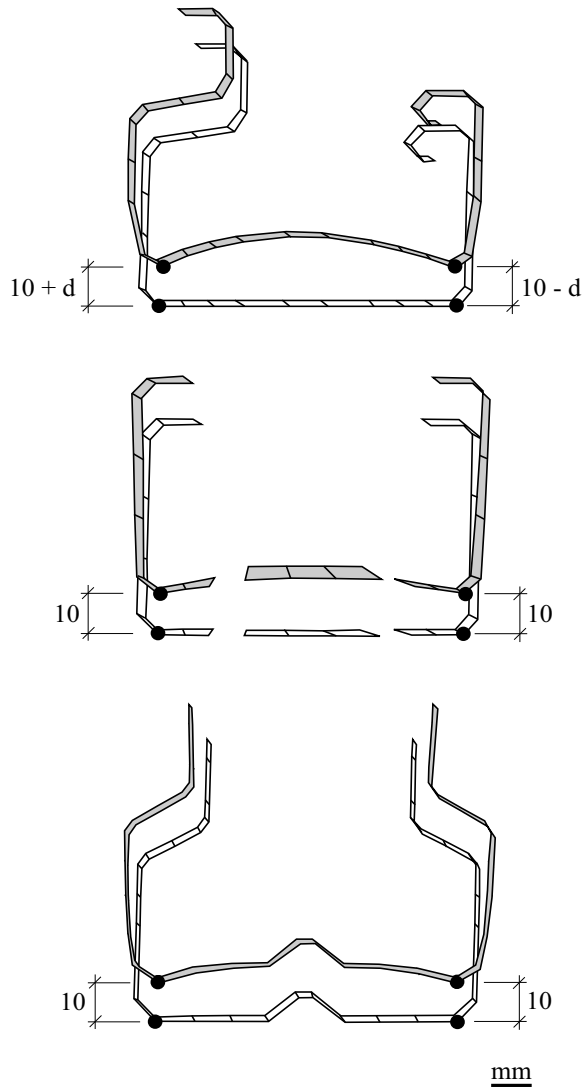

Figure 3: Deformed cross sections.

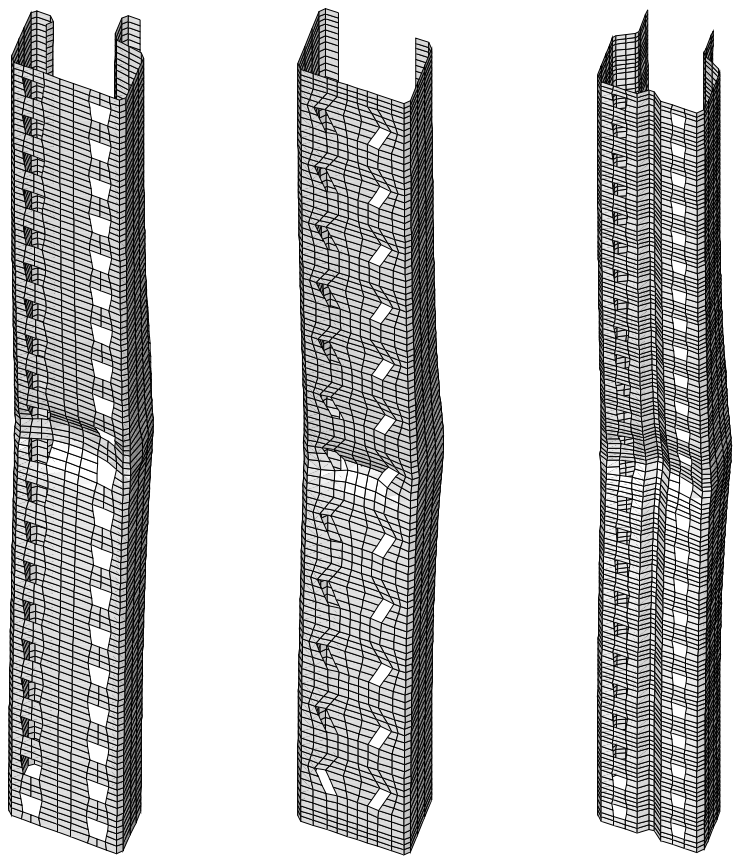

Figure 4: Columns with 10 mm damage.

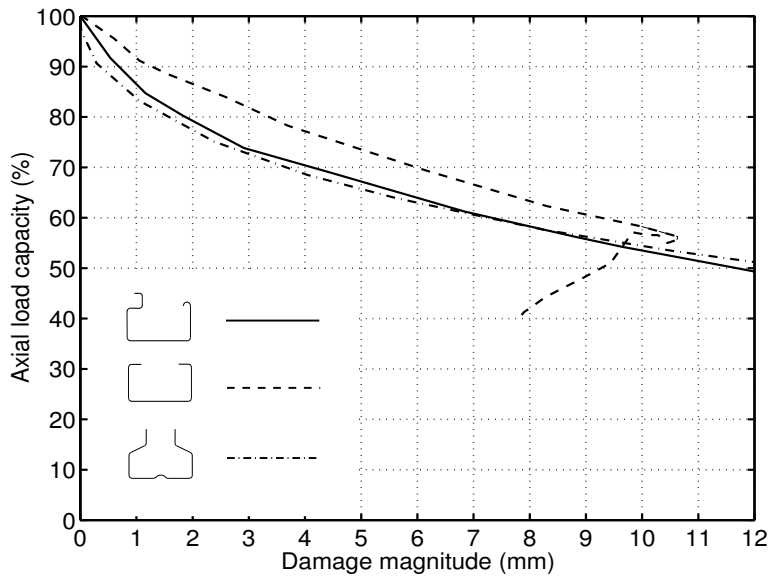

Figure 5: Load-carrying capacity as function of damage magnitude (Simulation I).

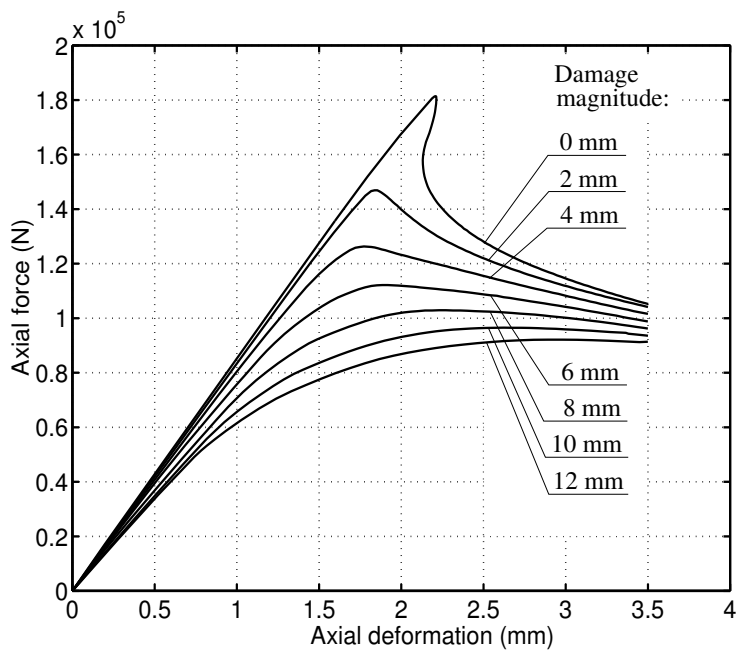

Figure 6: Axial force as function of axial compression for the asymmetric profile.

3.2 Simulation II

The preloading part of this simulation was divided into two steps, identical with the first and second steps of the previous simulation. Thus the boundary conditions allowed the columns to rotate around the axis parallel to the broad side when the axial compression step was applied. The extent of damage was represented as before with the displacements of two nodes at the middle of each column, but the damage magnitude was determined after the second preloading step (Fig. 2). The magnitudes of the different modes of deformation increased almost in proportion to the damage, and it was possible to achieve much higher damage magnitudes than with the previous simulation. Fig. 7 shows the axial load-carrying capacity of the different profiles as a function of the damage magnitude. The 100% load-carrying capacity corresponds to 142 kN for the asymmetric profile, 131 kN for the C profile, and 169 kN for the Ω profile. The reduction of load-carrying capacity due to different damage magnitudes was roughly the same for all the profiles. As in the previous simulation, damage of 10–12 mm resulted in reduction of the load-carrying capacity of 40–50%. Damage of 20 mm resulted in approximately 60% reduction of the load-carrying capacity.

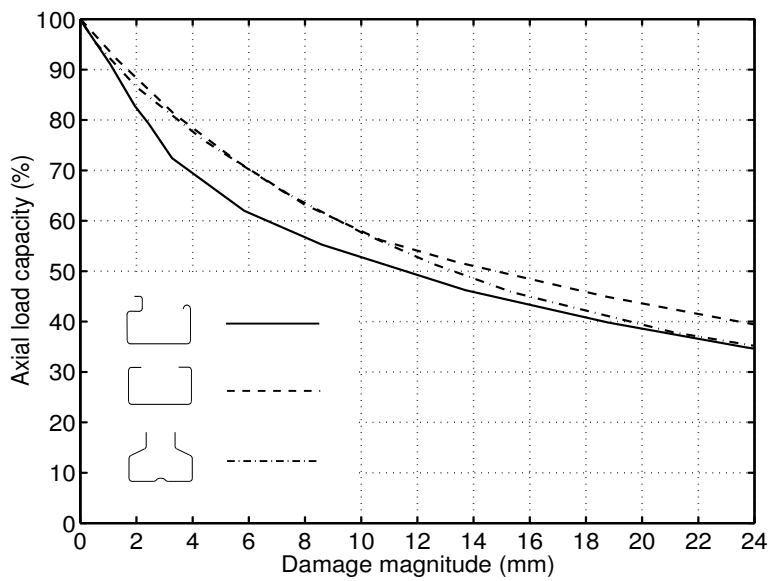

Figure 7: Load-carrying capacity as function of damage magnitude (Simulation II).

3.3 Simulation III

This simulation was performed to investigate the effects of damage caused by impacts to the corners of the profiles. Fig. 8 shows the steps in the simulation. In the first preloading step a rigid body was pressed laterally to the corner of each column at an angle of 45° to the broad side. The supports allowed the columns to rotate around the axes normal to the upright axis, but no twisting was allowed around the upright axis. Then, in the second step, the rigid body was released. Damage was defined as the

displacement, in the plane of the cross section, of the indented corners when the second preloading step was completed. Damage of different extent consisted mainly of bending of the columns, and only moderate distortion of the cross sections occurred. Damage was therefore sufficiently represented by the adopted definition.

As in the previous simulations, the columns were compressed through the centroidal axis in the final load step. Fig. 9 shows the axial load-carrying capacity as a function of the damage magnitude. The 100% load-carrying capacity corresponds to 115 kN for the asymmetric profile, 131 kN for the C profile, and 169 kN for the Ω profile. As the axes parallel to the broad side coincide perfectly with the minor axes of inertia for the symmetric profiles, the load-carrying capacities of those columns were equal to those of simulation II. For the asymmetric profile, however, the load-carrying capacity was 19% lower due to the difference in boundary conditions.

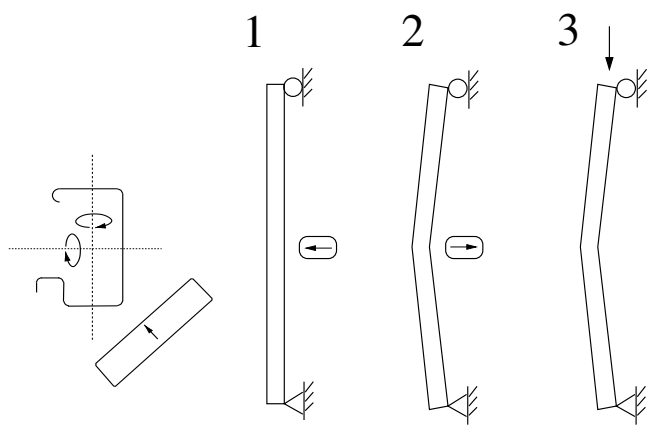

Figure 8: Boundary conditions and load steps in simulation III.

4 Experimental Verification

To evaluate the reliability of the numerical simulations, a laboratory test series was performed. Only the profile with asymmetric cross section was tested, and only one set of boundary conditions was considered. Furthermore, the test series was restricted to six 1250 mm long specimens, of which four were exposed to damage before the axial load-carrying capacity was evaluated.

4.1 Test Setup

The ends of each specimen were welded to rectangular steel plates with edges parallel to the broad side of the profile. The arrangement consisted of a preloading part and an axial compression part. In the first step of the preloading, a solid steel bar, with the same dimensions as the rigid body in the numerical simulations, was pressed to the broad side as indicated in Fig. 10. In the second step, the steel bar was released and the damage magnitude, as previously defined, was recorded. In the last step of the test, the specimen was put into axial compression as shown in Fig. 11. It was compressed

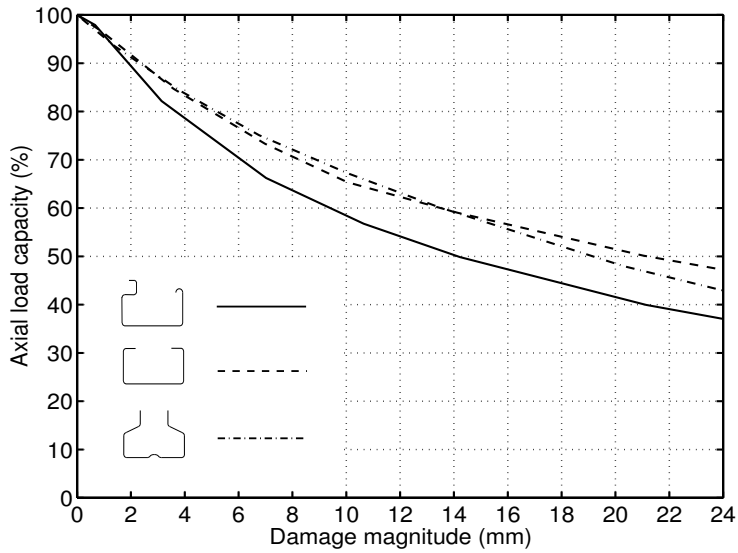

Figure 9: Load-carrying capacity as function of damage magnitude (simulation III).

through the centroidal axis, and a small ball, 28.5 mm in diameter, was placed between two steel plates at each support so that the ends of the profile were free to rotate in any direction.

Figure 10: Compression of a steel bar to the broad side of a column.

Figure 11: Axial compression of a damaged column.

4.2 Comparative Computer Simulation

The boundary conditions in the experimental arrangement differed slightly from those in the second numerical simulation. To imitate the conditions during the test series as closely as possible, an additional simulation was performed. The steps are shown in Fig. 12. In the first preloading step, a rigid body was pressed to the broad side of the profile. The ends of the columns were free to rotate around the axes normal to the upright axis. In the second step, the rigid body was released and the columns were free to rotate around the upright axis as well. Finally, the columns were compressed through the centroidal axis while the boundary conditions allowed them to rotate as in the second load step.

The material parameters were, as previously, evaluated from tension tests of small specimens of steel sheet. However, the properties of specimens from the same delivery as the columns used in the laboratory test series differed from those previously adopted. Due to these new material tests, the yield stress was 15% lower (328 MPa instead of 385 MPa) in this simulation than in simulations I–III.

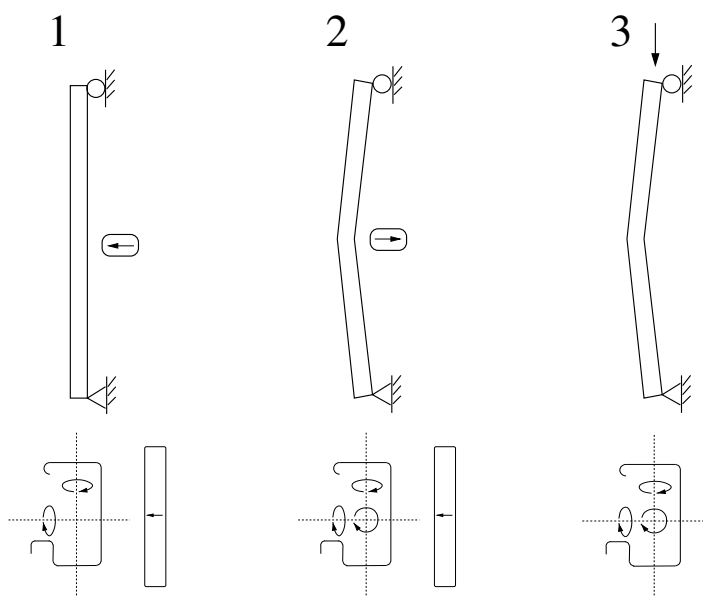

Figure 12: Boundary conditions and load steps in the comparative simulation.

4.3 Results

The results of the laboratory test series in terms of the axial load-carrying capacity, and the corresponding damage magnitudes, are shown in Table 1. The reduction in load-carrying capacity in percent of the capacity of the undamaged column, according to the comparative computer simulation, is also shown. Specimens one and two were not exposed to any preloading, but even the undamaged columns were a little curved, giving displacements of the midsections in relation to the ends. This is equivalent to damage according to the definition. Specimens three and four were aimed to receive

damage of 15 mm, and specimens five and six were aimed to receive damage of 20 mm. Guided by the numerical simulations, the displacement controlled lateral impress of the steel bar was 10 mm deeper than the desired damage magnitudes.

The results from the numerical simulation were in good agreement with the laboratory test series. Fig. 13 shows the results of the test series and the corresponding simulation. The test specimens are represented by the circles, and the computational results are represented by the curve. The load-carrying capacity is shown as a function of the damage magnitude. The 100% load-carrying capacity corresponds to 103 kN, which was the load-carrying capacity for an undamaged column according to the numerical simulation.

Specimen	Damage[a] (mm)	Capacity[b] (kN)	Reduction[c] (%)
1	0.4	97	−5.4
2	0.5	102	−0.5
3	13.6	63	−38.5
4	14.2	57	−44.4
5	21.8	45	−56.1
6	18.9	51	−50.2

Table 1. [a]Damage magnitude. [b]Load-carrying capacity according to laboratory test. [c]Reduction in load-carrying capacity compared to undamaged column in comparative computer simulation.

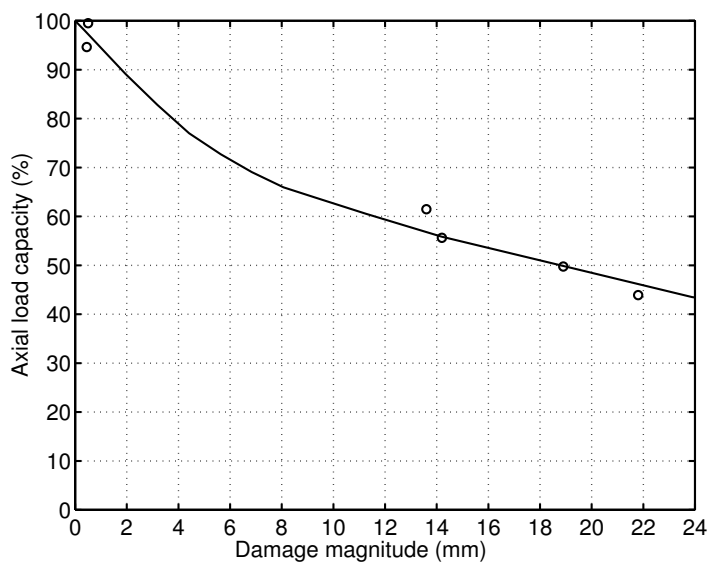

Figure 13: Load-carrying capacity according to the laboratory test series, and the corresponding numerical simulation.

5 Conclusions

Thin-walled steel columns with channel sections damaged by truck impacts are treated in this paper. The study comprised a C profile, an Ω profile, and a profile with asymmetric cross section. Numerical simulations and a verifying laboratory test series were presented. The numerical simulations considered impacts in different directions, for rigid supports as well as for pin-ended supports.

The different profiles were affected by damage to approximately the same extent. For example, it was found that damage corresponding to 10 mm displacement of the midsections of columns with length of 1250 mm resulted in 33–47% reduction of the axial load-carrying capacity. The lower value corresponds to the Ω profile damaged by a rigid body pressed laterally to the column at an angle of 45° to the broad side of the cross section, simulation III. The higher value corresponds to the asymmetric profile damaged by a rigid body pressed laterally to the column in direction normal to the broad side of the cross section (simulation II). The mode of failure for the columns where for all three profiles a combination of flexural and distortional buckling.

The laboratory test series only comprised the asymmetric profile. Damage of 0–22 mm was tested and the results, both in terms of load-carrying capacity and deformation modes, were in good agreement with the results of the corresponding numerical simulation. The work presented in this paper is aimed at increasing the knowledge about how damage to upright members in pallet racks affects their load-carrying capacity, and to increase safety at the working sites where pallet racks are used. Effort is made to present the results in terms that are easy to relate to actual damage in industrial rack and shelving systems.

Acknowledgements

The work was financially supported by the Swedish Council for Work Life Research and carried out in cooperation with the Swedish National Testing and Research Institute. The authors gratefully acknowledge the contributions of Krystoffer Mroz, MSc., at the Swedish National Testing and Research Institute, and Karl-Gustav Carlsson, MSc., at Constructor Sweden AB concerning the contents and scope of the study.

Some earlier work concerning the load-carrying capacity of pallet racks is presented in Mroz (1995), and in Olsson and Sandberg (1998).

References

ABAQUS. (1996). Hibbit, Karlsson, and Sorensen, Inc., Pawtucket, R.I., USA.

Clarke, M. J. (1994). "Chapter 6: Plastic-zone analysis of frames." *Advanced analysis of steel frames: Theory, software, and application*, W. F. Chen, and S. Toma, eds., CRC Press, London.

Davies, J. M., and Leach, P. (1992). "Some applications of generalized beam theory." *11th Int. Spec. Conf. on Cold-Formed Steel Struct.*, Center for Cold-Formed Steel Structures, University of Missouri-Rolla, St. Louis, 479–501.

Hancock, G. J. (1985). "Distortional buckling of steel storage rack columns." *J. Struct. Engrg.*, ASCE, 111(12), 2770–2783.

Mroz, K. (1995). "Load-carrying capacity of pallet racks." *SP Rep. 1995:07,* Build. Technol., SP-Swedish National Testing and Research Institute, Borås, Sweden.

Olsson, A., and Sandberg, G. (1998). "Parameter studies on pallet racks." *Rep. TVSM-7122,* Div. of Struct. Mech., Lund Institute of Technology, Lund, Sweden.

Rasmussen, K. J. R., and Rondal, J. (1997). "Strength curves for metal columns." *J. Struct. Engrg.*, ASCE, 123(6), 721–728.

Schardt, R. (1989). *Verallgemeinerte Technische Biegetheorie (Generalized beam theory).* Springer, Berlin (in German).

Paper V

Failure Sensitivity Analysis of Engineering Structures

by

Göran Sandberg and Anders Olsson

Computers and Structures 72(4–5) 525–534

Failure Sensitivity Analysis of Engineering Structures

Göran Sandberg[1] and Anders Olsson[2]

Computers and Structures 72(4–5) 525–534

Abstract

The present paper suggests a method to consider uncertainties in engineering structures in a computational scheme. Latin hypercube sampling is used to prepare input data of probabilistic parameters for subsequent deterministic simulations where the mechanical response is evaluated. The approach is applied on a pallet rack system where damaged columns and connector stiffnesses are considered as probabilistic parameters. The mechanical simulations are performed with the finite element method, and full advantage is taken of existing commercial code.

Keywords: finite element method, sensitivity analysis, uncertainties, probabilistic parameters, Latin hypercube sampling, pallet rack.

1 Introduction

Computational mechanics has led to elaborate deterministic numerical methods and models, including sophisticated strategies for dealing with a variety of mechanical processes. Nowadays it is common practice in the design of engineering structures to rely on computational analysis. However, in most design cases the engineer is left with uncertainties about how to actually model a structure. The uncertainties can be directed towards the stiffness values of structural members or connections, or geometrical or material properties. Also production errors or damage, caused by accidents or inadequate management, are in many civil engineering structures uncertain parameters that should be considered in the analysis. Another question is how the load is applied and, in dynamic analysis, the time history of the load.

There is a growing realization that unavoidable uncertainties must be considered in a computational scheme to produce reliable computational and engineering results. Traditionally, designers have used safety factors to provide increased confidence in the structural performance. However, this approach does not take into account the underlying, more sophisticated probability characteristics and does not provide the designer with adequate information about the reliability. This has lead to rather extensive research aiming to combine efficient methods of structural analysis with stochastic analysis where the influence of random variables is evaluated.

[1]Prof. Division of Structural Mechanics, Lund University, P.O. Box 118, SE-221 00, Lund, Sweden.
[2]Division of Structural Mechanics, Lund University, P.O. Box 118, SE-221 00, Lund, Sweden.
Telephone: +46 46 222 46 89. Fax: +46 46 222 44 20.

The finite element method, which is the dominating numerical tool in deterministic analysis, is the basis of many methods involving random parameters. Stochastic finite element approaches are based on the representation of stochastic fields as a series of random variables. The probabilistic design parameters are represented in the system matrices, often at the element level, by submatrices containing the nominal or mean values of the uncertain parameters and other submatrices considering the perturbation of the parameter values. The size of the system matrices increases rapidly with the number of probabilistic parameters and the order of the series expansion, see e.g. Jensen [1]. Kleiber and Hien [2] give a theoretical background in stochastic finite element analysis. The applicability of these methods is, however, limited since they in most cases are not capable of dealing with problems involving non-linearities or dynamic loading. Furthermore they are accurate only for small values of variability of the stochastic properties. Many methods also place restrictions on the element mesh.

A simple and widely used strategy for dealing with probabilistic parameters is Monte Carlo Simulations. The probabilistic input parameters are sampled from their distributions and a number of deterministic computations are performed to provide information about the distribution of the output parameters. This approach is the most accurate one and it is able to handle any mechanical processes which the deterministic methods are dealing with. The disadvantage is the computational cost, frequently very high due to the repeated analyses that have to be performed. In order to keep the computational cost low and be able to handle complex mechanical processes, combinations of stochastic finite element approaches and Monte Carlo simulations are suggested, see e.g. Papadrakakis and Papadopoulos [3]. A remaining disadvantage, however, common for most probabilistic methods, is the need for considerable revision in the finite element software developed for deterministic analysis.

In the present paper a Monte Carlo simulation approach, based on the Latin hypercube sampling plan, is applied to analyse the failure sensitivity of a complex civil engineering structure in an efficient manner. Latin hypercube sampling gives a good representation of the input distribution with proportionately few samples. The structure considered is a pallet rack system of a type frequently used in industry. The influence of damage to thin-walled steel columns and the influence of variations in connector stiffnesses are investigated. The sampling plan is only used to prepare the input data for the subsequent analyses. Thus the influence of uncertainties are evaluated without any revision of the deterministic finite element code, in this case ABAQUS [4]. The present procedure is aimed not only towards advanced and unique problems, but also towards everyday engineering design practice.

Sensitivity has a precise mathematical significance. In this paper, however, sensitivity is more of system sensitivity for engineering structures. Thus it has here a more general meaning.

2 Latin Hypercube Sampling

The Latin hypercube sampling plan was theoretically described in 1979 in a paper by McKay et al. [5]. The desired accuracy in the estimated distribution function determines the required number of simulations. Let n denote the required number of simulations and k the number of uncertain parameters; the sampling space is then k-dimensional.

The sampling plan is constructed as follows. For each of the k parameters, divide the outcome into n intervals with equal probability of occurrence and construct a column matrix with permutations of the integers $1, 2, \ldots, n$. Note that two such matrices can be identical. By putting the column matrices together, an $n \times k$-matrix is obtained. Each row in that matrix defines a k-dimensional hypercube cell in the sampling space. Take one random sample from each such cell. For two input variables with a uniform (0,1) distribution and five simulations, a possible sampling plan is shown in Fig. 1. Note that the samples are spread over the entire sampling space as the generation of the Latin hypercube sampling plan requires one sample from each row and each column. If n samples from the entire sampling space had been chosen completely at random, there is a risk that they would form a cluster and some parts of the sample space would not be investigated. For sampling in higher dimensions than three it is not possible to visualize the sampling plan, but it is clear that n samples spread over the whole sampling space are obtained. An interesting overview on different sampling plans is found in Kjell [6], and applications to structural analysis are suggested in Sandberg et al. [7].

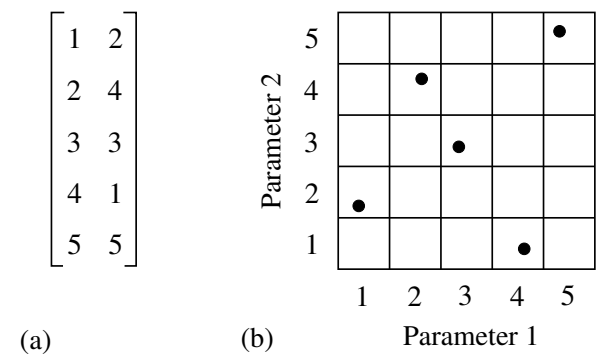

Figure 1: Latin cube, two parameters and five calculations. The 5×2 matrix (a) determines the plan illustrated in (b).

3 Load-carrying Capacity of Pallet Racks

The development of pallet racks and other load-carrying systems is undergoing a rapid growth, and progressively higher pallet racks are being designed. The development is requested by industry, and the competition between different manufacturers makes it necessary to minimize the cost of materials and production. Uncertainties in strength and stiffness of different structural members occur and cause uncertainties in the structural performance. This results in difficulties in achieving valid guarantees of the load-carrying capacity. To preserve the safety and serviceability at the working site, additional knowledge concerning the mechanical behaviour and the influence of changing different parameters in pallet racks is therefore needed.

In this paper the influence of two different parameters are studied with respect to the load-carrying capacity. At first the effect of damage to thin-walled steel columns with open cross-sections is evaluated. Damage could for instance be caused by trucks

running into the columns. The study comprises a close, deterministic investigation of the reduction in load-carrying capacity of individual columns due to different damage levels, and a global, probabilistic analysis of the influence of damaged columns in an entire pallet rack system. The analysis of the local, single column, level is only briefly discussed in this paper, see Olsson and Sandberg [8] for further details. The second parameter is the stiffness of the connectors between columns and horizontal beams. The influence of variations in stiffness between different connectors is investigated.

3.1 Damaged Thin-walled Steel Columns

A model of an upright profile is built up of shell elements. The model describes the geometry of the profile in detail and is able to capture both in-plane and out-of-plane deformation of the cross-section. An elasto-plastic material model is used, and large deformation theory is applied. The length of the column is 1,250 mm, which corresponds to the height of one compartment in the global pallet rack considered in the following study.

Simulations are performed to apply damage of different magnitudes to the profile and evaluate the influence of damage on the axial load-carrying capacity. The first part of the simulation, divided into three steps, applies the damage to the structure. At first the broad side at the middle of the column is compressed by a rigid body in direction normal to the broad side. There is no friction between the rigid body and the deformable structure. The column is supported so that it is free to rotate around the in-plane axis of the cross-section, parallel to the broad side. Then the rigid body is released and loses contact with the structure. If the compression was big enough to cause yielding in the material, there will be remaining deformations in the structure. Finally the ends of the column are bent so that the cross-sections at the supports end up normal to the original upright axis. Fig. 2 shows the result of these steps in the simulation, a damaged column. Depending on the magnitude of the rigid body compression, different damage levels are obtained. Damage is represented by the imperfection, or the displacement of the cross-section at the middle of the column.

The second part of the simulation puts the column into axial compression. Fig. 3 shows the axial force as a function of the axial displacement for a number of columns with different damage levels (0–12 mm) and Fig. 4 shows the remaining load-carrying capacity as a function of the initial damage level. It is shown that even very small damage causes significant reduction in strength and stiffness. For example, a 12 mm imperfection causes a 50% reduction of the axial load-carrying capacity. However, to investigate the global influence of damage an entire pallet rack must be analysed.

3.2 Damaged Columns Modelled by Beam Elements

To achieve a reasonable size of the stiffness matrix of a global pallet rack model, the properties of damaged columns must be transformed from the shell model to a more simple beam model. In the shell structure, damage involved bending of the upright axis as well as in-plane deformation of the cross-section. To capture the effects of damage in the beam model, changes in two different characteristics are performed. The first change affects the geometry. An imperfection, equal to the damage level defined for the shell model, is introduced. This decreases the stiffness and strength of the beam structure,

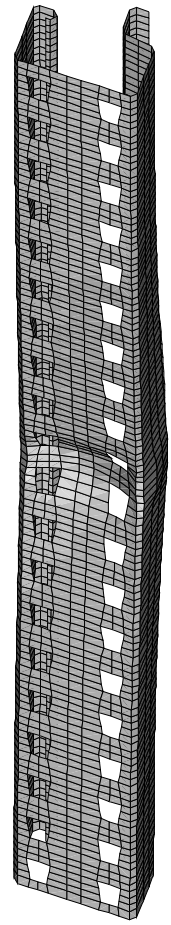

Figure 2: Damaged column according to the computer simulation.

but not as mush as the corresponding damage in the shell structure. To adjust the damage effects, the material properties are involved. For increasing damage levels the yield stress of the material in the beam structure is decreased. The reduction of the yield stress is adjusted to achieve equal reduction in load-carrying capacity according to the different models. The calibration results in good agreement concerning axial stiffness, axial load-carrying capacity, and stiffness to bending. Fig. 5 shows the principal features of the calibration process.

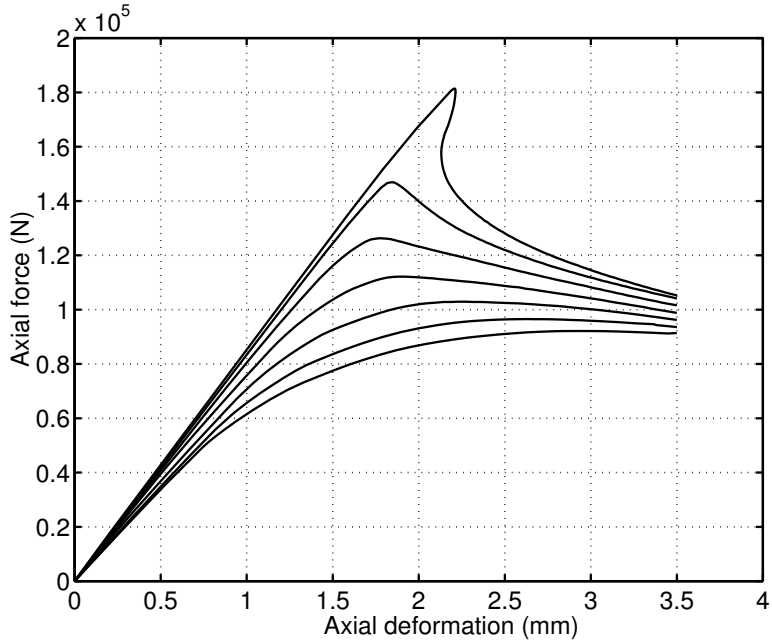

Figure 3: Axial force as a function of axial deformation.

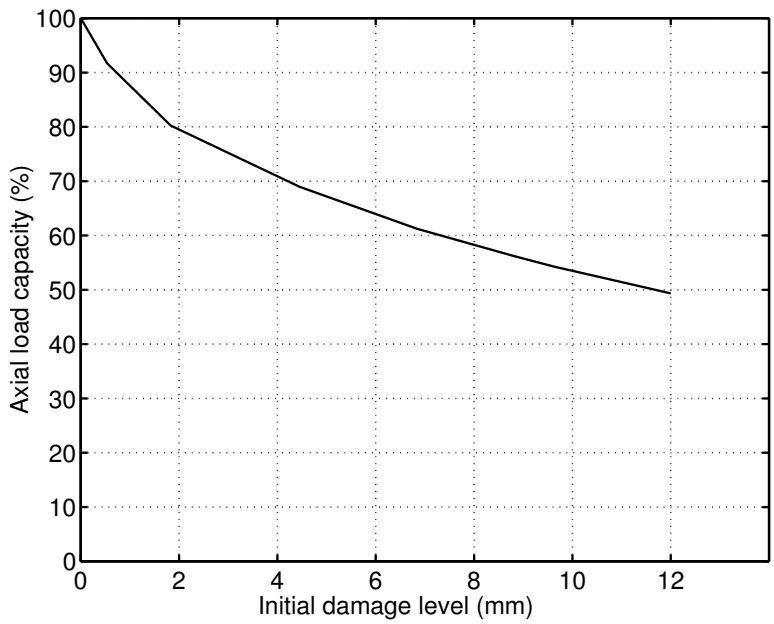

Figure 4: Remaining load-carrying capacity as a function of initial damage level.

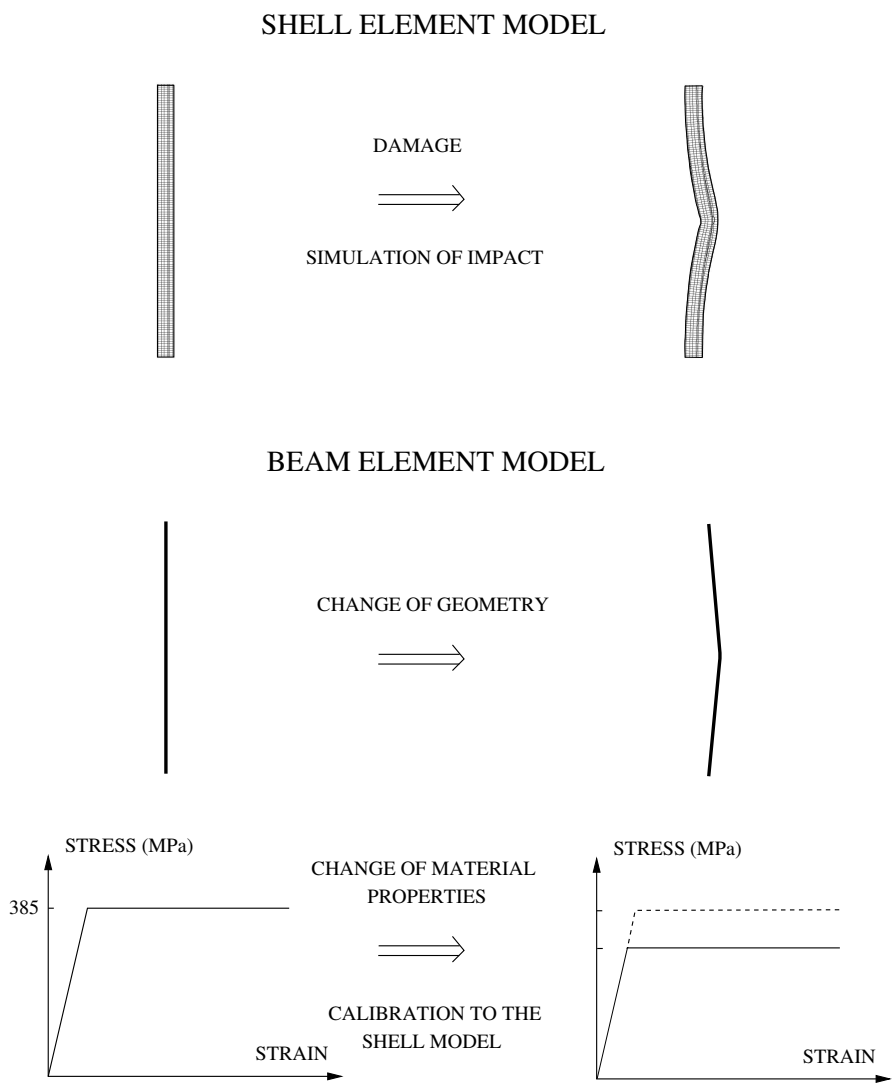

Figure 5: Damage as applied to the shell element model and to the beam element model.

3.3 Global Analysis of a Pallet Rack

The pallet rack in the present study contains five sections and four horizontal beam levels. Fig. 6 shows the geometry of the structure. The components in the pallet rack are typical for many racking systems used in industry. Laboratory tests, as well as numerical simulations, are performed to evaluate their mechanical properties, see Mroz [9].

The columns are modelled by beam elements which are able to capture torsion and warping of the cross-section. The horizontal beams are modelled by ordinary beam elements according to Timoshenko beam theory, and the diagonal elements, used for stabilization of the pallet rack in the cross-aisle direction, are modelled by truss elements, i.e. with pinned connections to the columns. The connections between the horizontal beams and the columns are modelled as finite elements with specified non-linear stiffness, evaluated from tests. The floor end connectors are modelled in the same manner. Large displacements are considered in the model as well as material non-linearities.

Fig. 7 shows the load configuration in the pallet rack. In the first load step the box loads and the corresponding horizontal loads are applied. Each box in the model represents a load of 10 kN and the horizontal loading amounts, in accordance with the FEM norm [10], to 0.31% of the vertical loading at the corresponding beam level. The pallet rack is also loaded by the weight of its own components. In the second load step the vertical loads at the columns at the top of the pallet rack and the corresponding horizontal loading are applied. The magnitude of the top loads is increased until failure occurs. Fig. 8 shows the three-dimensional structure of the pallet rack without damage, and the failure mode due to the loading applied, a global down-aisle sway mode.

3.4 Damage Distribution in Pallet Racks

As the exact damage locations and damage magnitudes in a pallet rack are not known, it is not possible to perform an accurate deterministic computation to evaluate the influence of the damage. However, if the distribution of damage is known or can be estimated, this would be enough to perform a probabilistic analysis and find the distribution of the global load-carrying capacity. Inspections of pallet racks have shown that the main part of the damage is located in the lower parts of the pallet racks since impacts often occur there. It is also clear that the loading is bigger in the lower parts of the structure and damage there is likely to be of greater importance than damage in the upper parts of the structure.

In the present analysis it is assumed that every column in the lowest level of the pallet rack is damaged. The damage is of the type presented above and is located with equal distance to the floor and the lowest horizontal beam level. The damage magnitudes for the 12 columns are assumed to be uniformly distributed in the interval 0–12 mm.

3.5 Probabilistic Analysis of Global Influence of Damage

The Latin hypercube sampling plan is used to choose damage magnitudes for the 12 columns for a number of finite element simulations. The technique is already generally described, but the procedure for the present application is also presented with an example where input data to four deterministic computations are to be performed. Twelve

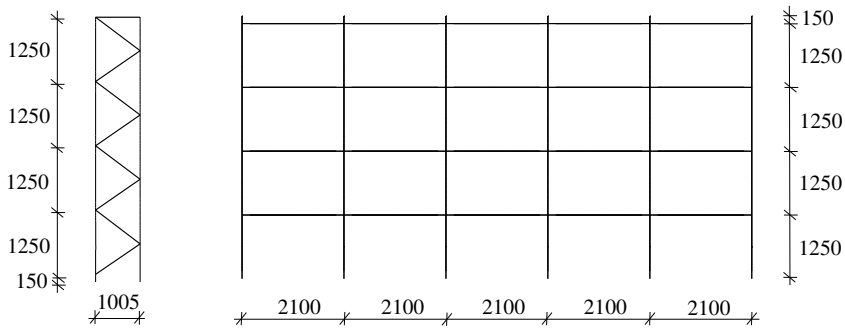

Figure 6: Geometry of the pallet rack. Lengths given in mm.

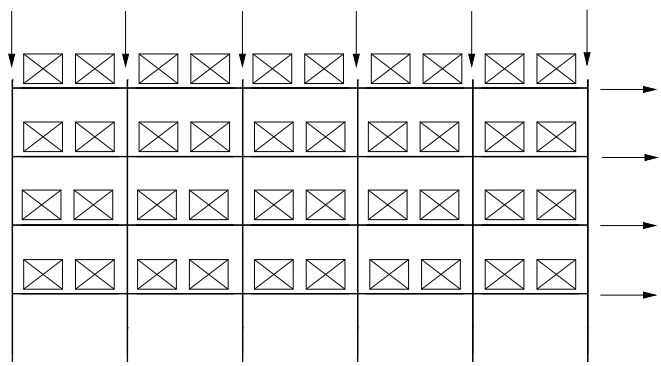

Figure 7: Load configuration in the pallet rack.

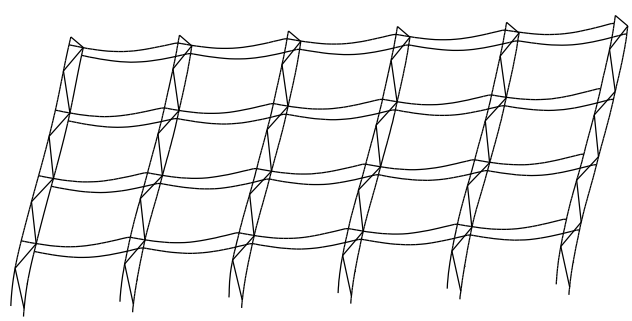

Figure 8: Failure mode for the pallet rack.

columns are damaged, i.e. $k = 12$, and four different damage cases are considered, i.e. $n = 4$. The sampling space for the 12 parameters is divided into four intervals.

$$Intervals: \begin{bmatrix} 1 \\ 2 \\ 3 \\ 4 \end{bmatrix} \quad correlates\ to \quad \begin{bmatrix} 0 - \frac{1}{4} \\ \vdots \\ \frac{3}{4} - 1 \end{bmatrix}$$

Twelve permutations of the damage intervals are performed.

$$Perm.\,1 = \begin{bmatrix} 3 \\ 1 \\ 4 \\ 2 \end{bmatrix} \quad Perm.\,2 = \begin{bmatrix} 1 \\ 4 \\ 2 \\ 3 \end{bmatrix} \quad \cdots \quad Perm.\,12 = \begin{bmatrix} 4 \\ 2 \\ 1 \\ 3 \end{bmatrix}$$

A matrix, four rows and 12 columns is established from the permutations.

$$\begin{bmatrix} 3 & 1 & \dots & 4 \\ 1 & 4 & \dots & 2 \\ 4 & 2 & \dots & 1 \\ 2 & 3 & \dots & 3 \end{bmatrix}$$

For each component, i.e. interval in the matrix above a random value is picked and multiplied by 12 mm. A new matrix is then established in which each line contains the damage magnitudes for the 12 columns for one deterministic computation.

$$\begin{bmatrix} 7.2 & 1.7 & \cdots & 9.2 \\ 1.9 & 11.6 & \cdots & 5.4 \\ 10.7 & 4.9 & \cdots & 0.8 \\ 3.4 & 7.1 & \cdots & 8.7 \end{bmatrix} \text{(mm)}$$

The damage magnitudes affect, as described above, the geometry and material for each of the 12 columns.

Fig. 9 shows the computational results in terms of the distribution of the load-carrying capacity for simulations with $n = 30$, $n = 100$ and $n = 300$. The load-carrying capacity is approximately uniformly distributed according to the simulations. The distributions become smoother when the number of samples increases, but even the 30-sample simulation gives a good representation of the variation of the load-carrying capacity. Failure arises for load levels between 0.68 and 0.86 (MN), where the latter value is equal to the failure load for a pallet rack without damage. The damage distribution causes a reduction in the load-carrying capacity of up to 20%. For all the damage cases considered in the simulations, the pallet rack fails in a global down-aisle sway mode as for a pallet rack without damage.

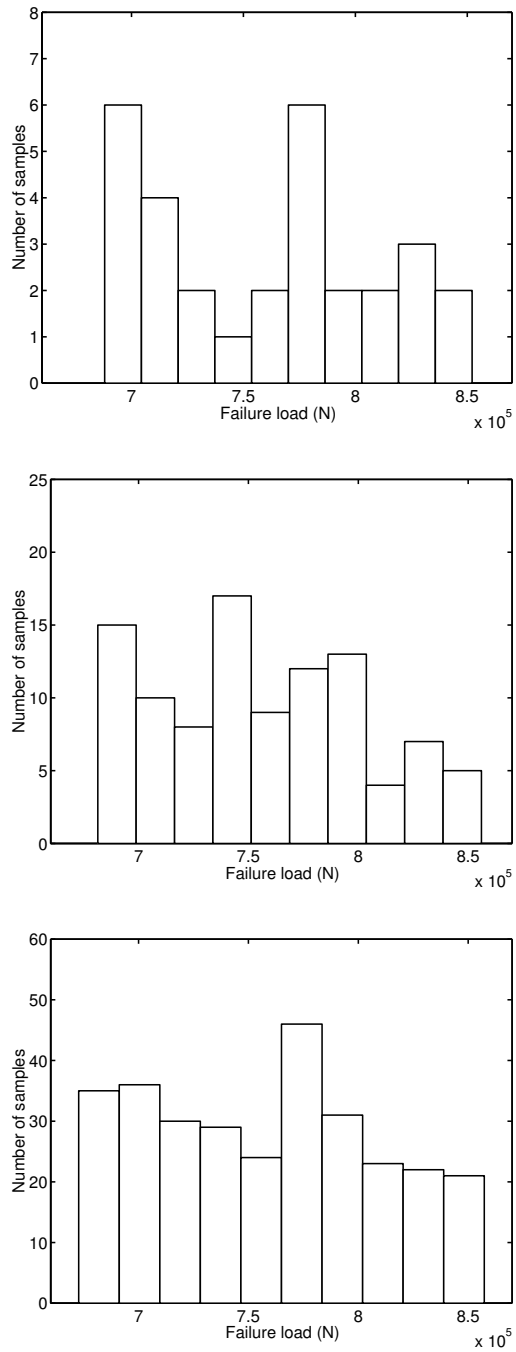

Figure 9: Distribution of the load-carrying capacity, with 30 samples, 100 samples, and 300 samples.

3.6 Stiffness of Beam end Connectors

Many pallet rack systems are designed without stabilizing bracing members in the down-aisle direction. The stiffness in that direction is then obtained with the framework of the horizontal beams and the columns. In this type of structures the stiffnesses of the beam end connectors are of vital importance for the behaviour of the pallet rack, and if failure occurs in a global down-aisle sway mode, as is the case for the pallet rack considered in this paper, the load-carrying capacity of the entire pallet rack is dependent on the stiffnesses of these connectors.

3.7 Connector Stiffnesses as Probabilistic Parameters

There are always individual differences in the stiffness relations of the beam-end connectors in a structure. Usually mean values of stiffness and failure moment, including safety factors, are evaluated from tests of a number of specimens and used as design values for all the connectors in the structure. In this study the sensitivity with respect to the failure load is investigated when individual connector stiffnesses, picked from known distributions, are applied to the pallet rack model. Fig. 10 shows the bending moment as a function of the rotation for five specimens tested according to the recommendations in FEM [10]. Five specimens are too few to draw any reliable conclusions about the distribution of the stiffness, but the aim of this analysis is to illustrate a method to evaluate the distribution of the load-carrying capacity when the distribution of the connector stiffnesses is known. It is assumed that the bending moment, at a number of different rotations, is normally distributed. Mean values and standard deviations are then computed. Fig. 11 shows a schematic sketch of the mean stiffness curve evaluated from the curves in Fig. 10. The lengths of the vertical bars indicate the size of the standard deviations at different rotations. Each bar is divided into a number of intervals where all the intervals represent equal probability.

Latin hypercube sampling is used to produce an optional number of stiffness intervals. From the sampling plan each connector stiffness is only represented by one interval from the uniform (0,1) distribution, as in the preceding study on damaged columns, but in the finite element model each stiffness curve is defined by five rotations and five corresponding bending moments. To prepare each curve, five random values are picked from its interval and mapped on five normal distributions, with mean values and standard deviations evaluated from the laboratory test. The mapping is performed according to Eq. (1) and illustrated in Fig. 12.

$$N(r) = \sqrt{2}\sigma \; erf^{-1}(2r-1) + m \tag{1}$$

where

$$erf(2r-1) = \frac{2}{\sqrt{\pi}} \int_0^{2r-1} e^{-t^2} dt \tag{2}$$

In Eq. (1) σ is the standard deviation, m is the mean value, r is a random value from the current interval, and $N(r)$ is the value of r mapped on the normal distribution. If the sampling space is divided into four intervals, 4×80 stiffness curves are established. A possible result of the procedure for one connector is shown in Fig. 13.

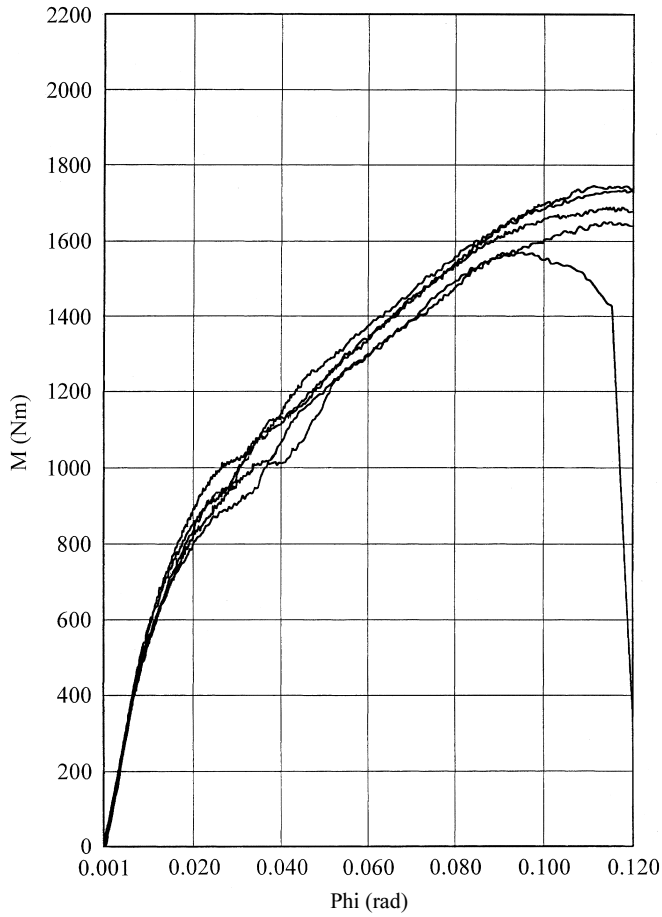

Figure 10: Stiffness curves of beam-end connectors according to laboratory test.

3.8 Influence of Variations in Connector Stiffnesses

Simulations with $n = 30$, $n = 100$ and $n = 300$ are performed. Fig. 14 shows the distribution of the load-carrying capacity according to the simulations, and Table 1 shows the mean values and the standard deviations of the connector stiffnesses and the load-carrying capacity. The standard deviation of the load-carrying capacity is very small compared to the standard deviations of the connector stiffnesses. This means that the global stiffness, and global load-carrying capacity are not very sensitive to variations around the mean values of the connector stiffnesses. This does not imply that the behaviour of the pallet rack is insensitive to variations of the mean value of the connector stiffnesses, but it could be concluded that in this particular case it is sufficient to treat the connector stiffnesses as deterministic parameters.

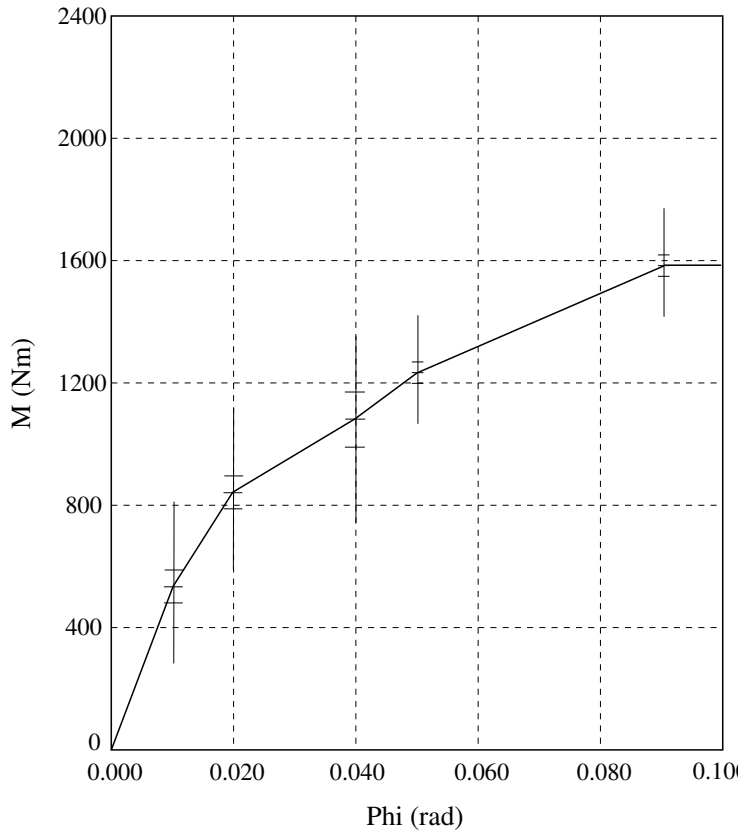

Figure 11: Mean stiffness curve of the beam-end connectors.

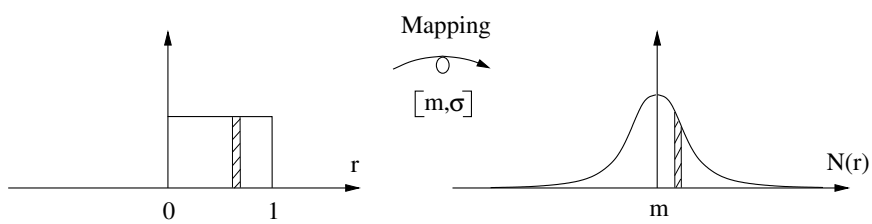

Figure 12: Mapping of a uniform distribution on a normal distribution.

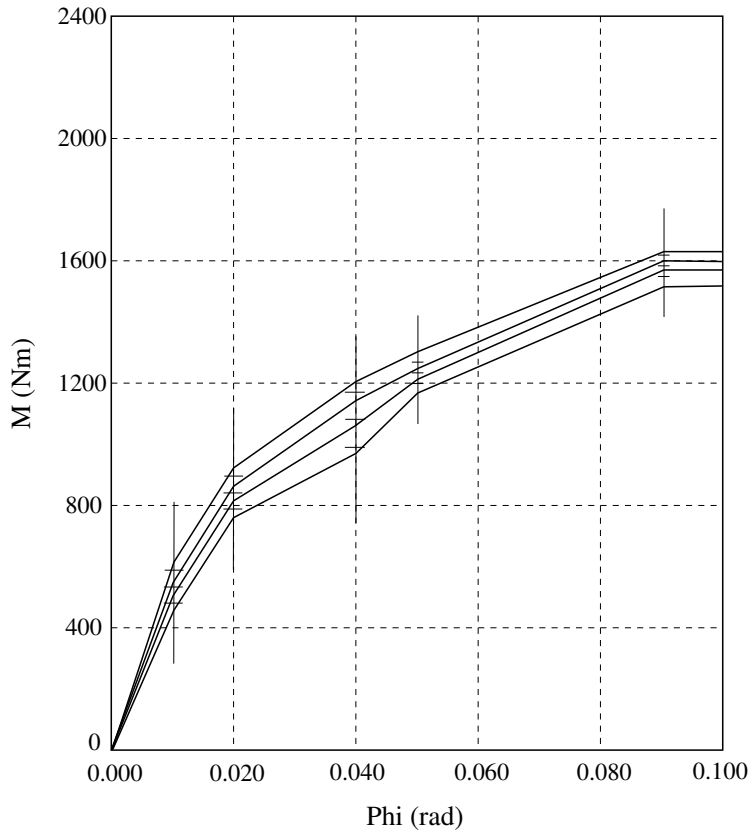

Figure 13: Possible generated stiffness curves.

Parameter	Mean value	Standard deviation	
$M(\phi = 0.010$ rad)	559 Nm	18.6 Nm	3.3%
$M(\phi = 0.020$ rad)	838 Nm	31.0 Nm	3.3%
$M(\phi = 0.040$ rad)	1092 Nm	48.5 Nm	4.4%
$M(\phi = 0.050$ rad)	1222 Nm	35.7 Nm	2.2%
$M(\phi = 0.090$ rad)	1592 Nm	34.0 Nm	2.1%
L-c. c. 30 samples	865.9 kN	3.19 kN	0.37%
L-c. c. 100 samples	865.8 kN	2.38 kN	0.27%
L-c. c. 300 samples	865.6 kN	2.68 kN	0.31%

Table 1. *Mean values and standard deviations of connector stiffnesses and load-carrying capacity (L.c.c).*

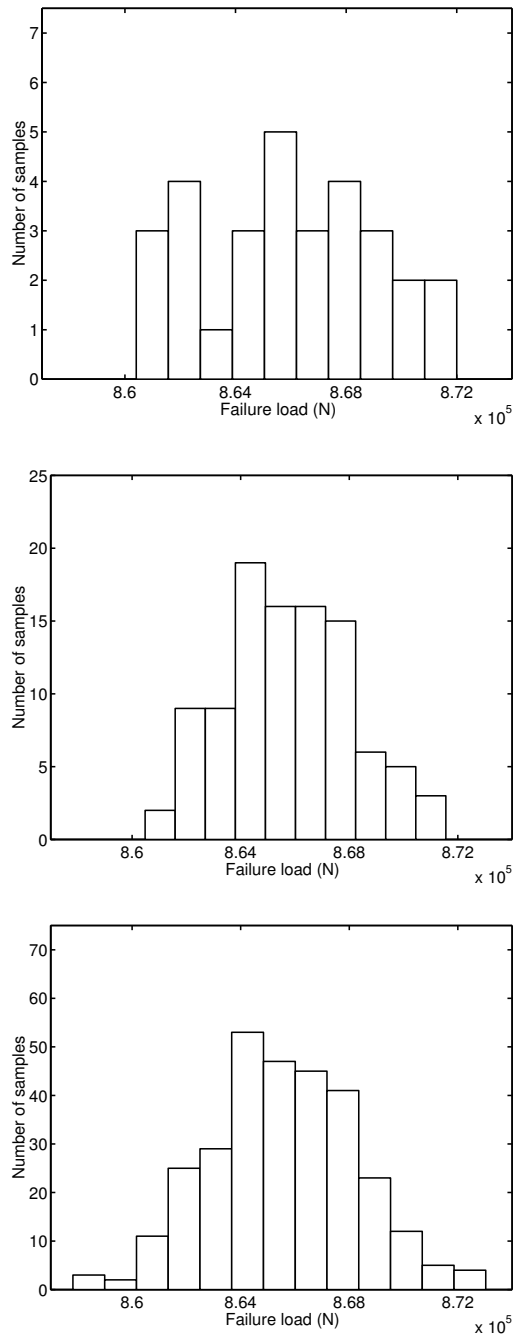

Figure 14: Distribution of the load-carrying capacity, with 30 samples, 100 samples, and 300 samples.

4 Summary and Conclusions

In this paper Latin hypercube sampling is used to prepare input data of probabilistic parameters to deterministic finite element analyses where non-linearities in structural behaviour are considered. An analysis of a pallet rack system shows that small damage to thin-walled steel columns is of great importance for the load-carrying capacity of the entire pallet rack as well as for the load-carrying capacity of individual columns. In a global pallet rack model damage is treated as a probabilistic parameter since it is impossible to predict the exact locations and magnitudes of damage. The simulation shows that damage corresponding to less than 12 mm imperfections causes reduction of the global load-carrying capacity of up to 20%.

The influence of deviations in the connector stiffnesses is also investigated. Laboratory tests of a few connectors are used to evaluate mean values and standard deviations of the stiffness relation. Synthetic stiffness curves are then generated and applied in the finite element model. The simulation shows that the global stiffness and thereby the load-carrying capacity are not very sensitive to deviations around the mean stiffness of the connectors.

The approach with Latin hypercube sampling allows the designer to analyse engineering structures, with probabilistic parameters, without keeping back the possibilities of using elaborate models and existing, deterministic codes. Compared to Monte Carlo simulations, where the samples are chosen completely at random, the representation of the distributions of the inputs are more accurate with the same number of samples.

References

[1] Jensen HA. A global sensitivity analysis in structural mechanics. Comput Struct 1995;56:903–15.

[2] Kleiber M, Hien TD. The stochastic finite element method. Chichester: Wiley, 1995.

[3] Papadrakakis M, Papadopoulos V. Robust and efficient methods for stochastic finite element analysis using Monte Carlo simulation. Comput Meth Appl Mech Engng 1996;134:325–40.

[4] Hibbitt, Karlsson, Sorensen. Inc. ABAQUS, Version 5.6., Pawtucket 1996.

[5] McKay MD, Conover WJ, Beckman RJ. A comparison of three methods for selecting values of input variables in the analysis of output from a computer code. Technometrics 1979;21:239–45.

[6] Kjell G. Computer experiments with application to earthquake engineering. Department of Mathematical Statistics, CTH, Studies in statistical quality control and reliability 1995 7, Gothenburg.

[7] Sandberg G, Kjell G, de Maré J. Computational planning using Latin hypercube sampling. Report TVSM-7118, Lund Institute of Technology, Division of Structural Mechanics, Lund 1997.

[8] Olsson A, Sandberg G. Parameter studies on pallet racks. Report TVSM-7122, Lund Institute of Technology, Division of Structural Mechanics, Lund 1998.

[9] Mroz K. Load-carrying capacity of pallet racks. SP report 1995:07, SP-Swedish National Testing and Research Institute, Building Technology, Borås 1995.

[10] Federation Européenne de la Manutention (pre Norm) Recommendations for the Design of Steel Static Pallet Racking (January 1996), Section X, Manchester 1996.

Paper VI

Probabilistic Analysis and Optimization of Roof Trusses

by

Anders Olsson

Submitted for publication in
Electronic Journal of Structural Engineering

Probabilistic Analysis and Optimization of Roof Trusses

Anders Olsson[1]
Division of Structural Mechanics, Lund University
Submitted for publication in Electronic Journal of Structural Engineering

Abstract

The influence of gaps between wooden members and displaced nail plates in roof trusses is investigated by means of probabilistic calculations and structural optimization. The employed mechanical model, using the finite element method, captures the non-linear behaviour of the nail-plate joints. The joint stiffness involves the size and location of the nail plate and the presence of contact or gap, respectively, between the wooden members. The analysis shows that even small initial gaps considerably increase the deflection of a roof truss. Misplaced nail plates also affect the deflection negatively, but it is also shown that the deflection can be significantly decreased, and the utilization of nail plates improved, by optimizing the nail-plate positions with respect to critical load cases and requirements.
Keywords: roof truss, nail-plate joint, geometrical imperfection, gap, finite element, probabilistic calculation, optimization.

1 Introduction

Wooden roof trusses with nail-plate joints are widely employed in modern roof construction. In Sweden, for example, roof trusses with nail-plate joints constitute the main load-carrying system of the roof structure in more than 50% of all residential buildings. This large volume makes a detailed understanding of the mechanical behaviour of these structures vital, as it is necessary in order to secure a satisfactory safety level and serviceability of the structures and to achieve an optimal use of resources in terms of material consumption and manufacturing control.

In addition to a detailed mechanical modelling of ideal roof trusses and nail-plate joints, it is important to consider uncertainties in material properties and in geometrical imperfections. Such uncertainties may significantly affect the stiffness and load-carrying capacity of wooden roof trusses. Variations in stiffness and strength of wood material have been studied by several researchers, e.g. Isaksson (1999), and probabilistic models for wood have been applied on roof trusses, aiming at a better understanding of the actual safety levels (Hansson 2001). Research with a probabilistic approach on geometrical imperfections in nail-plate joints have, however, to the author's knowledge, not

[1]Division of Structural Mechanics, Lund University, P.O. Box 118, SE-221 00, Lund, Sweden. Telephone: +46 46 222 46 89. Fax: +46 46 222 44 20.

been carried out before. The present paper is the result of ongoing research on roof-truss modelling and geometrical imperfections. It presents models and calculations of the influence of misplaced nail plates and gaps between wooden members in roof trusses. The research also aims at the development and comparison of methods for probabilistic analysis and optimization that can be efficiently employed in conjunction with non-linear finite element models of roof trusses and structural systems in general.

2 Modelling of Roof Trusses

2.1 Overview of Methods

In commercial software for roof-truss analysis, the nail-plate joints are typically regarded as either rigid or pin-ended, and the wooden members are modelled by beam elements with a linear elastic behaviour. Several such models have been collected and evaluated by Petersson and Olsson (1994) and Olsson and Rosenqvist (1996). In reality, however, nail-plate joints have complicated stiffness properties. The load-deformation relation cannot be expected to behave linearly and when approaching the limit-state loading, the failure of a joint, and thereby the entire truss, may be caused by different phenomena such as fracture in the wooden members, pull-out behaviour of the nails or buckling of the nail plates. Thus, this type of modelling only gives rough predictions of failure or unacceptable deformations through indirect criteria specified by structural codes. The codes, in turn, must rely on more advanced models and calculations in combination with laboratory tests.

Linear and non-linear elastic models considering joint deformations have also been developed. Foschi (1977) presented a model for nail-plate joints, capable of capturing the nail stiffness for different orientations in relation to the loading and wood-fibre direction. It was also capable of capturing local plate buckling and gaps or contact, respectively, between wooden members. The key work by Foschi has been followed by further development, modifications and software development (e.g. Petersson and Olsson 1994; Olsson and Rosenqvist 1996; Nielsen 1996; Berglund and Holmberg 2000; Ellegaard 2001).

More advanced models, using 2D or 3D finite elements, plasticity theory and fracture mechanics, must be employed in order to capture the nail-plate joint behaviour in detail when loaded until failure. Some work in this area has also been carried out (e.g. Nielsen 1996 and Kevarinmäki 2000), but these models have only been employed on single joints and are primarily suitable for research on details of the mechanical behaviour of joints and for calibration of simplified joint models.

Our purpose is investigating the impact of gaps between wooden members, and the influence of randomly misplaced nail plates, on the deformations of roof trusses. This requires a large number of computer runs which is why it is important that a single deterministic calculation can be carried out at a low computational cost. The Foschi type model fulfils our requirements, and a simple version of this model will be employed here. The following presentation of the mechanical model is similar to the presentation and model by Nielsen (1996), although it differs in some respects.

2.2 A Non-linear Model for Nail-plate Joints

A roof truss can be divided into nail-plate joints and wooden members between the joints. The wooden members between the joints are modelled herein by Timoshenko beam elements, which are located in the system lines. The wooden members are assumed to behave linearly elastic.

The joints are modelled by three different types of elements, namely: nail elements, splice elements and contact elements. A nail element represents the nails of a plate area fastened into one wooden member. The splice element represents the plate covering the border between two wooden members. It is connected, in the model, to two nail elements. The splice element captures the normal and shear deformations of the plate. The contact element is used to capture the contact pressure between wooden members. A gap may be initially present between wooden members due to tolerances and fabrication errors, but contact may occur as a consequence of the roof-truss deformation when loaded. It is required, of course, that an initial gap is closed in order to put the contact element into action. Finally, rigid connections are employed in the model, too. They are used to couple other elements and transfer forces and moments due to the geometry of the joint and the model. Fig. 1 shows an arbitrary nail-plate joint and the elements used in the modelling. Below follows the derivations of the element stiffness matrices of the joint elements.

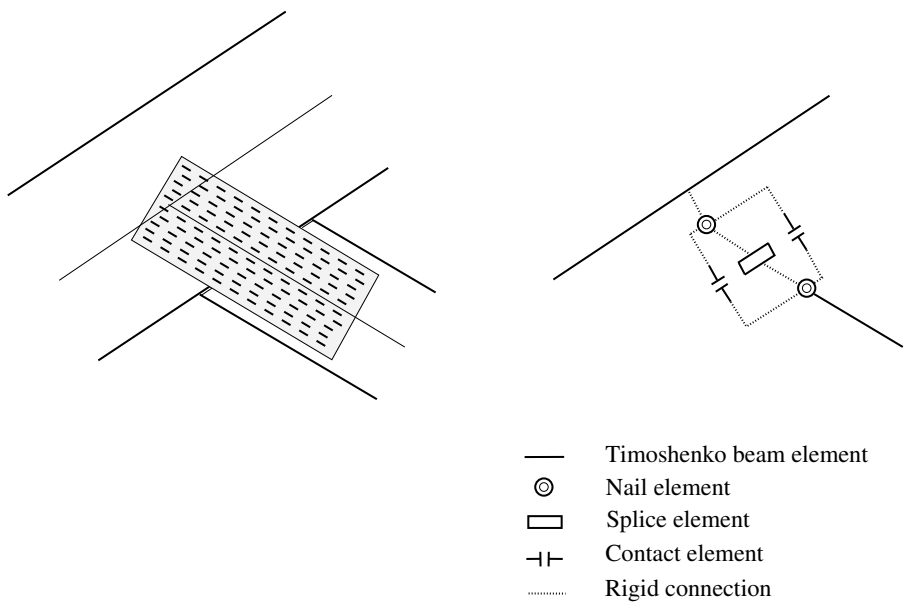

Figure 1: Nail-plate joint and corresponding mechanical model. Different element symbols are introduced.

2.2.1 The Nail Element

Each nail of the nail-plate area contributes to the stiffness of the corresponding nail element. The contribution of a nail to the rotational stiffness is dependent on the

distance to the rotational centre. This is captured by the distance to the nodal points of the nail element, i.e. to the reference positions in the wooden and nail-plate parts respectively. An important assumption is that the plate area and the corresponding wooden area of the nail element transform and rotate rigidly, i.e. do not deform. Fig. 2 shows the local coordinate system of a nail element along with the global coordinate system of the model. It also shows the nodal points of the nail element and the position of an arbitrary location i in the nail-plate area. Thus, even though the nail-element symbol introduced in Fig. 1 indicates that both nodes of the element are located at the same position, this is only one possible choice. The node positions may be chosen arbitrarily.

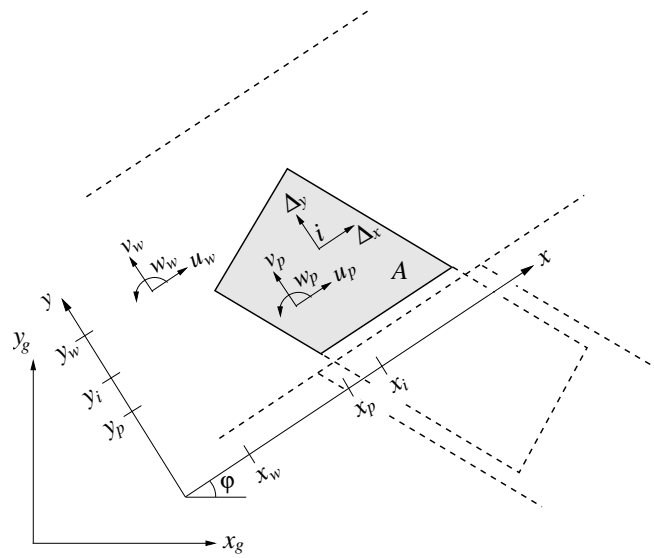

Figure 2: Global and local coordinate systems of a nail element and delimitations of the corresponding nail-plate area. The degrees of freedom of the node of the plate are denoted $[u_p, v_p, w_p]$ *and the degrees of freedom of the node of the wood are denoted* $[u_w, v_w, w_w]$.

The absolute displacement between the wood and the plate in point i of the nail-plate area is calculated as

$$\Delta = \sqrt{\Delta_x^2 + \Delta_y^2} \tag{1}$$

where Δ_x and Δ_y are the displacements in the x-direction and in the y-direction, respectively, calculated as

$$\Delta_x = \mathbf{q}_x^T \mathbf{u}^{(n)}; \quad \Delta_y = \mathbf{q}_y^T \mathbf{u}^{(n)} \tag{2}$$

where, with reference to Fig. 2,

$$\mathbf{q}_x = [1 \;\; 0 \;\; -(y_i - y_w) \;\; -1 \;\; 0 \;\; (y_i - y_p)]^T \tag{3}$$

$$\mathbf{q}_y = [0 \;\; 1 \;\; (x_i - x_w) \;\; 0 \;\; -1 \;\; -(x_i - x_p)]^T \tag{4}$$

$$\mathbf{u}^{(n)} = [u_w \quad v_w \quad w_w \quad u_p \quad v_p \quad w_p]^T \tag{5}$$

The displacement between two arbitrary points, in the plate and in the wood respectively, can thus be uniquely determined by the translations and rotations of the nodal points.

The stiffness relation adopted in the model, Eq. (6), was suggested by Foschi (1977).

$$p(\Delta) = (p_0 + k_1\Delta)\left(1 - exp\left(\frac{-k_0\Delta}{p_0}\right)\right) \tag{6}$$

The force, p, on a nail in position i is a function of the absolute displacement between the plate and the wood, Δ, and three stiffness parameters. These parameters, p_0, k_0 and k_1, can be estimated by means of laboratory tests. The parameters may be functions of the angle between the grain direction of the wood and the principal axis of the plate, and of the direction of the force transmitted by the nail (Foschi 1977). In our simplified version of the model, however, and in accordance with Nielsen (1996), the stiffness parameters are assumed to be independent of directions. Fig. 3 illustrates the force-displacement curve and shows the significance of p_0, k_0 and k_1 in the model.

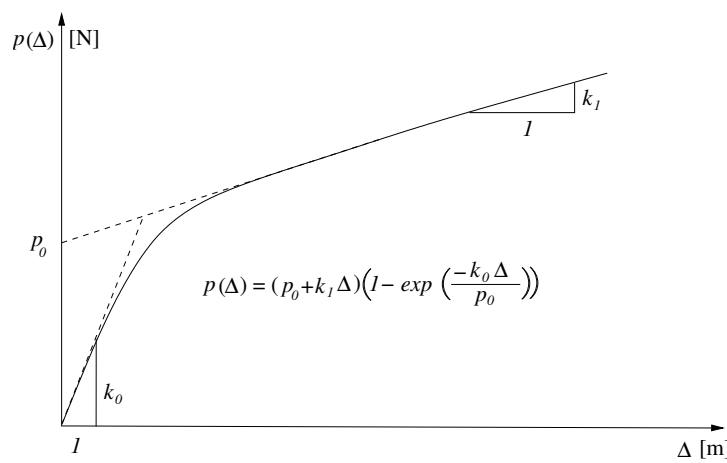

Figure 3: Force-displacement relation for one nail of the plate area represented by the nail element, and definitions of the model stiffness parameters.

The secant and tangent stiffness matrices of the nail element, in the local coordinate system, can now be established. The reader may consult Nielsen (1996) for details in the derivation of the secant stiffness matrix using the principle of virtual work. Only the resulting expression is presented herein. The secant stiffness matrix, $\mathbf{K}_s^{(n)}$, can be expressed as

$$\mathbf{K}_s^{(n)} = \int_A \Im \frac{p(\Delta)}{\Delta}(q_x q_x^T + q_y q_y^T)dA \tag{7}$$

where $\Im$ is the nail density, i.e. the number of nails per unit area, and A is the nail-plate area represented by the nail element. As a typical nail element comprises a large number of nails, it is practical to consider the nails and their stiffness contributions as smeared

out over the plate area and thus calculate the stiffness matrix of a nail element by numerical integration over the plate area of the element. The tangent stiffness matrix, $\mathbf{K}_t^{(n)}$, is finally expressed as

$$\mathbf{K}_t^{(n)} = \int_A \Im \frac{\partial p(\Delta)}{\partial \Delta} (q_x q_x^T + q_y q_y^T) dA \tag{8}$$

2.2.2 The Splice Element

The splice element is used to model the plate area close to the splice between two wooden members. The nails are ineffective in this area because they are located between the wooden members or very close to the edges of the wooden members. As the nails are cut out from the plate, the remaining, perforated plate area, shaded in Fig. 4, consists of a network of approximately rectangularly formed small pieces. In the models presented by Foschi (1977) and Nielsen (1996), the plate area of the splice element was modelled by a number of beam elements representing the plate material between the holes. In the present model, the stiffness of the splice element is captured by adopting a non-linear spring stiffness [N/m^2] in the x-direction and in the y-direction, respectively, along the splice, see Fig. 4. The advantage of this approach is that the stiffness is smeared over the length of the splice and thereby continuous. The beam approach, on the other hand, represents the splice by a discrete number of small beams. This difference is important as regards to probabilistic calculations and optimization of the structure later on.

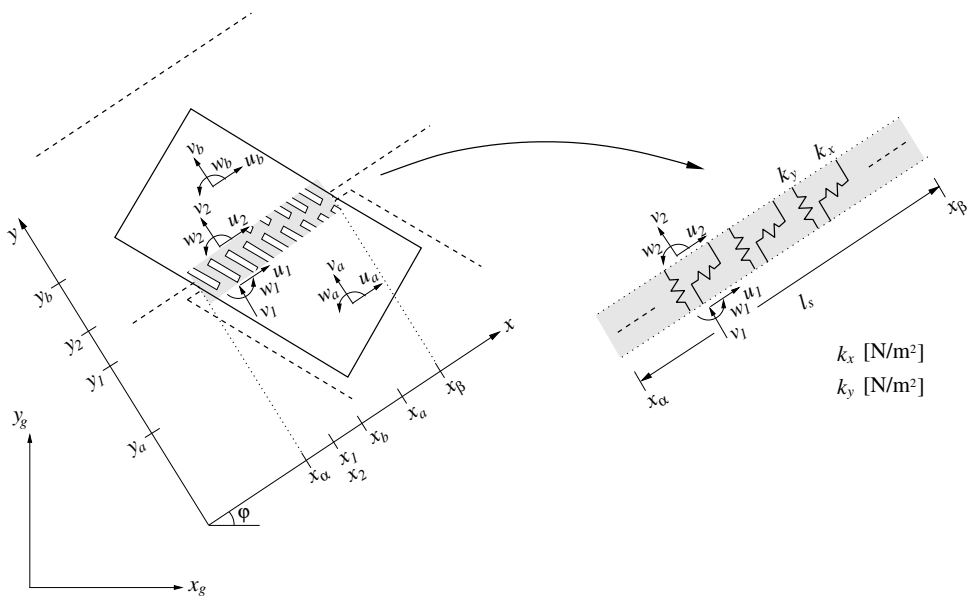

Figure 4: Geometry, degrees of freedom and coordinate systems of a splice element. The degrees of freedom of the nodal points are denoted $[u_a, v_a, w_a]$ *and* $[u_b, v_b, w_b]$*, respectively, and the translations and rotations in some position along the splice are denoted* $[u_1, v_1, w_1]$ *and* $[u_2, v_2, w_2]$*, respectively.*

As the adjacent plate areas represented by the nail elements are assumed to be rigid, the displacement of each point along the borders of the splice element, $x_\alpha \leq x \leq x_\beta$ and $y = y_1$ or $y = y_2$, see Fig. 4, is uniquely determined by the translations and rotations of the nodal points of the splice element. The locations of the nodal points, a and b, are arbitrary.

The kinematic relation between the nodal points and the positions along the edges of the splice area is expressed by

$$\bar{\mathbf{u}} = \mathbf{D}\mathbf{u}^{(s)} \tag{9}$$

where

$$\bar{\mathbf{u}} = \begin{bmatrix} u_1 & v_1 & w_1 & u_2 & v_2 & w_2 \end{bmatrix}^T \tag{10}$$

$$\mathbf{u}^{(s)} = \begin{bmatrix} u_a & v_a & w_a & u_b & v_b & w_b \end{bmatrix}^T \tag{11}$$

and, with $x = x_1 = x_2$,

$$\mathbf{D} = \begin{bmatrix} 1 & 0 & y_a - y_1 & & & \\ 0 & 1 & x - x_a & \mathbf{0} & & \\ 0 & 0 & 1 & & & \\ & & & 1 & 0 & y_b - y_2 \\ & \mathbf{0} & & 0 & 1 & x - x_b \\ & & & 0 & 0 & 1 \end{bmatrix} \tag{12}$$

In correspondence with the displacement vectors, $\mathbf{u}^{(s)}$ and $\bar{\mathbf{u}}$, force vectors are defined by $\mathbf{f}^{(s)}$ and $\bar{\mathbf{f}}dx$. The force components and moment components of $\mathbf{f}^{(s)}$ correspond to the translation directions and rotations of $\mathbf{u}^{(s)}$ and the components of $\bar{\mathbf{f}}$ correspond in the same way to the components of $\bar{\mathbf{u}}$. The vector $\mathbf{f}^{(s)}$ is related to $\bar{\mathbf{f}}$ as

$$\mathbf{f}^{(s)} = \int_{x=x_\alpha}^{x_\beta} \mathbf{D}^T \bar{\mathbf{f}} dx \tag{13}$$

and the relation between $\bar{\mathbf{f}}$ and $\bar{\mathbf{u}}$ is expressed by

$$\bar{\mathbf{f}} = \bar{\mathbf{K}}\bar{\mathbf{u}} \tag{14}$$

where

$$\bar{\mathbf{K}} = \begin{bmatrix} k_x & 0 & 0 & -k_x & 0 & 0 \\ 0 & k_y & 0 & 0 & -k_y & 0 \\ 0 & 0 & 0 & 0 & 0 & 0 \\ -k_x & 0 & 0 & k_x & 0 & 0 \\ 0 & -k_y & 0 & 0 & k_y & 0 \\ 0 & 0 & 0 & 0 & 0 & 0 \end{bmatrix} \quad [N/m^2] \tag{15}$$

The parameters k_x and k_y are the spring stiffness of the splice element in the x-direction and y-direction, respectively, per unit length along the splice. By inserting Eq. (9) and Eq. (14) into Eq. (13), the local finite element equation is established by

$$\mathbf{f}^{(s)} = \mathbf{K}^{(s)}\mathbf{u}^{(s)} \tag{16}$$

where the stiffness matrix, $\mathbf{K}^{(s)}$, is given by

$$\mathbf{K}^{(s)} = \int_{x=x_\alpha}^{x_\beta} \mathbf{D}^T \bar{\mathbf{K}} \mathbf{D} dx \tag{17}$$

Finally, the spring stiffness, k_x and k_y, must be supplied to the model and a bi-linear relation between stiffness and displacement is adopted herein, see Fig. 5. As for the nail element, the secant stiffness matrix as well as the tangent stiffness matrix are derived, but since a general expression for the stiffness matrix is already given, Eq. (17), it only remains to supply values for k_x and k_y for the two alternative stiffness matrices. However, even though the values of the parameters in the x-direction and in the y-direction may differ, the same procedure is employed for the derivation of k_x and k_y. Therefore, only the derivation of k_x is presented below. (k_y can be derived by replacing index x by index y in Eqs. (18)–(20), and by replacing $[u_1(x), u_2(x)]$ by $[v_1(x), v_2(x)]$ in Eq. (20)). For the secant stiffness matrix the value assigned to k_x is

$$\begin{aligned} k_x &= \frac{k_x^0 c_x^c + k_x^c(\delta_x - c_x^c)}{\delta_x}, && \delta_x < c_x^c \\ k_x &= k_x^0, && c_x^c \le \delta_x \le c_x^t \\ k_x &= \frac{k_x^0 c_x^t + k_x^t(\delta_x - c_x^t)}{\delta_x}, && \delta_x > c_x^t \end{aligned} \tag{18}$$

and for the tangent stiffness matrix the value assigned to k_x is

$$\begin{aligned} k_x &= k_x^c, && \delta_x < c_x^c \\ k_x &= k_x^0, && c_x^c \le \delta_x \le c_x^t \\ k_x &= k_x^t, && \delta_x > c_x^t \end{aligned} \tag{19}$$

where δ_x is the displacement defined by

$$\delta_x = u_2(x) - u_1(x) \tag{20}$$

The parameters k_x^c, k_x^0, k_x^t, c_x^c and c_x^t are defined by Fig. 5 and should be determined by means of laboratory tests.

2.2.3 The Contact Element

Contact pressure between wooden members arises in different locations of the roof truss when it is loaded, unless the initial gaps between the wooden members are too large. Contact elements should therefore be added to the model in locations where contact pressure may occur. Fig. 6 shows the locations of two contact elements capturing the potential contact pressure between two wooden members. A contact element may be coupled to the beam elements of the wooden members by auxiliary beam elements or by geometrical transformations directly to the nodes of the beam elements representing the wooden members. The stiffness matrix of a contact element is derived below with respect to the degrees of freedom located where the contact takes place.

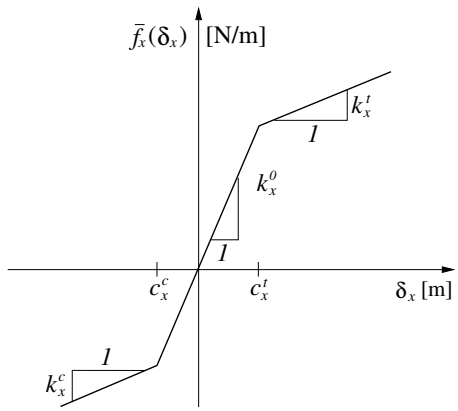

Figure 5: Bi-linear spring stiffness in the x-direction. c_x^c and c_x^t indicate critical displacements for which the tangent stiffness changes. The tangent stiffness for different displacements, δ_x, is represented by k_x^c, k_x^0 and k_x^t, respectively.

The important parameters of a contact element are: the initial gap size between the wooden members, the normal stiffness of the contact element when put into action and the coefficient of friction between the wooden members.

The element displacement vector is defined, with reference to Fig. 6, as

$$\mathbf{u}^{(c)} = \begin{bmatrix} u_A & v_A & u_B & v_B \end{bmatrix}^T \tag{21}$$

The criterion for contact between the wooden members at the location of the element is

$$v_A - v_B \geq g \tag{22}$$

where g is the initial gap size. The element stiffness matrix of the contact element can, in the local coordinate system, be expressed as

$$\mathbf{K}^{(c)} = \begin{bmatrix} k_f & 0 & -k_f & 0 \\ 0 & k_n & 0 & -k_n \\ -k_f & 0 & k_f & 0 \\ 0 & -k_n & 0 & k_n \end{bmatrix} \quad [N/m] \tag{23}$$

where k_n is the normal stiffness perpendicular to the edges of the two wooden members, and k_f is the shear stiffness caused by friction between the wooden members. k_f is a function of the normal force and the coefficient of friction. In the following derivations, however, friction is neglected, giving $k_f = 0$.

The element equation in local coordinates can be expressed as

$$\mathbf{f}^{(c)} = \mathbf{K}^{(c)}\mathbf{u}^{(c)} \tag{24}$$

where the four components of the force vector, $\mathbf{f}^{(c)}$, correspond to the four components of the displacement vector, $\mathbf{u}^{(c)}$.

The remaining task is to determine the value of the normal stiffness component, k_n, of $\mathbf{K}^{(c)}$. As before, the tangent as well as the secant stiffness matrices will be considered.

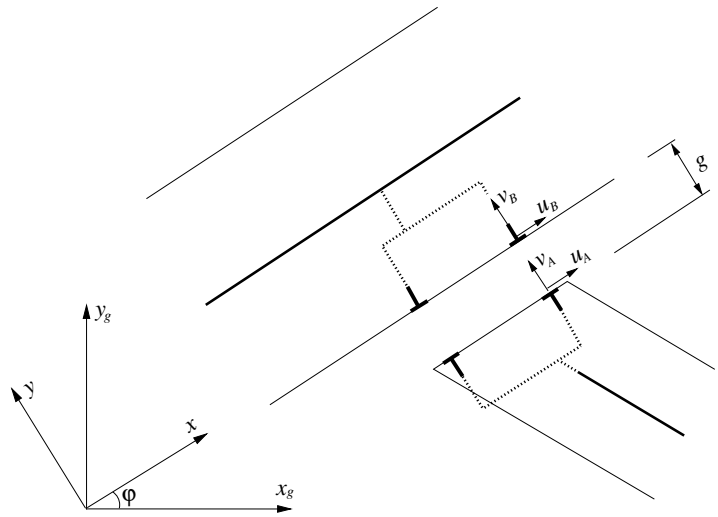

Figure 6: Contact elements for modelling of contact pressure between wooden members.

The tangent and secant stiffness k_t and k_s, respectively, are indicated in Fig. 7. For the tangent stiffness matrix, k_n is given by

$$\begin{aligned} k_n = k_t &= 0, \qquad && d < g \\ k_n = k_t &= \frac{EA_c}{L}, \qquad && d \geq g \end{aligned} \tag{25}$$

where d is the current relative displacement, $v_A - v_B$. E is the modulus of elasticity of the wood material, which depends on the angles between the fibre directions of the wooden members and the contact surface. A_c is the estimated area of the contact surface between the members represented by the contact element, and L is the length of the wood material in contact pressure modelled by the contact element. It may be noted that the estimated parameters E, A_c and L are only employed in order to find a physical foundation for the estimation of the stiffness $k_s(d \geq g)$. If $k_s(d \geq g)$ can be estimated by laboratory experiments, E, A_c and L are not needed.

The secant stiffness, k_s, is a function of the tangent stiffness parameter, k_t, and the initial gap size, g. For the secant stiffness matrix, k_n is defined by

$$\begin{aligned} k_n = k_s &= 0, \qquad && d < g \\ k_n = k_s &= \frac{k_t(d-g)}{d}, \qquad && d \geq g \end{aligned} \tag{26}$$

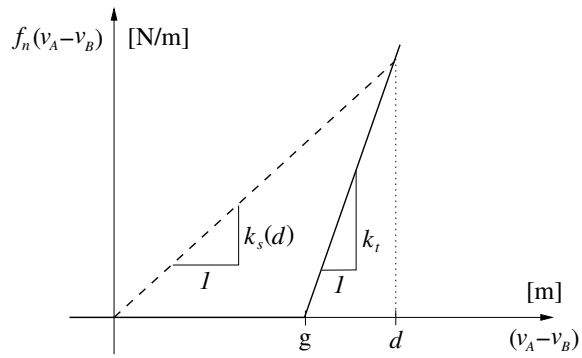

Figure 7: Contact force, f_n, as a function (solid line) of relative displacement and initial gap size. The tangent stiffness, k_t, and the secant stiffness, k_s, are illustrated. d is the current relative displacement.

2.3 Application on a Roof Truss

The elements presented are now employed in the analysis of a complete roof truss using the software MATLAB (2002) and the finite element toolbox CALFEM (1999). The considered roof truss is a common symmetric W-truss with a roof angle of 20° and a span of approximately eight metres. The geometry of the truss and the nail-plate joints is shown in Fig. 8, and the mechanical model of the joints, using the element symbols defined in Fig. 1, is presented in Fig. 9. The same truss was analysed by Nielsen (1996), and some material properties for the nail-plate joints are taken from his work.

Table 1 states the parameters of the truss elements. The first column contains the stiffness parameters of the wooden members. E_0 is the modulus of elasticity in the fibre direction and E_{90} is the modulus of elasticity in the direction perpendicular to the fibre direction. G is the shear modulus. These wood parameters could be chosen differently depending on strength class, load duration and climate conditions for the structure. For our purposes, however, i.e. calculating the influence of geometrical imperfection, it is sufficient to choose realistic stiffness values for the wooden members and not define under which precise conditions the chosen values are valid. Column two and column three of Table 1 state the parameters of the nail elements and the splice elements, respectively. The parameters originate from the plate type *GNA20S* produced by *MiTex* (former *Gang-Nail Systems*), and the given values are valid for single nail plates. As nail plates are present on both sides of the wooden members of the truss, double nail elements and splice elements are assembled in the model.

The normal, tangent stiffness of the contact elements in action depends on the estimated contact area, A_c, the estimated length of the contact zone, L, and the modulus of elasticity of the wood in compression, E, which is highly dependent on the angle between the contact pressure and the wood-fibre direction. The employed stiffness of each contact element, $k_t = EA_c/L$, is, with reference to the contact element numbering of Fig. 9, supplied in the fourth column of Table 1.

Two different load cases are considered in the present study. Load case A, shown in Fig. 10, represents a realistic loading in relation to the design of the truss. Load case B is simply twice the loading of load case A. Load case B is hardly realistic for the truss

under consideration, but it is useful for studying the effects of geometrical imperfections when the joints are heavily loaded.

Wooden members	Nail element par.	Splice element par.	Contact stiffness
$E_0 = 7200$ MPa	$p_0 = 150$ N	$k_x^c = 86.8$ MN/m^2	(1) $k_t = 14.5$ MN/m
$E_{90} = 240$ MPa	$k_0 = 900$ N/m^2	$k_x^0 = 4630$ MN/m^2	(2) $k_t = 29.5$ MN/m
$G = 480$ MPa	$k_1 = 900$ kN/m	$k_x^t = 86.8$ MN/m^2	(3a) $k_t = 295$ MN/m
	$\Im = 14650$ nails/m^2	$k_y^c = 3.44$ MN/m^2	(3b) $k_t = 295$ MN/m
		$k_y^0 = 183$ MN/m^2	(4a) $k_t = 254$ MN/m
		$k_y^t = 3.44$ MN/m^2	(4b) $k_t = 254$ MN/m
		$c_x^c = 0.0022$	(5) $k_t = 15.1$ MN/m
		$c_x^t = 0.0022$	
		$c_y^c = 0.01$	
		$c_y^t = 0.01$	

Table 1: Parameters of the truss elements. The first column contains the stiffness parameters of the wooden members. The second and third columns state the parameters of the nail elements and the splice elements, respectively, and the fourth column states the normal stiffness of the contact elements.

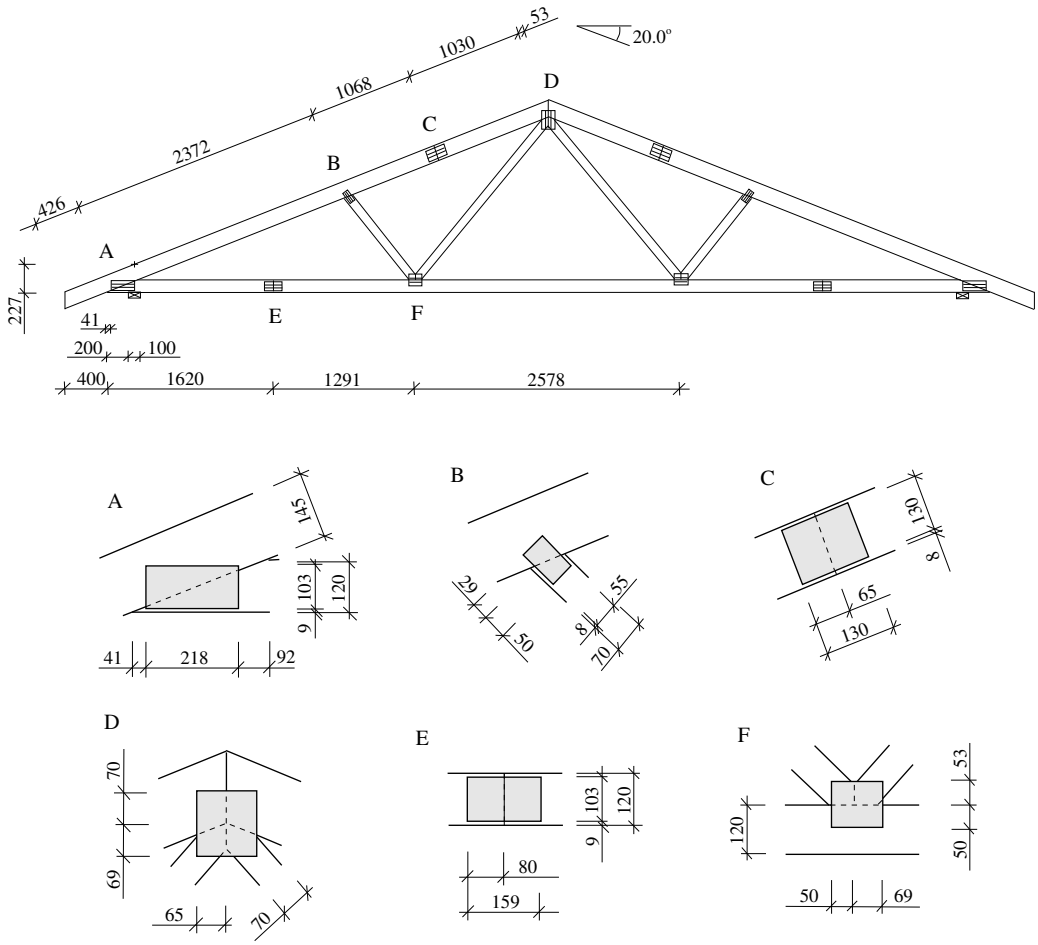

Figure 8: Geometry of a symmetric, 20°, W-truss, including the nail-plate locations. Lengths are given in mm.

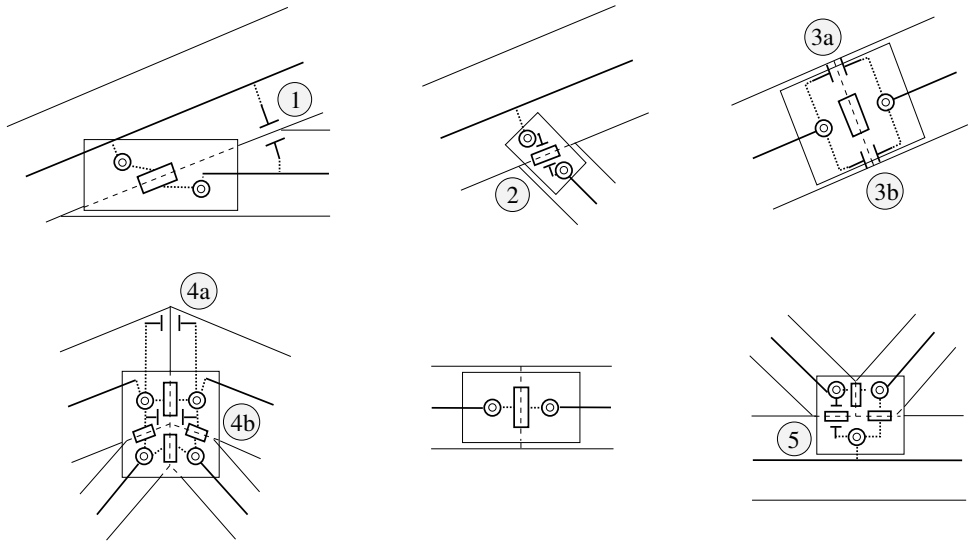

Figure 9: Mechanical model of the nail-plate joints using nail elements, splice elements and contact elements. The numbering refers to the contact elements.

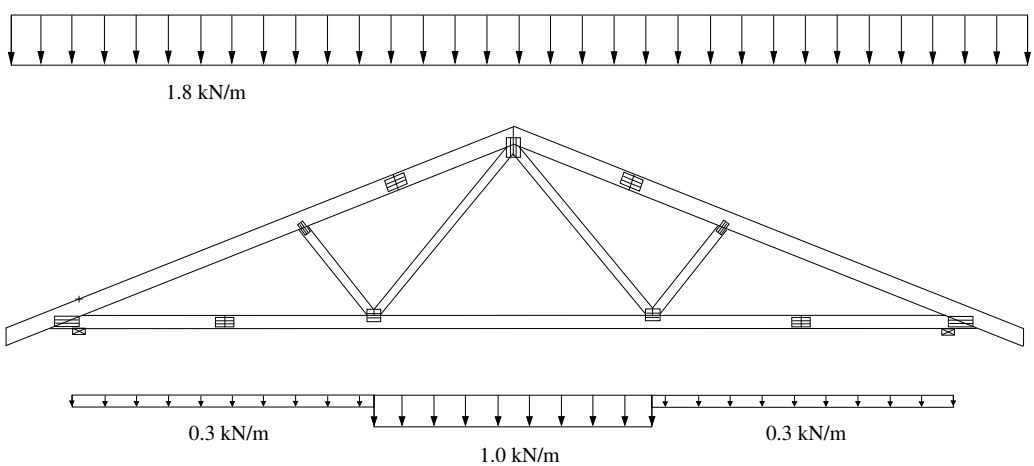

Figure 10: Definition of load case A.

2.3.1 Results

The results presented here are restricted to the deflection of the truss. The deflection supplies a measure of the overall stiffness of the truss, and requirements on the deflection are often critical for the design of roof trusses.

The maximum deflection of the truss under consideration takes place in the middle of the chord. This is indicated in Fig. 11, which shows the deformation mode of the entire truss for load case A. The relation between the deflection of the middle of the chord and the applied loading is shown in Fig. 12. The different curves represent cases with: initial contact between the wooden members, no contact between the wooden members and rigid nail-plate connections. The stiffness curve representing the rigid connection model shows that a substantial part of the deflection depends on the limited stiffness of the wooden members, modelled by Timoshenko beams. Otherwise, the deflection for this model would be smaller. However, even though the stiffness of the nail-plate joints is relatively high, the presence of contact between the wooden members makes a significant contribution to the overall stiffness compared to the case without any contact between the wooden members. Lack of contact also results in a more pronounced non-linear behaviour as larger deformations are reached in the nail-plate joints.

Depending on the load level, the maximum deflection of the truss differs about 15–25% for models with initial contact compared to models without any contact between the wooden members. For load case A, the deflection is 18.6 mm in case of initial contact and 21.3 mm in case of no contact. For load case B, the deflections are 38.9 mm and 48.4 mm for initial contact and no contact, respectively. In reality, the initial gap may close as a result of deformations in the nail-plate joints subjected to loading. Large initial gaps, however, may not close for any realistic loading on the roof truss and the magnitude of the initial gap is therefore of vital importance for the overall stiffness and deformation of the truss.

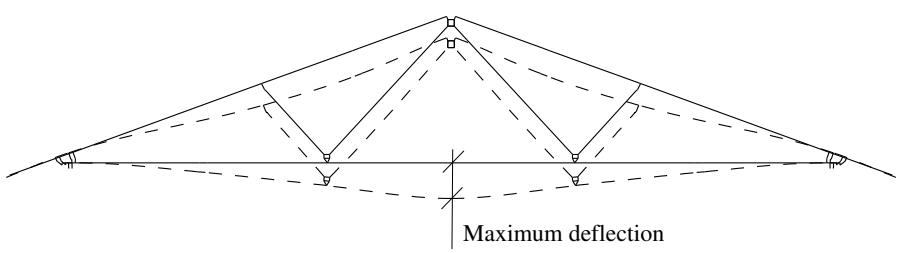

Figure 11: Deformation mode of the W-truss, with initial contact between wooden members, subjected to load case A. The deformation is shown with a magnification factor of twenty.

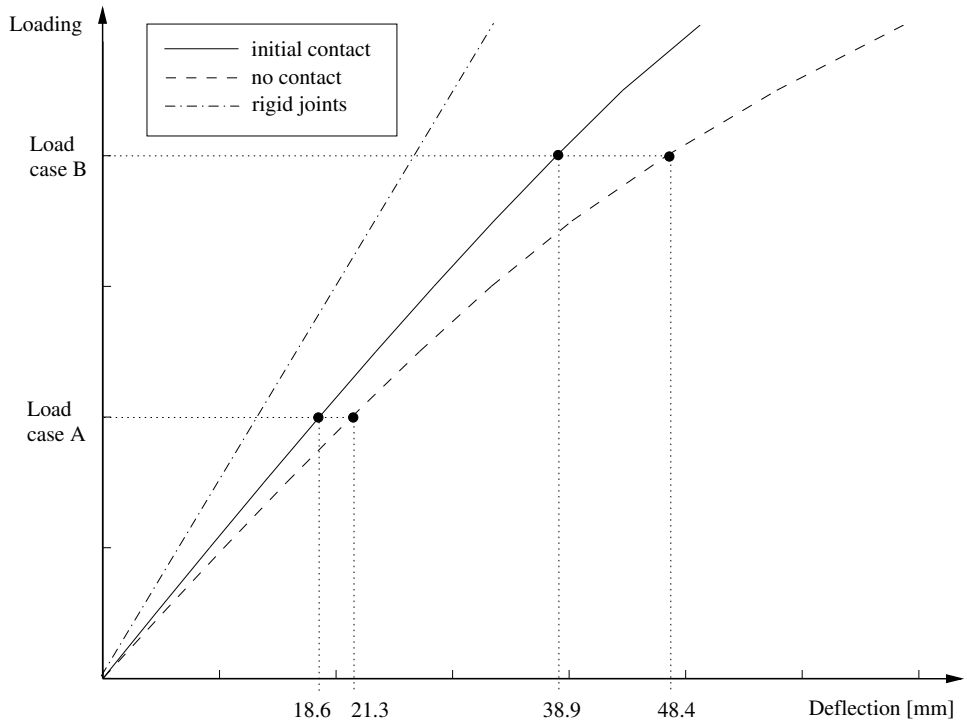

Figure 12: The relation between loading and deflection for cases with initial contact between wooden members, and no contact between wooden members, respectively. The stiffness curve of a roof-truss model with rigid joints is also presented.

3 Geometrical Imperfections

3.1 Gaps Between Wooden Members

The computational results presented above comprise the case of initial contact between all pairs of wooden members, and the case of no contact between any wooden members. Below follows a parameter study on gaps at different locations and a probabilistic analysis of the influence of randomly distributed gaps in a roof truss.

3.1.1 Parameter Study on the Effect of Gaps

For each pair of wooden members, for which contact as well as gaps are possible and have an influence on the behaviour of the truss, the effects of gaps of different magnitudes are investigated. Table 2 and Table 3 state, for load cases A and B, respectively, the relative increase in deflection of the roof truss for gaps of different magnitudes and at different locations. The numbering, 1–5, corresponds to the contact location numbering of Fig. 9. For those joints modelled by more than one contact element (joints 3 and 4), the same initial gap size is assumed to be present throughout the splice. In each case of Tables 2–3, initial contact between wooden members is assumed at all other locations of the roof truss.

Gap size	1	2	3(a–b)	4(a–b)	5
0.25 mm	1.003	0.999	1.012	1.019	1.015
0.50 mm	1.006	0.999	1.013	1.036	1.025
1.00 mm	1.006	0.999	1.013	1.055	1.025
1.50 mm	1.006	0.999	1.013	1.055	1.025

Table 2: For load case A, influence of gaps of different magnitudes at different positions where contact matters. The values given are the ratio between the deflection of the truss with a certain gap, and the deflection of the truss with initial contact.

Gap size	1	2	3(a–b)	4(a–b)	5
0.25 mm	1.002	0.999	1.007	1.010	1.007
0.50 mm	1.003	0.999	1.012	1.018	1.015
1.00 mm	1.007	0.999	1.020	1.035	1.028
1.50 mm	1.008	0.999	1.020	1.054	1.028
2.00 mm	1.008	0.999	1.020	1.073	1.028
4.00 mm	1.008	0.999	1.020	1.106	1.028

Table 3: For load case B, influence of gaps of different magnitudes at different positions where contact matters. The values given are the ratio between the deflection of the truss with a certain gap, and the deflection of the truss with initial contact.

The most important location, with respect to contact vs gap, is joint 4, at the top of the roof truss. An initial gap here results in an increase in deflection of, at most, 5.5% for load case A, and 10.6% for load case B. For load case B, however, the initial gap must be almost 4 mm in order to remain open when the entire load is applied, whereas for load case A, an initial gap of 1 mm remains open. An initial gap of 1 mm gives, for load case B, an increase in deflection of 3.5%.

A gap at joint 2 actually decreases, though not significantly, the deflection of the chord. This result may surprise at first glance, but the deflection of the middle of the chord does not capture the complete behaviour of the truss. For example, a gap at joint 2 also results in increased deflection of the rafter for the same load cases.

In contrast to a gap at joint 2, a gap at joint 5, at the opposite end of the short diagonal wooden member, has a significant and increasing effect on the deflection. It is actually the second most important contact location after the top joint. The reason is that a gap/contact at joint 5 has a direct impact on the internal forces and the deformations of the entire nail plate connecting the chord and the two diagonal members. A gap at joint 5 thus increases the internal forces and the deformations of the adjacent nail and splice elements, coupled to the chord and the longer diagonal.

Joint 3, the splice joint of the rafter, is sensitive even to small gaps. An initial gap of 0.25 mm in this single joint results in, for load case A, an increase of 1.2% of the deflection.

A gap at joint 1, the heel joint, does not have a major effect on the deflection. The reasons are that the contact element is relatively weak as it models wood in compression

in the weak direction parallel to the fibre direction, and that friction between wooden members is ignored. Also, the size of the nail plate at the heel joint is quite large, giving a stiff connection and only small relative displacements of the wooden members in the direction perpendicular to the contact surface. Therefore, the additional effect of contact between the chord and the rafter is moderate.

For load case A, no initial gap of more than 1 mm closes during loading. Thus, the deflection for a case with a gap exceeding 1 mm coincides with a case where contact is ignored. For load case B, larger gaps are closed during loading, but when the initial gap size is increased above a certain level, this has no impact, according to the model, on the behaviour of the roof truss. The reason is that the employed model does not capture phenomena such as buckling of the nail plates, caused by large gaps, as the stiffness of the splice elements are not sensitive to the gap size. Therefore, the present model, and consequently our results, are not valid for very large gaps. However, in contrast to available commercial software using very simple mechanical models, the employed model allows the modifications required with a reasonable additional effort.

3.1.2 Probabilistic Analysis of the Influence of Gaps

The presence of gaps in manufactured roof trusses is a consequence of lack of precision, and possibly lack of control, in the manufacturing process. Gaps are therefore randomly distributed and a roof truss may contain several gaps of different sizes at different joint locations. A proper analysis of the influence of gaps must therefore involve probabilistic calculations, where the presence of gaps is modelled by statistical distributions. These distributions should rely on thorough investigations of the actual gap sizes present in manufactured roof trusses. Unfortunately, however, no such investigation is available at this point. Instead, we must make reasonable assumptions and rely on these assumptions in the following calculations.

Four different distributions of the initial gap sizes are considered. In each case, a uniform distribution is assumed and the intervals are $[0 : 0.25]$, $[0 : 0.5]$, $[0 : 1.0]$ and $[0 : 1.5]$ mm, respectively. In total, nine pairs of wooden members are modelled by twelve contact elements, see Fig. 9 (not showing joints represented by their reversed joints). No correlation or dependence is assumed between the gap sizes at different locations within the roof truss.

The probabilistic analysis is performed using Monte Carlo simulations and the Latin hypercube sampling plan. The Latin hypercube sampling plan, first proposed by McKay et al. (1979), is more efficient than standard Monte Carlo sampling, as it accurately represents the distributions of the input data, in this case the gap sizes, with a reasonable sample size. The method has been further developed for different purposes by several researchers [e.g. Owen (1994); Olsson and Sandberg (2001)] and has been evaluated for structural mechanics applications by Olsson (1999).

The results of the probabilistic analysis are shown in Fig. 13 and Fig. 14 for load cases A and B, respectively. The histograms, comprising one thousand deterministic calculations each, show the distributions of the roof-truss deflection (the deflection of the middle of the chord) for the four different distributions of the gap size. The deflections for the extreme cases, with initial contact and no contact between wooden members, respectively, are marked by dashed lines in the histograms. The deflections for the cases with initial gap sizes equal to the upper limits of the distributions (0.25, 0.5, 1.0 and

1.5 mm, respectively) are marked in the histograms by dotted lines.

It is clear from Figs. 13–14 that even a small initial gap, gap < 0.25 mm, significantly affect the deflection of the truss. For initial gap sizes equal to 0.25 mm, the deflection is increased by 7.5% and 4.0%, for load cases A and B, respectively, compared to the truss with initial contact. It is interesting to note that for load case A, a small gap results in a larger relative increase of the deflection than for load case B. Gaps larger than approximately 1 mm, on the other hand, have a larger impact on the deflection for load case B.

The probabilistic results presented by the histograms give useful information on the probability for a certain deflection to be exceeded. However, without going into details about exact probabilities, it is clear that for each gap distribution and each load case, there is a significant risk that the deflection comes close to the upper bound of that particular case, i.e. close to the dotted line in the histogram. For load case A, assuming the wide gap intervals of $[0 : 1.0]$ and $[0 : 1.5]$ mm, it even seems reasonable to neglect the contact between wooden members when calculating the deflection.

It is finally concluded that a thorough investigation of the actual presence of gaps in roof trusses would be most interesting in order to establish a valid statistical distribution of the gap size. It would also be very interesting to study, by means of laboratory tests and advanced finite element calculations, the behaviour in bending and compression of nail-plate joints when large gaps between wooden members are present. Such an investigation would probably imply a sensitivity to the gap size in the properties of the splice element.

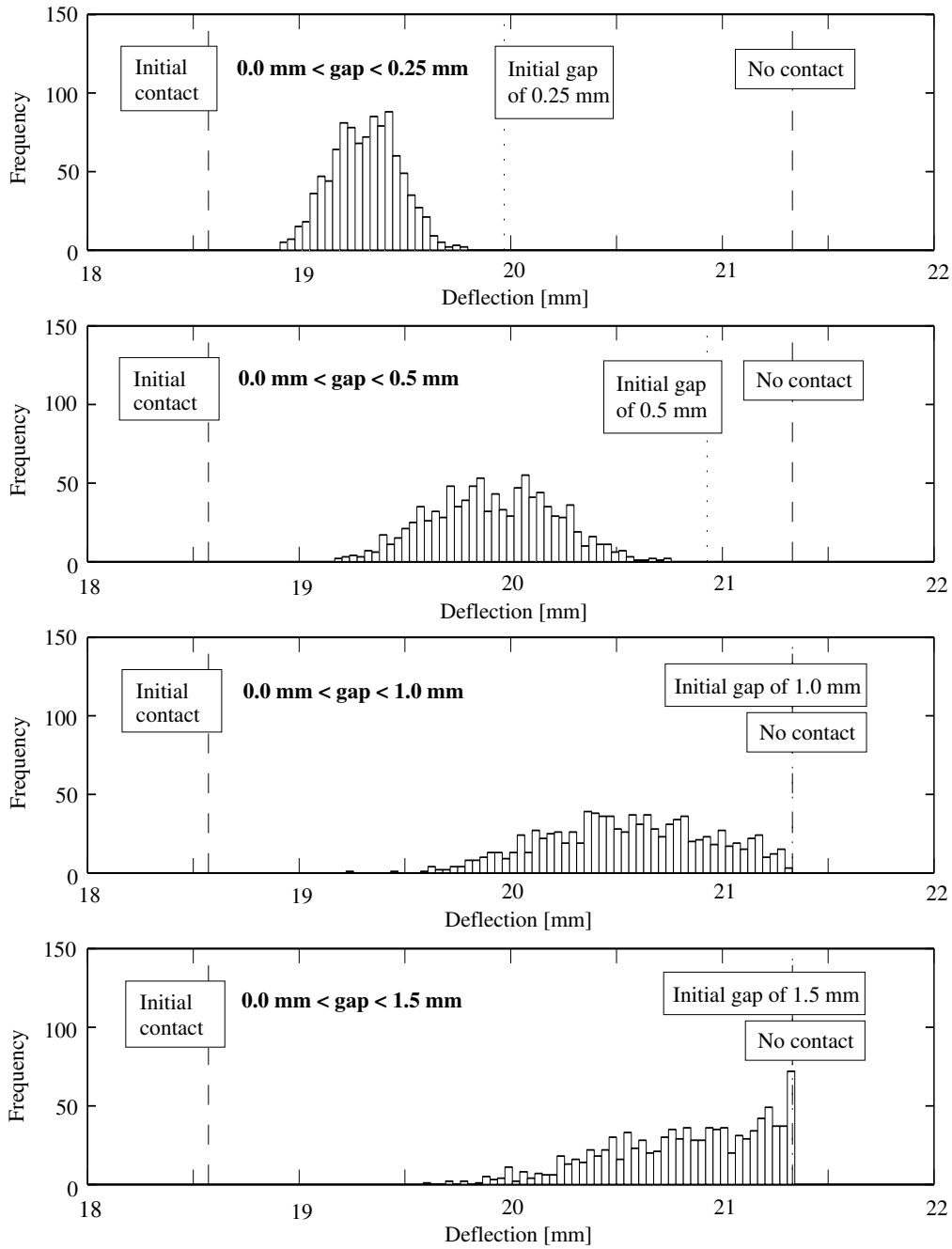

Figure 13: Histograms of the roof-truss deflection corresponding to load case A, and four different uniform distributions of the gap size.

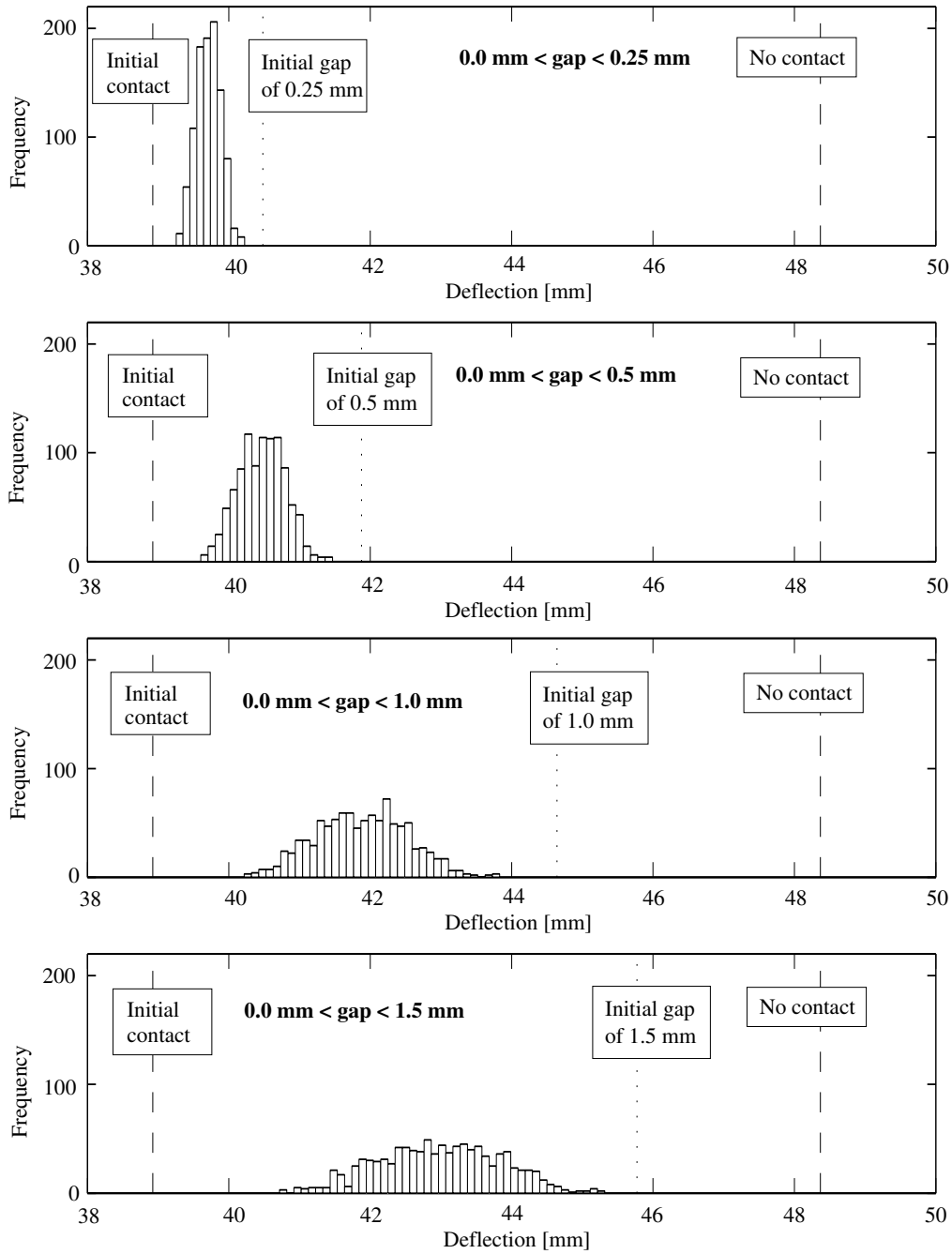

Figure 14: Histograms of the roof-truss deflection corresponding to load case B, and four different uniform distributions of the gap size.

3.2 Location of Nail Plates

In contrast to models frequently employed in industry, the model employed here captures the exact nail-plate location when calculating the deformations. Thus, we are able to investigate the effects of changes in the nail-plate locations. Displacements of nail plates in relation to the prescribed locations may occur as a result of lack of precision in the manufacturing process and it is investigated how such random misplacement influences the behaviour of the roof truss. Another aspect considered is the possibility of improving the roof-truss behaviour with respect to some critical criterion, in this case the deflection of the middle of the chord, by performing an optimization procedure on the nail-plate locations.

Nail plates are located on both sides of the wooden members, and this is modelled, as before, by double nail and splice element stiffness. Thus, the plates on the opposite sides of the wooden members (with identical xy-coordinates) are restricted, in the present model, to move in the same way.

3.2.1 Probabilistic Analysis on Misplaced Nail Plates

In similarity with the analysis of gaps between wooden members, a probabilistic analysis of misplaced nail plates is carried out. The probability distribution of the misplacement of the nail plates should, preferably, be founded on a thorough investigation of actual nail-plate locations of manufactured roof trusses. As no such investigation is available, the employed distribution of misplacement is instead founded on typical tolerances for nail-plate locations. A misplacement of, at most, 5 mm is often accepted, and a uniform distribution in the interval $[-5 : 5]$ mm is therefore adopted here for the misplacement in the length direction and cross direction, respectively, of each nail plate.

The probabilistic analysis is performed using Monte Carlo simulations and the Latin hypercube sampling plan. Cases with initial contact between wooden members as well as without any contact between wooden members are considered, and simulations are carried out for load cases A and B, respectively. For each of the four combinations, a probabilistic analysis consisting of one thousand deterministic calculations is carried out. The resulting deflections of the middle of the chord are visualized by the histograms in Figs. 15–16.

The distributions of the roof-truss deflection appear, in all the cases, to be approximately normally distributed with a moderate standard deviation. Of course, however, the intervals between the largest and smallest possible deflections are limited as the nail-plate displacements are moderate and limited. It is also clear from Figs. 15–16 that the influence of misplaced nail plates is larger for roof trusses without contact between wooden members than for roof trusses with initial contact, and larger for load case B than for load case A. For load case B and no contact between wooden members, the difference between the smallest and largest deflection is about 5%, or a 2.5 mm deflection. For load case A and initial contact, the difference is only about 2%, or a 0.5 mm deflection. The reason is that for load case B, the nail plates are heavily loaded and have a lower tangent stiffness. Small changes in positions, therefore, have a large impact on the deformation. Also, in case of no contact between wooden members, the nail plates constitute the only load carriers between the wooden members, and the overall stiffness and deformation of the truss are more sensitive to changes of the nail-plate positions

than if contact is present.

The deflection for the case with nominal positions of the nail plates is marked in Figs. 15–16 and it is obvious that the nominal nail-plate positions do not result in minimal deflection of the middle of the chord. For all four cases considered, a significant number of the random nail-plate configurations give lower deflections than the nominal configuration. This observation turns our interest towards an optimization of the nail-plate positions with respect to the deflection.

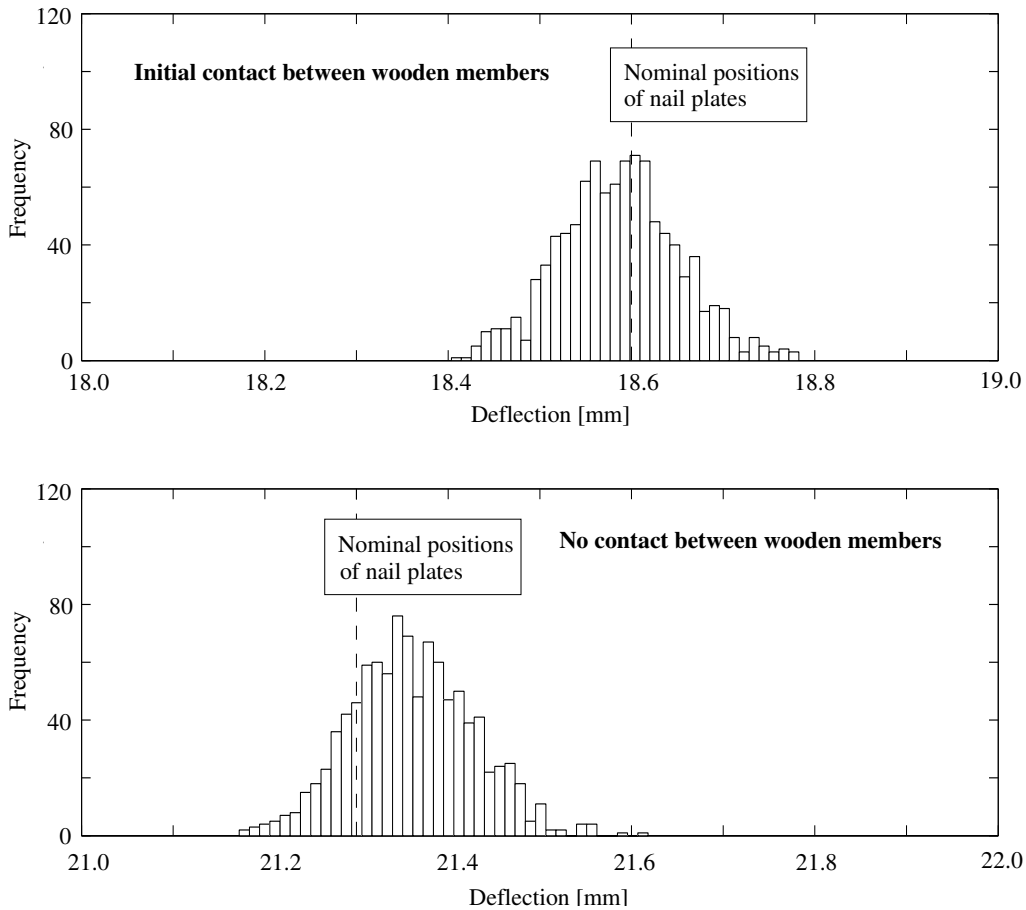

Figure 15: Histograms of the roof-truss deflection corresponding to load case A, and uniformly distributed displacements of nail plates, $[-5 : 5]$ *mm. Cases with initial contact and no contact between wooden members, respectively, are presented.*

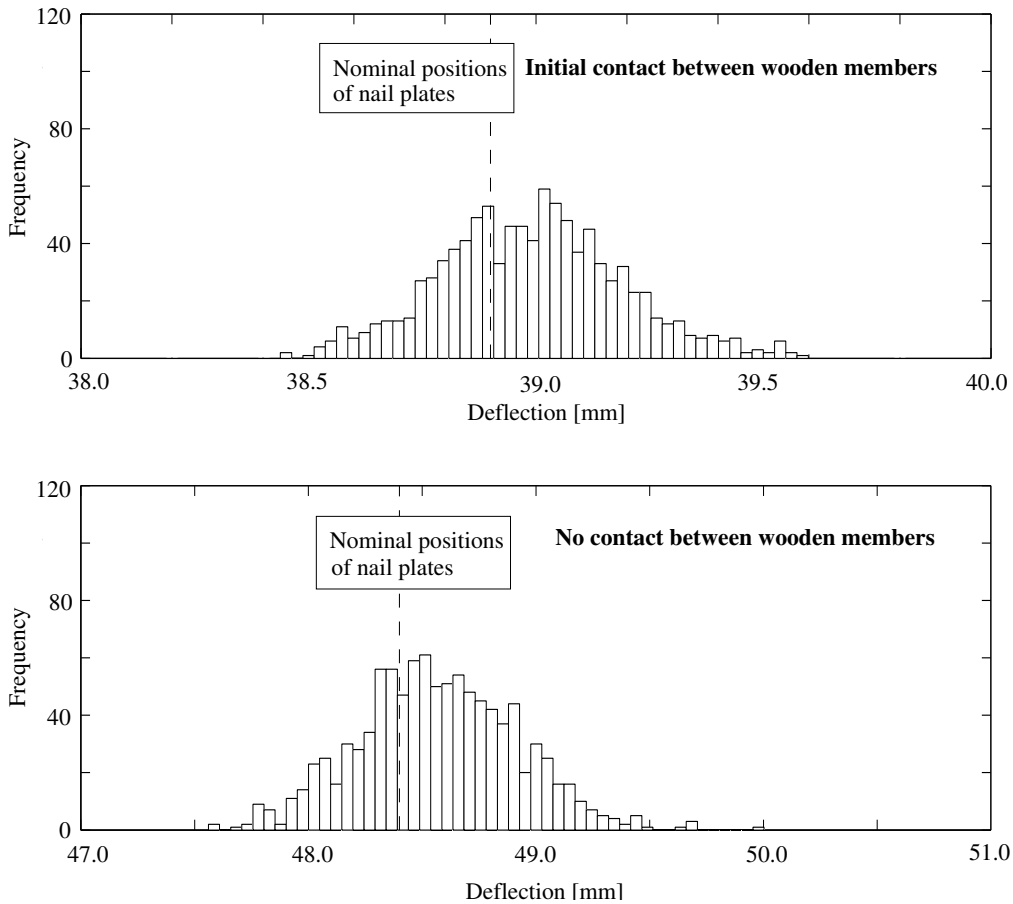

Figure 16: Histograms of the roof-truss deflection corresponding to load case B, and uniformly distributed displacements of nail plates, $[-5 : 5]$ *mm. Cases with initial contact and no contact between wooden members, respectively, are presented.*

3.2.2 Optimization of Nail Plate Positions

It is fundamental for all optimization that a certain function of the involved variables is defined for evaluation. In the present case, the selected function is the deflection of the middle of the chord. The purpose is to find the nail-plate configuration that minimizes this deflection. The displacements of the nail plates in the length direction and cross direction, see Fig. 17, are thus the variables determining the deflection.

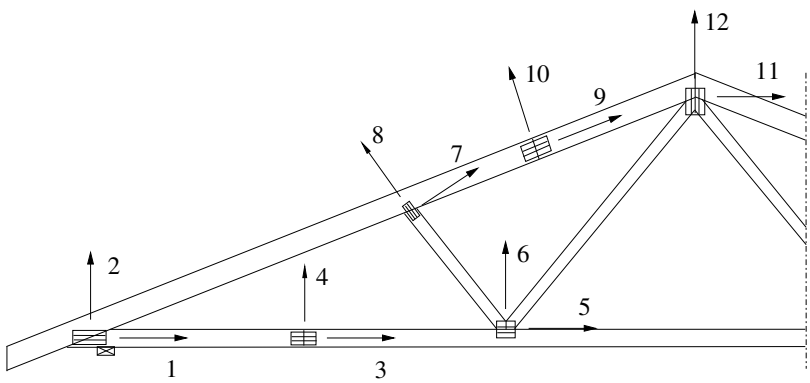

Figure 17: Left part of the roof truss with definition and numbering of displacement directions of the nail plates.

Different constraints, i.e. restrictions on the optimization variables, may be applied in the search for the optimal solution. In the present case, restrictions are placed on the displacements of the nail plates. For example, the plate connecting the chord with the two diagonal wooden members is not allowed to be moved more than 5 mm in its length and cross directions, respectively. The reason is that, for the present load cases, an extreme displacement of this nail plate, towards loss of connection between the short diagonal and the other wooden members, would be favourable for the deflection under consideration. It is obvious, however, that such a displacement would be far from optimal with respect to other demands on the roof truss and for other load cases.

The analysis comprises the four cases considered in the investigation of misplaced nail plates, i.e. with and without contact between wooden members, and load cases A and B, respectively. The resulting optimal nail-plate displacement, with reference to the variable numbering of Fig. 17, are presented in Table 5 along with the corresponding deflections of the middle of the chord. Displacements restricted by constraints are marked by a (C) in Table 5.

According to the calculations, the optimum location for the nail plate at the heel joint is fairly close to the nominal position. A moderate displacement to the right and downwards is, however, favourable for decreasing the deflection. This holds for all four cases considered, but the exact optimal displacement differs somewhat for the different cases. No constraints are activated at the heel joint.

The nail plates at the splice joints, connecting the wooden members of the chord and the rafter, respectively, are moved towards the upper edges of the wooden members. For all cases considered, the best location is such that the upper edges of the nail-plates coincide with the upper edges of the wooden members. This is a reasonable result

	Initial contact		No contact	
Displacement	Load case A	Load case B	Load case A	Load case B
1	1.9 mm	2.2 mm	2.4 mm	3.2 mm
2	−3.9 mm	−4.4 mm	−0.5 mm	−0.6 mm
3	−0.1 mm	−0.1 mm	−0.1 mm	−0.2 mm
4	9.0 mm (C)	9.0 mm (C)	9.0 mm (C)	9.0 mm (C)
5	5.0 mm (C)	5.0 mm (C)	5.0 mm (C)	5.0 mm (C)
6	5.0 mm (C)	5.0 mm (C)	4.3 mm	3.4 mm
7	0.6 mm	0.3 mm	1.0 mm	0.4 mm
8	−0.1 mm	−0.1 mm	−0.1 mm	−0.1 mm
9	0.1 mm	0.1 mm	0.1 mm	0.2 mm
10	9.0 mm (C)	9.0 mm (C)	9.0 mm (C)	9.0 mm (C)
11	0.0 mm	0.0 mm	0.0 mm	0.0 mm
12	−5.0 mm (C)	−5.0 mm (C)	5.8 mm	7.3 mm
Reduction of deflection	1.6%	2.4%	1.7%	3.8%

Table 4: Nail-plate displacements, in relation to the initial positions, giving minimum deflection of the chord of the roof truss. Activated constraints are indicated by (C). The resulting reductions of the deflection are also supplied.

knowing that the maximum tension at the splice joint of the chord, as well as the maximum compression at the splice joint of the rafter, are located at the upper edges. It is assumed herein that the nails remain effective even if they are located close to the edges of the wood. It should also be noted that a different load case could give maximum tension at the lower edge of the splice joint of the chord, which would result in a nail-plate displacement towards the lower edge at this joint.

The nail plate connecting the chord with the two diagonal members of the roof truss is moved upwards and towards an increased connection between the chord and the long diagonal member. The displacement of the nail plate is limited by constraints allowing only 5 mm displacements in the length and cross directions of the plate.

The optimal position of the nail plate at the top joint depends on the presence of contact between the two rafters. In case of initial contact, the plate is displaced downwards, increasing the connection between the long diagonal elements of the roof truss and the rafters. The two rafters are connected by contact pressure in combination with the nail plate. On the other hand, in the cases of no contact between the wooden members, the nail plate is displaced upwards. In this case the nail plate is moved towards a stiffer connection between the rafters.

The results of the optimization procedure with respect to the target function, the deflection of the middle of the chord, are also presented in Table 5. The reduction of the deflection is 1.6–3.8%, compared to the deflection with nominal nail-plate positions, where the higher value is valid for load case B, in case of no contact between wooden members. This reduction is modest, but significant. In the design of a roof truss, there

is often a critical deflection for one load case that must not be exceeded. If calculations, considering a preliminary design, show that the allowed deflection will be exceeded, it may be a solution to perform optimization on the nail-plate positions aiming at decreased deflection. This is, of course, an attractive option compared to increasing the dimensions of wooden members and nail plates.

3.2.3 The Optimization Procedure

Finally, a few comments on the optimization procedure should be supplied. A traditional optimization procedure using the steepest descent method is employed. In brief, starting at the nominal nail-plate positions, the gradient of the target function, i.e. the deflection, is calculated with respect to the nail-plate displacements. Then the quadratic fit method is employed. The target function is evaluated at two additional locations along the direction of the calculated gradient, giving that the deflection is known at three different locations, and that a quadratic polynomial can be fitted to these values. The polynomial, in turn, suggests a new position along the gradient direction for which the target function is minimized (according to the quadratic approximation). Then a new gradient is calculated at this new position and the procedure proceeds with a new quadratic fit, and so on. The procedure is a common strategy in structural optimization and a textbook on the subject has been written by Luenberger (1989).

An important detail in the implementation of the present optimization problem is the calculations of gradients. The gradient is calculated numerically, and a general perturbation procedure, for calculating the gradient once, would require a complete calculation of the deflection for twenty-two different nail-plate configurations (as the truss has eleven nail plates, each with two displacement degrees of freedom). However, as the non-linear model is elastic, i.e. the response is path independent, the gradient can be calculated by only performing one additional increment, and not a complete solution, for each of the twenty-two nail-plate displacements. This feature is very important for the computational efficiency, giving that the optimization procedure can be carried out at a very low computational cost, namely the cost of solving the problem for one nail-plate configuration times three (for the quadratic fit) times the number of iterations for convergence (about five or ten). The strategy for effective calculations of gradients in non-linear elastic problems has been presented in detail by Liu and Der Kiureghian (1991).

4 Concluding Remarks and Further Research

An investigation of the influence of geometrical imperfections in roof trusses has been carried out using a non-linear model capable of considering the stiffness of nail-plate joints, including contact pressure between wooden members.

A gap between wooden members, compared to initial contact between members, was found to be of great importance for the deflection and overall stiffness of the considered 20^o W-truss. For moderate loading, the deflection of the middle of the chord was about 15% larger for the case without contact, and the difference was even larger for higher loading. It was also found that small initial gaps between wooden members, less than 0.5 mm, distributed at different locations in the truss, result in a significant impact on

the deflection.

Further work on gaps between wooden members should comprise a thorough investigation of actual gap sizes present in manufactured roof trusses. Also, laboratory tests on nail-plate joints, in order to calibrate stiffness properties of nail plates and contact pressure, should be carried out. In particular, the friction coefficients for different wood fibre directions, and the influence of the butt effect, should be evaluated and considered in the calculations. The butt effect means that sawn surfaces of wood, pressed into each other in the fibre direction, tend to have a relatively low initial contact stiffness. Moreover, the splice elements of the mechanical model should be modified, according to laboratory tests, to be able to capture the effects of very large gaps between wooden members. Such gaps could be disastrous for the behaviour of the truss. In addition, the dependence on the angle between the plate direction and the splice direction should be evaluated and considered for the stiffness parameters of the splice element. Finally, not only stiffness and deformations should be considered in the evaluations, but also the ultimate strength of roof trusses.

Misplaced nail plates may have a negative effect on the stiffness and deflection of the roof truss. However, if the misplacement magnitudes are moderate, less than 5 mm, the influence on the deflection is much smaller than the influence of gaps between wooden members. Controlled displacements of nail plates, on the other hand, can be used in order to improve the behaviour of the roof truss. It was shown that the deflection can be reduced by about 2–4%, depending on the load case and the presence of contact. Moreover, it was shown that the employed non-linear and elastic mechanical model can, at a low computational cost, be combined with an optimization procedure adapted for the problem.

One type of geometrical imperfection, not considered here, is poorly pressed nail plates. Such nail plates have reduced stiffness and strength and the problem should be considered in a way similar to the types of geometrical imperfections treated here, in combination with laboratory work.

The conclusions from research on geometrical properties of wooden roof trusses with nail-plate joints can be used for the development of more accurate and complete computer software than those employed in industry today. The suggested models and routines can be used not only to increase the safety and performance of roof trusses, but also to improve the utilization of material, components and tolerances in industry.

References

Berglund, P. and Holmberg, J. (2000). "CALROOF - Program for Modelling of Roof Trusses Considering Flexibility of Joints," *Rep. TVSM-5099*, Division of Struct. Mech., Lund Univ., Lund, Sweden, (in Swedish).

CALFEM. (1999). "A finite element toolbox to MATLAB, Version 3.3" *Rep. TVSM-9001*, Division of Struct. Mech., Lund Univ., Lund, Sweden.

Ellegard, P. (2001). "Analysis of Timber Joints With Punched Metal Plate Fasteners - With Focus on Knee Joints," *ISSN 1395-7953 R0206*, Dept. of Build. Techn. and Struct. Eng., Aalborg Univ., Aalborg, Denmark.

Foschi, R. (1977). "Analysis of Wood Diaphragms and Trusses, Part II: Truss-plate Connections," *Can. J. Civ. Eng.*, **4**, 353–362.

Hansson, M. (2001). "Reliability of Timber Structural Systems," *Rep. TVBK-1022*, Division of Struct. Eng., Lund Univ., Lund, Sweden.

Isaksson, T. (1999). "Modelling the Variability of Bending Strength in Structural Timber," *Rep. TVBK-1015*, Division of Struct. Eng., Lund Univ., Lund, Sweden.

Kevarinmäki, A. (2000). "Semi-Rigid Behaviour of Nail-plate Joints," *Rep. TKK-TRT-109*, Lab. of Struct. Eng., Helsinki Univ. of Tech., Espoo, Finland.

Liu, P.-L. and Der Kiureghian A. (1991). "Finite Element Reliability of Geometrically Nonlinear Uncertain Structures," *J. Eng. Mech.*, **117**, 1806–1825.

Luenberger, D. (1989). "Linear and Nonlinear Programming," *Addison-Wesley Publication Company*, Menlon Park, California.

MATLAB. (2002). "High-performance numerical computation and visualization software, Version 6.1", *The Math Works Inc*, Natic Ma.

McKay, M. D., Conover, W. J., and Beckman R. J. (1979). "A Comparison of Three Methods for Selecting Values of Input Variables in the Analysis of Output from a Computer Code," *Technometrics*, **21**, 239–245.

Nielsen, J. (1996). "Stiffness Analysis of Nail-plate Joints Subjected to Short-term Loads," *ISSN 1395-7953 R9613*, Dept. of Build. Techn. and Struct. Eng., Aalborg Univ., Aalborg, Denmark.

Olsson, A. (1999). "Modelling Damage and Stochastic Properties in Engineering Structures," *Rep. TVSM-3037*, Division of Struct. Mech., Lund Univ., Lund, Sweden.

Olsson, A. and Rosenqvist, F. (1996). "Comparative Calculations of Deflections in Wooden Roof-trusses Connected with Nail Plates," *Rep. TVSM-5066*, Division of Struct. Mech., Lund Univ., Lund, Sweden, (in Swedish).

Olsson, A.,, and Sandberg, G. (2001). "Latin Hypercube Sampling for Stochastic Finite Element Analysis," *J. Eng. Mech.*, **128**, 121–125.

Owen, A. B. (1994). "Controlling Correlations in Latin Hypercube Samples," *J. American Stat. Ass.*, **89**, 1517–1522.

Petersson, H. and Olsson, K.-G. (1994). "Simple Models for Roof Truss Analysis," *Proc. of COST C1 Workshop*, Prague, Czech Republic.